GENESIS OF THE KARAALİ (ANKARA, TURKEY) Fe-Cu SULFIDE MINERALIZATION

A THESIS SUBMITTED TO
THE GRADUATE SCHOOL OF NATURAL AND APPLIED SCIENCES
OF
MIDDLE EAST TECHNICAL UNIVERSITY

BY

ALİ İMER

IN PARTIAL FULFILLMENT OF THE REQUIREMENTS
FOR
THE DEGREE OF MASTER OF SCIENCE
IN
GEOLOGICAL ENGINEERING

JANUARY 2006

Approval of the Graduate School of Natural and Applied Sciences

Prof. Dr. Canan ÖZGEN
Director

I certify that this thesis satisfies all the requirements as a thesis for the degree of Master of Science.

Prof. Dr. Vedat DOYURAN
Head of Department

This is to certify that we have read this thesis and that in our opinion it is fully adequate, in scope and quality, as a thesis for the degree of Master of Science.

Dr. Steven K. Mittwede	Assist. Prof. Dr. A. Pırıl ÖNEN
Co-Supervisor	Supervisor

Examining Committee Members

Prof. Dr. M. Cemal GÖNCÜOĞLU	(METU,GEOE)	_____
Assist. Prof. Dr. Pırıl ÖNEN	(METU,GEOE)	_____
Dr. Steven K. Mittwede	(Müteferrika Ltd.)	_____
Prof. Dr. Nilgün Güleç	(METU, GEOE)	_____
Prof. Dr. Asuman TÜRKMENOĞLU	(METU,GEOE)	_____

I hereby declare that all information in this document has been obtained and presented in accordance with academic rules and ethical conduct. I also declare that, as required by these rules and conduct, I have fully cited and referenced all material and results that are not original to this work.

Name, Last Name: Ali İmer

Signature:

ABSTRACT

GENESIS OF THE KARAALİ (ANKARA, TURKEY) Fe-Cu SULFIDE MINERALIZATION

İMER, Ali
M.Sc., Department of Geological Engineering
Supervisor : Assist. Prof. Dr. A. Pırıl ÖNEN
Co-Supervisor : Dr. Steven K. Mittwede
January 2006, 157 pages

With the closure of Neo-Tethys in the Early Tertiary, oceanic crustal material was accreted along the İzmir-Ankara-Erzincan Suture Zone. The Ankara mélange developed within this suture zone and contains Cretaceous ophiolitic fragments, some of which host significant Fe-Cu sulfide mineralization. Such mineralization is observed as massive to disseminated pyrite-chalcopyrite hosted by pillow to massive basalts in a dismembered and tectonically imbricated ophiolite block near Karaali, Ankara. Basaltic host rocks lack most of their primary mineral assemblages and textural relationships. As a consequence of greenschist-facies metamorphism and hydrothermal alteration, the basalts were strongly albitized and propylitized prior to late-stage argillic alteration, which is proximal to the main mineralized zone. Sulfide mineralization occurs in a massive sulfide lens and laterally extensive, 10-meter-thick zone of anastomosing quartz-sulfide veins. Other than pyrite and chalcopyrite, bornite, covellite and sphalerite also occur as minor sulfide phases, and the source of sulfur is determined to have been magmatic on the basis of ^{34}S isotope analyses. A series of geochemical analyses suggest that the basaltic host rocks formed within a subduction-related tectonic setting, and the mineralization is thought to have formed during a medium-temperature hydrothermal event which was followed by another later period of low-temperature hydrothermal activity. Field, petrographical and geochemical

evidence show that the Karaali Fe-Cu mineralization is genetically correlative with the Cyprus and Küre massive sulfide deposits, and may be classified as a “Cyprus-type” massive sulfide deposit.

Keywords: Ankara mélange, Karaali, ophiolite, massive sulfide, Cyprus-type.

ÖZ

KARAALİ (ANKARA, TÜRKİYE) Fe-Cu SÜLFİT CEVHERLEŞMESİNİN OLUŞUMU

İMER, Ali
Yüksek Lisans, Jeoloji Mühendisliği Bölümü
Tez Yöneticisi : Yrd. Doç. A. Pırıl ÖNEN
Yardımcı Tez Yöneticisi : Dr. Steven K. Mittwede
Ocak 2006, 157 sayfa

Neo-Tetis'in Erken Tersiyer'de kapanması ile bu okyanusta oluşmuş olan okyanus kabuğu malzemesi İzmir-Ankara-Erzincan Kenet Kuşağı boyunca yığışmıştır. Bu kenet kuşağında gelişmiş olan Ankara melanjı, bazıları önemli Fe-Cu sülfit cevherleşmelerine ev sahipliği yapan Kretase yaşlı ofiyolit parçaları içerir. Benzeri cevherleşmeler Karaali, Ankara yakınlarındaki parçalanmış ve tektonik olarak dilimlenmiş bir ofiyolit bloğunda bulunan yastık ve masif bazaltlarda masif ve dağılmış haldeki pirit-kalkopirit şeklinde görülür. Bazaltik anakayalar birincil mineral topluluklarının ve dokusal ilişkilerinin büyük bölümünü yitirmiştir. Yeşilşist fasiyesindeki metamorfizmanın ve hidrotermal alterasyonun sonucu olarak bazaltlar yoğun biçimde albitleşmiş ve propilitize olmuş, ayrıca geç evrede de ana cevherleşme bölgesi yakınlarında arjillik alterasyona uğramıştır. Sülfit cevherleşmesi massif sülfit lensi ve yanal olarak süreklilik gösteren, 10 metre kalınlığında örgü tipi kuvars-sülfit damarları şeklindedir. Pirit ve kalkopirit dışında bornit, kovellin ve sfalerit ikincil sülfit fazlarıdır. Cevherleşmedeki sülfürün kaynağı ^{34}S izotop analizi sonucunda magmatik olarak belirlenmiştir. Bir dizi jeokimyasal analiz sonucunda bazaltik anakayanın dalma-batma ile ilişkili bir tektonik ortamda oluştuğu ve cevherleşmenin geç evreli, düşük sıcaklıklı bir hidrotermal aktivite tarafından izlenen tahmini olarak orta sıcaklıklı bir hidrotermal evre sonucunda gerçekleştiği belirlenmiştir. Arazi, petrografi ve jeokimya çalışmalarının ışığında

Karaali Fe-Cu cevherleşmelerinin Kıbrıs ve Küre'deki masif sülfit yataklarıyla oluşumsal açıdan ilişkili olduğu ve "Kıbrıs-tipi" bir yatak olarak sınıflandırılabileceği ortaya konmuştur.

Anahtar Kelimeler : Ankara melanjı, Karaali, ofiyolit, massif sülfit, Kıbrıs-tipi.

in memories
of
Ersin İmer and Prof. Dr. Ayhan Erler…

ACKNOWLEDGMENTS

I would like to express my sincere gratitude to my supervisor, Assist. Prof. A. Pırıl Önen, for her patience, guidance and critical suggestions through every step of this study.

This thesis could not have been written without Dr. Steven K. Mittwede, who not only served as my co-supervisor, but also encouraged and guided me throughout my scientific research with his critical views and suggestions.

I am deeply indebted to my instructors Prof. Dr. Demir Altıner, Prof. Dr. Cemal Göncüoğlu, Prof. Dr. Haluk Akgün, Prof. Dr. Nilgün Güleç, Prof. Dr. Erdin Bozkurt, Prof. Dr. Asuman Türkmenoğlu, Assoc. Prof. Dr. Bora Rojay, Assoc. Prof. Dr. İlkay Kuşçu, Assist. Prof. Dr. Fatma Toksoy Köksal and Res. Assist. Mustafa Koçkar for their never-ending support and critical suggestions both during my undergraduate and graduate studies.

I would like to extend my thanks to Dr. Nurullah Hanilçi (İstanbul University) for performing the fluid-inclusion analyses, and to Mr. Okan Zimitoğlu and Dr. Semih Gürsu (MTA) for their help in taking photomicrographs of polished sections.

Thanks also go to Mr. Orhan Karaman for preparing the thin sections.

I would like to express my gratitude to my friends Hakan Akan, Evren Yücel, Onur Gezen, Ulaş Avşar, Kaan Sayıt, Sinan Öztürk and Mert Bildiren for their never-ending support.

Finally, and most importantly, I wish to extend my deepest thanks to my mother, Arsal İmer, for her moral and financial support throughout my life.

I would like to dedicate this thesis to two people who are not with us now but who, nevertheless, influenced me profoundly. First of all, to my father, Ersin İmer, who guided me but never prevented my desire to seek new ideas and try to go beyond; secondly, to Prof. Dr. Ayhan Erler, whom I never met but have heard much of and whose example has served as an inspiration to me.

TABLE OF CONTENTS

LIST OF TABLES

LIST OF FIGURES

CHAPTER 1

INTRODUCTION

1.1 Purpose and Scope

Massive and disseminated pyrite-chalcopyrite mineralization, much of which appears to occur in fault-hosted veins, is exposed near Karaali, Ankara Province, Turkey. In Karaali, the mineralization historically produced a significant amount of Cu and, possibly lesser Au, as reflected by the ~70,000 ton slag heap in Karaali. An unpublished C^{14} age determination from charcoal engulfed in Karaali slag has yielded an age of ~950 yr B.P (W.E. Sharp and S.K. Mittwede, unpublished data). The present study aims to determine the relationship of this mineralization to the adjacent and proximal altered pillow basalts, gabbros and serpentinites, which presumably represent a dismembered, tectonically imbricated (partial) ophiolite complex.

The eastern Mediterranean region hosts many ophiolite-hosted massive sulfide deposits, and the Troodos Massif of Cyprus and the Semail Ophiolite of Oman have deposits of considerable size and grade (e.g., Constantinou and Govett, 1972; Coleman, 1977; Adamides, 1980; and Franklin et al., 1981). Similarly Turkey, which is also located in this region, has significantly productive massive sulfide deposits especially in the western/central Pontides (e.g., the Küre district in Zonguldak) and in southeastern Anatolia (the Ergani district in Elazığ and the Madenköy district in Siirt) (e.g., Bamba, 1976; Erdoğan, 1977; Erler, 1984; Güner, 1982; Çağatay, 1993; and Koç et al., 1995).

Along the İzmir-Ankara-Erzincan suture zone, which represents the closure of Neo-Tethys, oceanic accretionary complexes are widely exposed. The North Anatolian Ophiolitic Mélange Belt is a major component of these complexes and

contains widely distributed blocks of ophiolitic fragments, massive and pillow basaltic lava flows, and Jurassic-Cretaceous carbonates. Despite their mélange character, some of the ophiolite fragments within this belt are well-preserved and are associated with massive sulfide mineralization. The present study aims to emphasize the presence and significance of such mineralization in the region.

Through geological mapping, petrographic investigation, whole-rock geochemical work, and isotope and fluid-inclusion studies, the genesis of the Karaali mineralization and the surrounding ophiolitic rocks will be established. This thesis further aims to evaluate and compare the results of these field and laboratory studies with those of the Cyprus and Küre massive sulfide deposits. Moreover, an attempt will be made to fit the Karaali mineralization into the existing general classification systems for volcanogenic massive sulfide deposits.

1.2 Geographic Setting

Karaali village lies at the northwestern edge of central Anatolia. The study area is located about 39 km south of Ankara on the Ankara-Bala road and has an approximate extent of 20 km^2 (Figure 1.1). Within this area, the focal point of the study of massive sulfide mineralization is the ophiolites which cover an area of 12 km^2. Beynam village is located at the northern end of the study area, while the southern perimeter is delimited by Karaali village.

The abandoned mine is situated 3 km from the center of Karaali village staying within a narrow valley called Karaboyalık (Figure 1.2). The southern flank of this valley is occupied by Otlubel Hill, and Yağmuryağan Hill lies on the northern flank.

1.3 Methods of Study

The present study involves two major types of research: field studies and laboratory studies. Field studies, including geological mapping and rock sampling, were begun in late August 2004, with a reconnaissance visit to Karaali village.

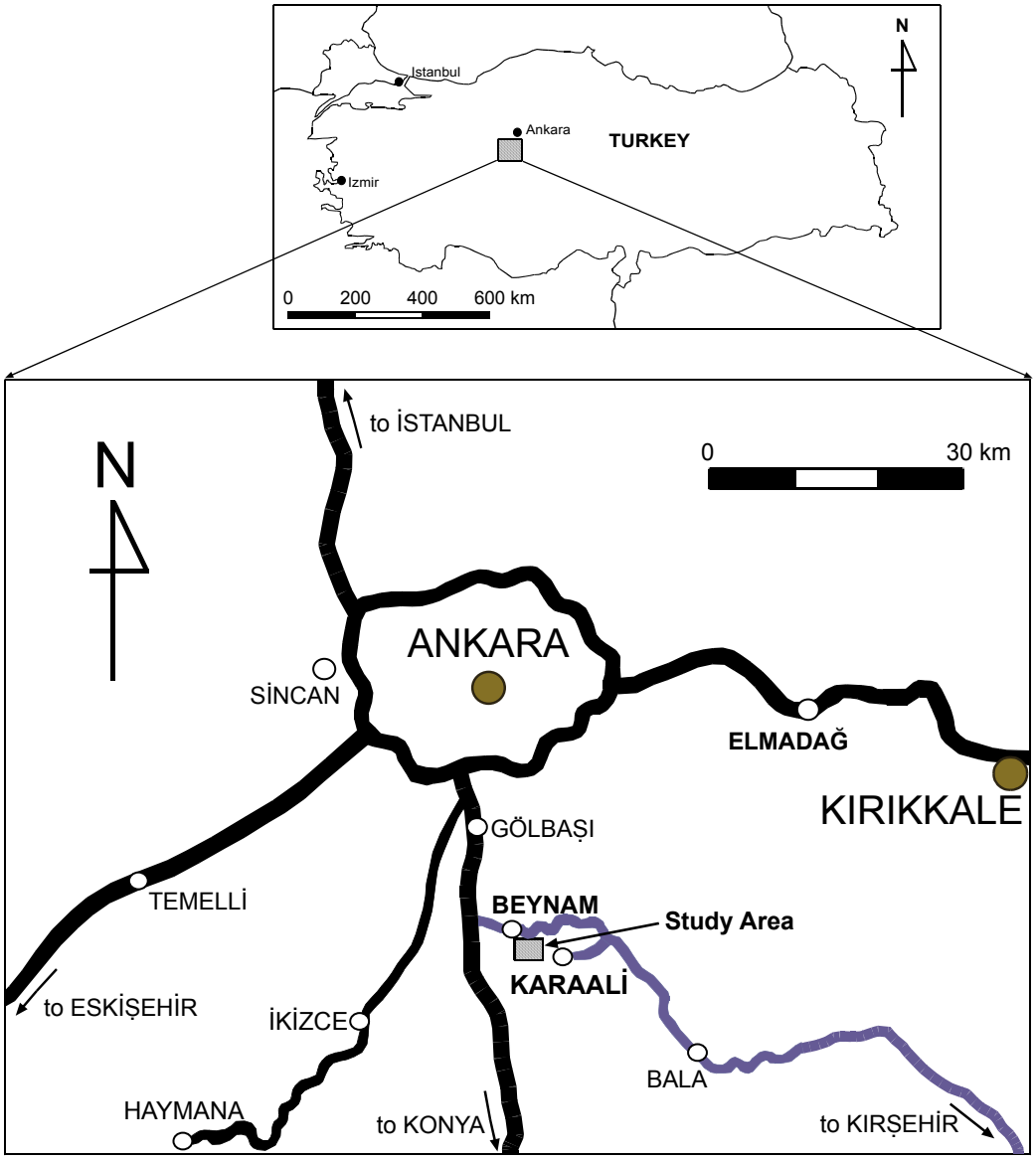

Figure 1-1. Location map of the study area.

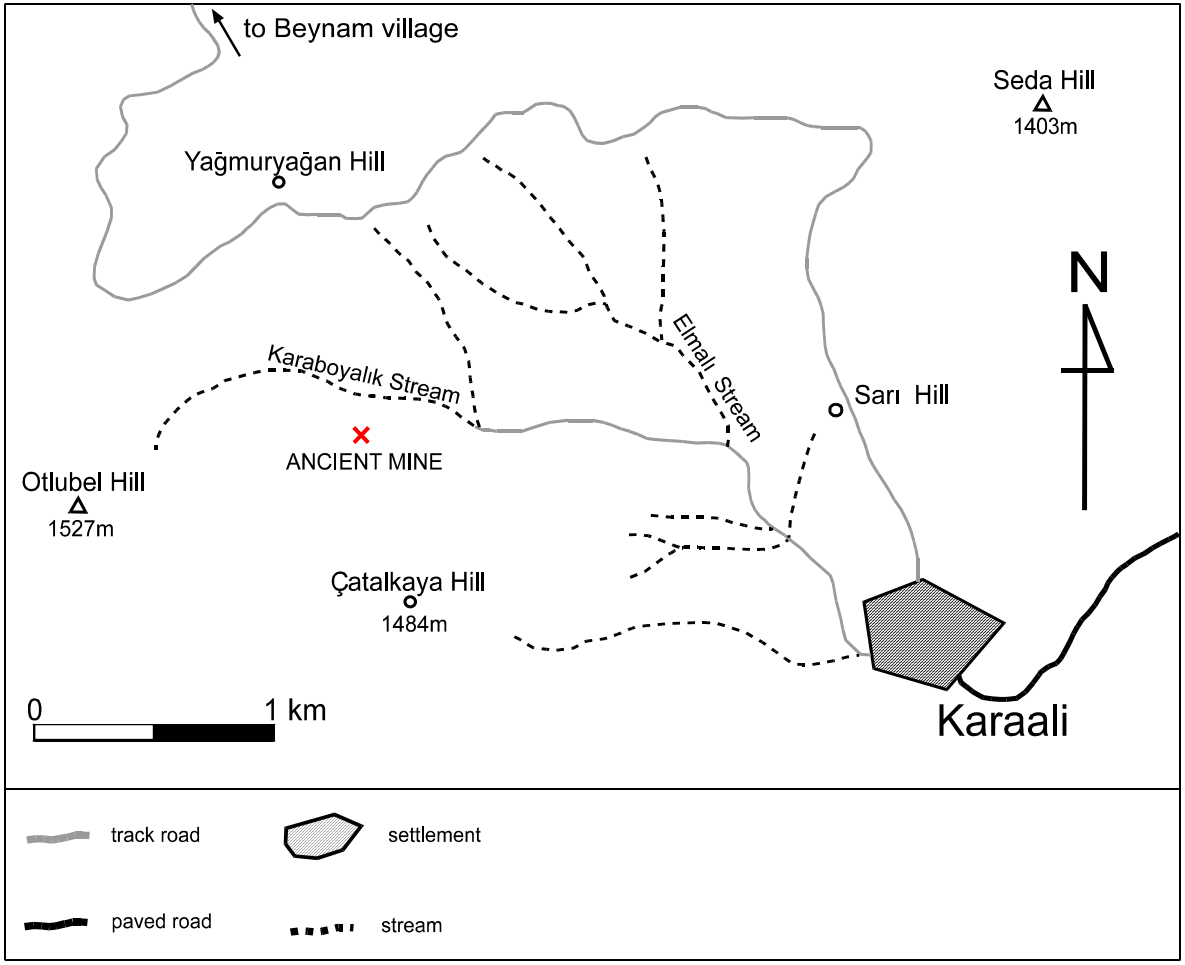

Figure 1-2. Outline map showing the site of mineralization and the ancient mine site.

Rock sampling entailed collecting 112 samples, most of which were taken from the ophiolite fragment between Karaali and Beynam villages. Systematic sampling has been carried out in close proximity to the main ore body along traverses extending from NE to SW, which cut the main orebody and underlying vein systems perpendicularly. In the meantime, a 1:25,000 scale geological map of the entire study area and a 1:5000 scale map of the mineralized horizons have been prepared (see Chapter 4).

Following field work, laboratory studies were carried out. These include preparation and study of thin and polished sections, whole-rock geochemical analyses of 18 samples, XRD analyses of four samples for determination of critical mineral assemblages, sulfur-isotope analyses of six sulfide ore-bearing samples, and fluid-inclusion microthermometric analysis of 12 samples from mineralized quartz-sulfide veins. Further details concerning analytical methods are given in the pertinent chapters.

1.4 Previous Studies

The North Anatolian Ophiolite Mélange (NAOM) represents allochthonous assemblages of the Neo-Tethyan İzmir-Ankara-Erzincan Ocean, which were emplaced southward onto the Tauride-Anatolide Platform during the Late Cretaceous (e.g., Rojay et al., 2001 and 2004). The NAOM consists of huge bodies of almost complete ophiolitic sequences and tectonic mélanges of the accretionary complex.

The most common and internationally known name given to this assemblage is the “Ankara Mélange” (Bailey and McCallien, 1950) – an Upper Cretaceous chaotic tectono-sedimentary ophiolitic mélange, comprising various blocks of dissimilar age, origin, facies, and size set in an intensely sheared and fine-grained matrix composed of ophiolitic-material-rich sandstone, shale, radiolarite, and pelagic mudstone (Rojay et al., 2001).

Bailey and McCallien (1950) stated that there are broken rocks, consisting mainly of graywackes, limestones, and the Steinmann Trinity (an association of serpentinite, pillow lava and radiolarite) around Ankara, and that these comprise a chaotic assemblage generally resembling a mélange. Bailey and McCallien (1950) then proposed that this broken mixed zone be termed “Ankara Mélange”. According to those authors, the Ankara Mélange is composed of fragments and masses of the component rocks (graywackes, limestones and the Steinmann Trinity) ranging up to kilometers in length.

Gansser (1959) suggested that the formation of the Ankara Mélange was related to the development of submarine olistostromes and its emplacement was mainly tectonically induced (gravity slumping and sliding). He also used the term “colored mélange” for the ophiolitic mélange in the region.

Boccaletti et al. (1966) divided the Ankara Mélange into two subgroups: (1) thick graywacke assemblages comprising low- to high-grade metamorphics and Paleozoic limestones with rare blocks of ophiolites; (2) a mixture of ophiolitic blocks with limestones and flysch-type sediments.

Sestini (1971) defined the Ankara Mélange as an assemblage of serpentinite, diabase/basalt, radiolarite, limestone, flysch packages, marl, lenses of shale, and polygenic breccia within an internally chaotic complex. His study also suggested that the formation mechanism of the mélange was the emplacement of ophiolites, such as gravity nappes, and that the relation between the Cretaceous flysch and the limestones was tectonic.

Norman (1973) studied the Ankara Mélange and the surrounding Cretaceous succession in detail and divided the mélange units into three, from west to east: metamorphic block mélange, mélange with limestone blocks, and ophiolitic mélange.

Çapan and Buket (1975) studied the Kalecik section of the Ankara Mélange and constructed a 1:25,000 scale geological map, partially grouping some of the

mélange units. They indicated the presence of limestone blocks (olistoliths), flysch-like sedimentary units and volcanics other than the already-known Steinmann Trinity (serpentinite-radiolarite-pillow lava) occurrences. According to that study, the age of ophiolite emplacement was established as the early stages of the Late Cretaceous, and the upper boundary for the formation of the mélange was delimited as Maastrichtian.

Batman (1978) studied the southwestern margin of the mélange and divided the mélange into two – namely, the Hisarlıkaya Formation and the Dereköy Formation – on the basis of the lithologies involved in these mélanges and their emplacement ages. The Middle-Upper Triassic Hisarlıkaya Formation comprises a shale-sandstone-graywacke section at its base, topped by exotic blocks of limestone that were carried by gravity sliding and slumping. Owing to the presence of the exotic limestone blocks, the Hisarlıkaya Formation was regarded as a counterpart of limestone block mélange. Moreover, the Dereköy Formation consists entirely of ophiolites and, as a result, belongs to the ophiolitic mélange.

Akyürek et al. (1979) studied the Çankırı section of the ophiolitic mélange. Naming the ophiolitic mélange in that region the “Eldivan Ophiolitic Mélange”, they determined an emplacement age within the Barremian and Cenomanian-Turonian interval. This section of the Ankara Mélange includes mainly gabbro, diabase, serpentinite, cherty limestone and radiolarite-mudstone.

Akyürek et al. (1980) studied the area around Eldivan, Şabanözü and Kalecik in detail, outlining the general stratigraphy of the region. According to the those authors, the ophiolites were emplaced into the region in the Early Cretaceous via undetermined tectonic processes and gained its mélange character by bringing up Jurassic-Early Cretaceous limestone blocks from a subduction zone that is assumed to be to the north.

Norman et al. (1980) defined the Ankara Mélange as a combination of Permian-Cretaceous limestone blocks, turbiditic limestones, pillow lavas, agglomerates,

serpentinites, and radiolarian cherts embedded in a matrix of shale and volcanic sand.

Ünalan (1981) constructed a local stratigraphic column for the southeastern part of the Ankara Province. According to him, the Ankara Mélange corresponds to a sedimentary succession in the Early Triassic to Late Cretaceous interval. Both at the top and bottom of the ophiolitic mélange Upper Senonian marine successions occur. Consequently, that study suggests that the ophiolitic mélange is formed in the Late Senonian in a marine basin.

Akyürek et al. (1984) revised the map of the ophiolite succession around Eldivan and delineated the succession as follows: an ultramafic section at the bottom comprising peridotite, dunite, harzburgite and pyroxenite; an upper section of gabbro and diabase dikes; and pillow lavas and pelagic sediments at the top. They reported that the internal structure of this allochthonous ophiolite complex is partially preserved and was emplaced during the Early Cretaceous –most probably in the Albian-Aptian interval- and found within a Cenomanian-Maastrichtian flysch in the form of olistostromes and olistoliths.

Norman (1984) restudied the Ankara Mélange and reinterpreted it as a subduction/accretion complex related to Early Mesozoic closure of Tethys. Based on the dominant lithologies he separated the mélange into three parts: metamorphic-block mélange, limestone-block mélange and ophiolitic mélange.

Tankut (1990) aimed to identify the geochemical characteristics and tectonic settings of the ultramafic and mafic rock clasts in the Ankara ophiolitic mélange (Keskin, Elmadağ and Beynam). According to her study, there are serpentinites, serpentinized peridotite, gabbro, dolerite, and basalts with radiolarites and pelagic limestones in the ophiolitic mélange. That study also indicates that the basic rocks show both mid-ocean ridge and island-arc affinities, indicating a possible back-arc basin tectonic setting.

Tankut and Gorton (1990) demonstrated the geochemical similarities of Edige ultramafic body to oceanic lithosphere via the use of detailed geochemical studies. According to those authors, incompatible trace-element chemistry of the rocks of Edige massif reveal that it is a remnant of an oceanic lithosphere fragment in the ophiolitic mélange.

Tankut and Sayın (1990) studied the Edige massif which is in the form of a large ophiolite block within the Ankara Mélange. The Edige massif comprises tectonites and cumulates, and the cumulate minerals are established to be the products of mid-ocean-ridge-type magma differentiation, with obvious ocean-floor metamorphism.

Koçyiğit (1991) studied several outcrop areas of Upper Cretaceous-Lower Tertiary sedimentary sequences in a NE-SW trending belt the northwest part of the Ankara Province. He suggested that these areas represent remnants of a peripheral accretionary fore-arc basin comprising the Haymana-Polatlı accretionary fore-arc basin during the Middle Campanian-Middle Eocene time.

Tüysüz et al. (1995) proposed that the Ankara-Erzincan Ocean (northern branch of Neo-Tethys) between the Sakarya and Kırşehir continents was closed along a two-folded subduction system. The ophiolitic belt, as a remnant of this ocean, was differentiated into two lithological units: an ophiolitic mélange and a volcanic-sedimentary association. The ophiolitic mélange consists of two distinct mélange units developed along different subduction zones. One of them, the northern mélange, developed along the southern margin of the Sakarya continent, whereas the southern mélange was a product of intra-oceanic subduction. On the other hand, the volcanic rocks of the volcanic-sedimentary association have been differentiated into two tectonomagmatic settings: island arcs and ocean islands.

Tankut et al. (1998) studied the chemistry of ophiolitic rocks from Edige, Kalecik and Beynam in the Ankara mélange and documented the nature of magmatism and tectonic affinity associated with oceanic crust and seamount generation in the northern branch of Neo-Tethys. Regarding the assortment tectonomagmatic

signatures of these ophiolitic rocks, they suggested three distinct episodes of volcanism, including an N-MORB sea-floor spreading volcanism at a mid-ocean ridge, a plume-related alkaline volcanism associated with the formation of volcanic build-ups and seamounts, and an arc-related volcanism in the Neo-Tethyan oceanic lithosphere in the upper plate of a north-dipping subduction zone.

Rojay et al. (2001) made an attempt at dating the Tethyan oceanic crust from pillow basalts within the Cretaceous ophiolitic mélange terrain, and at determining the original tectonic setting prior to mélange formation. In the light of field, geochemical and paleontological data they suggested that the ocean-island signature of basalts may represent the presence of an intra-plate hot spot on the oceanic crust. The study also verified the inferred age of Middle Jurassic to Early Cretaceous for the inter-pillow biomicrites, signifying the time interval for seamounts in the region.

Rojay et al. (2004) presented a similar study (in the general context of the 2001 paper) on the dating and geochemistry of isolated pillow basalts in the North Anatolian ophiolitic mélange. With the addition of new data, this study also supports the presence of a seamount on the Neo-Tethyan oceanic crust during the Early Cretaceous.

1.5 Previous Studies of Mineralization in the Study Area

The Fe-Cu sulfide mineralization near Karaali previously attracted some geologists to the area, especially in the mid-nineties. Although much of the ore seemed to been removed by earlier civilizations, the Institute of Mineral Research and Exploration (MTA) carried out some fieldwork in the area and searched for prospects.

Birgi (1944) carried out fieldwork in the Karaali area and simply stated the geology of the area with supplementary petrographic examinations and geochemical analyses. Birgi, in his report, indicated the grade of Cu as 0.93% and estimated

reserves of 7000 tons of Cu. Birgi (1944) also pointed out that there is gold in significant quantities (40 g/t) and recommended further studies in the area.

Brabers (1964) performed a study mainly concerning the economic significance and potential of several areas of Cu-Au mineralization around Bala, Ankara, which included the Fe-Cu sulfide mineralization of Karaali. The report considered the recommendations of Birgi (1944) and focused on the geochemical aspects of the mineralization with more detailed analyses. Brabers (1964) proposed that gold is totally absent in the area and there are no important copper reserves in the region.

CHAPTER 2

OPHIOLITES AND OPHIOLITE-RELATED MINERALIZATION: A REVIEW

2.1 Introduction

Ophiolites represent ocean crust and mantle formed at oceanic spreading centers. These centers occur either at mid-ocean ridges, in pull-apart intra-arc oceanic basins, at active back-arc basins, and at extensional zones in the centers of forearcs during the initial development of island arcs (Moores, 2003).

The term “ophiolite” (meaning snake-rock in Greek) was first used by a French geologist, Alexander Brongniart in 1813 in order to refer to a suite of ultramafic to mafic magmatic rocks closely associated in the field. However; it was Gustav Steinmann, a German geologist, who clearly defined the ubiquitous association of serpentinite, diabase-spilites, hypabyssal and plutonic mafic rocks, and radiolarian chert, which was later termed the “Steinmann Trinity” (Moores, 2003). Subsequently, the definition and extent of the term “ophiolite” has been modified many times, and in 1972, a Penrose conference on ophiolites was held which has been regarded as a “turning point” in the understanding of ophiolites. The definition agreed on at the Penrose Conference was as follows:

Ophiolite refers to a distinctive assemblage of mafic to ultramafic rocks. It should not be used as a rock name or lithologic unit in mapping. In a completely developed ophiolite, the rock types occur in the following sequence:

- ultramafic complex, consisting of variable proportions of harzburgite, lherzolite, and dunite, usually with a metamorphic tectonic fabric (more or less serpentninized);

- gabbroic complex, ordinarily with cumulus textures commonly containing cumulus peridotites and pyroxenites and usually less deformed than the ultramafic complex;

- mafic sheeted-dike complex;

- mafic volcanic complex;

- associated rock types include (1) an overlying sedimentary section typically including ribbon cherts, thin shale interbeds and minor limestones; (2) podiform bodies of chromite generally associated with dunite; and (3) sodic felsic intrusive and extrusive rocks.

Faulted contacts between mappable units are common. Whole sections may be missing. An ophiolite may be incomplete, dismembered, or metamorphosed ophiolite. Although ophiolite generally is interpreted to be oceanic crust and upper mantle, the use of the term should be independent of its supposed origin (Anonymous, 1972). (Dilek, 2003)

This definition, evidently, is not valid for all of the ophiolites (including the most well-preserved examples) recognized up until now, and studies of various ophiolites over the last few decades clearly support this idea. However, today most researchers agree on the idea that ophiolites are fragments of fossil oceanic lithosphere that have been thrust over or obducted onto continental margins at consuming plate boundaries (Coleman, 1971; Dewey and Bird, 1971; Dewey, 1976; Dewey, 2003).

When their mineralization potentials are considered, ophiolites are one of the major focal points in the exploration for different types of ore deposits. The main mineral deposit types that develop in ophiolites are volcanogenic massive sulfides, orthomagmatic deposits (chromite and PGE) asbestos and supergene deposits of laterites. Among these, the massive-sulfide and chromite deposits are the most significant mineral-deposit types (Coleman, 1977).

The main metallogenic interest pertaining to ophiolites has, without doubt, been concentrated either on the pillow basalts or on the deeper, ultramafic portions of the complexes. Especially massive, stratabound, base-metal sulfide ores and deposits of chromite/PGE and asbestos are of main primary interest (Vokes et al., 1990).

2.2 Deposit Types in Ophiolites

The variety of ophiolite-related mineral deposits was mainly recognized during intensive studies of the Troodos ophiolite in Cyprus, particularly in the 1970s and early 1980s. Pouit (1984), Laznicka (1985) and O'Hanley (1996) presented important reviews of ophiolite-hosted mineralization by combining data gathered from different localities around the world, including Newfoundland, the Apennines, and the Alpine chain, in addition to Cyprus.

Based on the Pouit (1984) classification, four main types of ophiolite-hosted mineral deposits are recognized:

A. massive pyritic, copper- and lesser zinc-bearing sulfides, in many cases pillowed basaltic lavas of ocean-floor type (Layer 2).

B. weak sulfidic (mainly pyrite±chalcopyrite) veins and disseminations in the sheeted dike complexes ("diabase complex") of Layer 3.

C. minor deposits of chalcopyrite-pyrrhotite, with or without gold values, toward the top of the gabbros of Layer 3.

D. often significant deposits of chromite, asbestos and (lesser) Fe-Cu-Ni-Co sulfides and PGE in the ultramafic rocks, both in the layered series and in the mantle harzburgites (Figure 2.1).

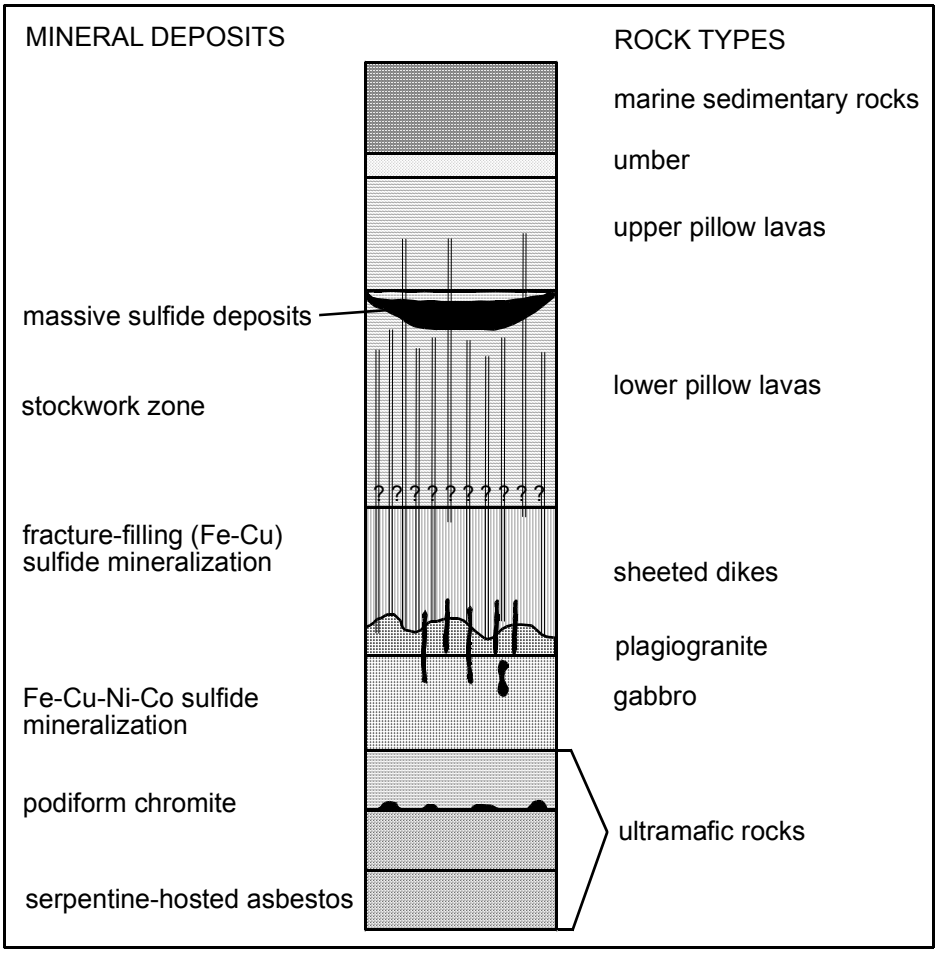

Figure 2-1. Diagrammatic composite geologic column of the Troodos ophiolite, showing the major lithologic units and the distribution of orebodies in the complex (after Constantinou, 1980; Robinson et al., 2003).

2.3 Volcanogenic Massive Sulfides

2.3.1 Introduction

Volcanic-hosted massive-sulfide deposits were recognized as a genetically distinct group during the 1950s (Franklin et al., 1981) and they occur in

association with most upper-crustal rock types. These type of deposits are an important source of copper, zinc, and lead in the world, and contain significant quantities of silver, gold, selenium, tin, and bismuth, as well as minor amounts of many other metals.

By definition, “massive-sulfide deposits are stratabound and in part stratiform accumulations of sulfide minerals which are normally composed of at least 60 percent sulfide minerals in their stratiform portions. The stratiform portion may comprise up to 100 percent of the total sulfide present, but many deposits have a substantial component of discordant vein-type sulfide mineralization, the “stringer zone”, mainly in the footwall strata” (Franklin et al., 1981) (Figure 2.2). Massive-sulfide deposits can occur in virtually any supracrustal rock type, although volcanic rocks and pelitic to semipelitic strata are the predominant host rocks. Deposits contain almost ubiquitous iron sulfides as the dominant sulfide species, with one or more of sphalerite, chalcopyrite, and galena as the principal economic minerals (Franklin et al., 1981).

Volcanic-associated stratabound massive-sulfide deposits are widely distributed throughout geologic time. The oldest occurrences of sulfide mineralization have been dated as pre-3700 and pre-3400 m.y.-old in Greenland and Western Australia, respectively (Sangster and Brook, 1977). On the other hand, currently active black smokers in the ocean-floor rift systems may be regarded as the youngest deposits of this type.

2.3.2 Classification

Since their first discovery in 1950s, economic geologists have made many attempts to classify volcanogenic massive-sulfide deposits. Various parameters such as metal associations, tectonic setting, or host-rock composition have been used for division of massive-sulfide deposits into distinct groups.

Hutchinson (1973) proposed a threefold classification system which is mainly based on ore compositions: (1) zinc-copper deposits, which are principally

Archean in age and volcanic hosted; (2) lead-zinc-copper-silver types, which occur in both volcanic and mixed volcanic and sedimentary strata, predominantly in Proterozoic and Phanerozoic rocks; and (3) cupreous-pyrite deposits, which are associated predominantly with mafic and ultramafic volcanic rocks, principally of Phanerozoic age (Franklin et al., 1981). In this classification system, Hutchinson combined ore compositions with environmental factors as secondary classification criteria.

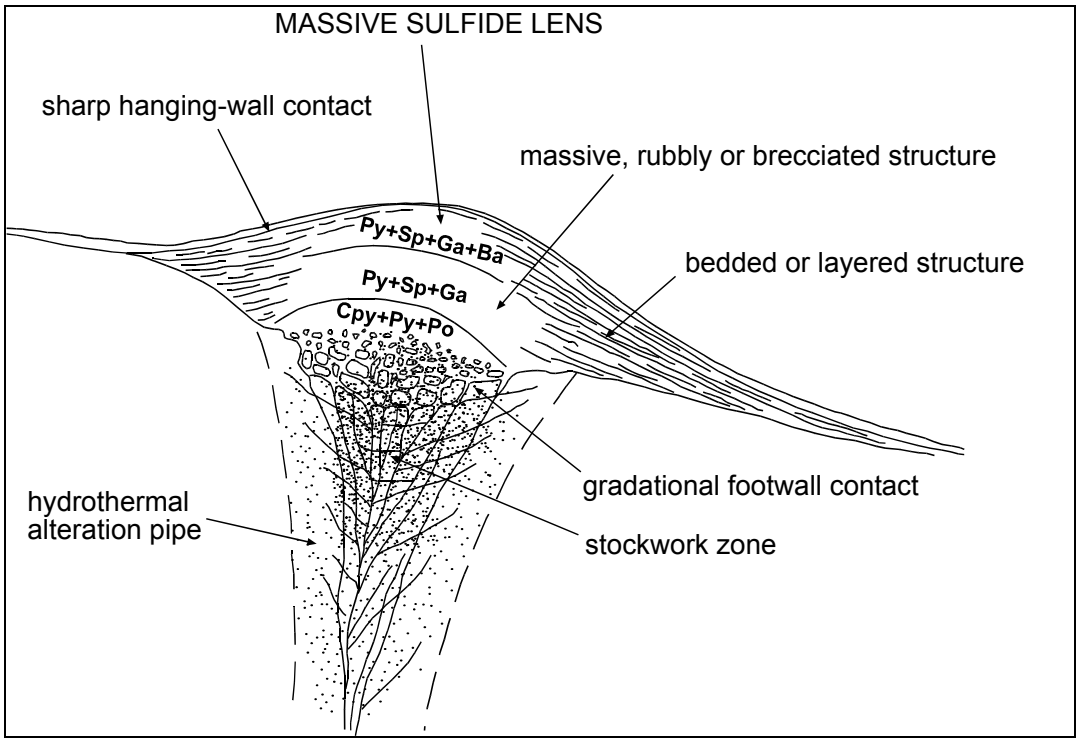

Figure 2-2. Idealized cross-section of a massive sulfide deposit (modified from Lydon, 1984) (py: pyrite, cpy: chalcopyrite, ga: galena, sp: sphalerite, ba: barite, po: pyrrhotite).

Subsequently, Sangster and Scott (1976) proposed a division into three types on the basis of environments: (1) deposits of a predominantly volcanic association;

(2) those of a predominantly sedimentary association; and (3) those of a mixed volcanic and sedimentary association.

Sawkins (1976) devised a three-fold classification system based on deposit characteristics, including composition of associated volcanics and tectonic setting:

(a) Cyprus type- associated with spreading ocean or back-arc spreading ridges and with basic volcanics, usually ophiolites;

(b) Besshi type- associated with the early part of the main calc-alkaline stage of island-arc formation;

(c) Kuroko type- associated with the later stages of island-arc formation and more felsic volcanics (Edward and Atkinson, 1986).

Another compositionally based approach was suggested by Solomon (1976), and divided the volcanic-hosted deposits into three: a zinc-lead-copper group; a zinc-copper group; and a copper group.

Franklin et al. (1981) followed a similar approach and identified two distinct groups: a copper-zinc group, and zinc-lead-copper group. The copper group of Solomon (1976) was omitted since the subdivision into copper and copper-zinc may be artificial due to copper-producing deposits having zinc (below the cut-off value) which is not reported (Edward and Atkinson, 1986).

In contrast to these classifications, Stanton (1978) suggested another classification system which considered the volcanic ores as belonging to one continuous spectrum showing geochemical evolution; namely, reflecting the evolution of calc-alkaline rocks in island arcs. He suggested that the mainly pyritic copper deposits are spatially and temporally associated with tholeiitic and ultrabasic rocks. With the change to calc-alkaline volcanism, the larger, zinc-rich deposits occur, while further development of the calc-alkaline trend toward dacite and rhyolite is accompanied by the occurrence of lead-bearing deposits (Edward and Atkinson, 1986).

Hutchinson (1980) combined the ore composition, the tectonic setting and the host rock aspects and proposed a four-fold division. This classification introduced the primitive (zinc-copper) in addition to Sawkins (1976) classification.

In a classification based on the composition of the dominant host rock, Klau and Large (1980), divided the volcanogenic massive sulfide deposits into mafic-volcanic, felsic-volcanic, and sedimentary types.

The classification systems mentioned above mainly concentrate on two principal approaches: a host-rock lithology approach (Sangster and Scott, 1976; Sawkins, 1976; Stanton, 1978; and Klau and Large, 1980) and an ore-composition approach (Solomon, 1976; and Hutchinson, 1980). Each classification method has its own advantages and disadvantages.

Preferring a classification system based on the composition of the ore is especially useful for determining the economic significance of the deposit that is sought. Also, such a classification enables the researchers to obtain the genetic evolution of the deposit itself (Franklin et al., 1981).

In contrast, applying a classification system based on geological environment is a particularly useful field system, as the principal stratigraphic elements of any deposit are recorded on geological maps. Knowing the geological characteristics of a site, one can easily target a deposit via this classification system (Franklin et al., 1981).

In general, by combining the plate-tectonic setting with localized tectonic and depositional environment and host rocks, Hutchinson's (1980) classification can be regarded as the most convenient classification system for the exploration geologist (Table 2.1). With the tectonic-setting approach, it can help in the selection of possible target areas on a global scale. Utilizing the localized tectonic and depositional environment systems will assist at the regional scale, while the host-rock compositions may be useful for determination of target areas. Therefore,

in this study, Hutchinson's (1980) classification is the main reference point for the classification of the Karaali massive sulfides.

2.3.2.1 Besshi Type

Besshi-type deposits occur in either clastic sedimentary and mafic marine volcanic rocks, or in basaltic tuffs and flows, shale and siltstone. These rocks formed or were deposited in oceanic extensional environments, more specifically in oceanic-ridge environments close to continental margins, in back-arc basins, and possibly in cratonic basins. The type example is the Besshi deposit in southwestern Japan that occurs in the Sambagawa metamorphic terrane (Hutchinson, 1980; Franklin et al. 1981; Cox and Singer, 1986; Höy, 1991).

Besshi-type deposits occur in thick sequences of clastic sedimentary rock and intercalated basalt overlain by dominantly argillaceous rocks. This deposit type consists of thin sheets of massive to well-laminated pyrite, pyrrhotite, chalcopyrite and sphalerite, and other sulfide minerals. Lesser minerals are magnetite, galena, bornite, and tetrahedrite. Gangue minerals are quartz, carbonate minerals, albite, white mica, and chlorite (Obolenskiy et al., 2003). The massive-sulfide layer comprises dominantly massive and banded pyrite and chalcopyrite, with minor sphalerite, magnetite and hematite. The banded ore occurs in the middle of the sulfide layer and consists of pyrite and chalcopyrite interlayered with magnetite-chlorite-quartz schist. Pyrrhotite is present in some of the deeper levels of the Besshi deposit, and cobaltite has been identified locally (Höy, 1991).

Wall rocks exhibit hydrothermal alteration and (or) chemical sedimentation that is coeval with deposition of massive-sulfide minerals. A footwall alteration zone, similar to those recognized in other copper-zinc deposits and lead-zinc-copper deposits, has not been recognized. Many Besshi-type deposits have variably developed silica-chlorite alteration zones (Obolenskiy et al., 2003).

2.3.2.2 Kuroko Type

Kuroko-type deposits, taking their name from the Miocene deposits of the Green Tuff belt of Japan, typically occur in association with arc-related felsic volcanics, specifically with subaquaeous, dacitic/rhyolitic lava domes and volcaniclastics. As Kuroko-type deposits commonly contain lead and precious metals in addition to copper and zinc, they are also referred to as polymetallic VMS deposits (Horihoshi, 1969; Garson and Mitchell, 1977; Höy, 1991, Taylor et al., 1995).

An idealized Kuroko deposit comprises three main zones: a low-grade stockwork zone with quartz veins, pyrite and chalcopyrite; yellow ore consisting mainly of pyrite and chalcopyrite; and overlying black ore- massive galena, sphalerite and barite with variable amounts of chalcopyrite and pyrite. The massive-sulfide lens may be overlain locally by barite containing minor pyrite, and occasionally by ferruginous chert (Höy, 1991).

Alteration zones in Kuroko deposits are well-developed. The stockwork zone and immediately adjacent deposits are characterized by magnesium chlorite-sericite alteration and, locally, silicification. Less intense sericite, sericite-montmorillonite and chlorite alteration surrounds the stockwork zone and may extend several hundred meters into the hanging wall. Locally, albite and potassium-feldspar occurs within this alteration zone. Clay alteration, dominantly montmorillonite, extends well beyond the limits of the immediate deposit alteration and grades laterally into regional zeolite-facies metamorphism characteristic of the Green Tuff beds. The deposit alteration patterns reflect strong magnesium metasomatism and, in the deposit footwall, silica and potassic metasomatism (Höy, 1991).

2.3.2.3 Cyprus Type

Cyprus-type deposits ideally occur in submarine, predominantly mafic tholeiitic or calc-alkaline volcanic sequences that occur in ophiolite sequences or greenstone belts. Dominant minerals are mainly pyrite, chalcopyrite, sphalerite, and lesser marcasite and pyrrhotite. Sulfide minerals occur in pillow basalt that is associated

with tectonized dunite, harzburgite, gabbro, sheeted diabase dikes, and fine-grained sedimentary rocks that form part or all of an ophiolite assemblage (Obolenskiy et al., 2003).

These deposits generally consist of a lens of massive sulfides underlain by a well-developed pipe-shaped stockwork zone. The massive sulfide lens consists of fine-grained pyrite and chalcopyrite, with accessory marcasite, sphalerite and galena. The top of the lens may be altered to a goethitic material, interpreted to be caused by submarine oxidation and indicative of formation on the sea floor (Constantinou and Govett, 1972). The massive-sulfide lens is usually overlain by unmineralized deep-water sediments or by pillow lavas (Höy, 1991).

Stockwork zones beneath Cyprus deposits consist of strongly altered and mineralized basalt. Stockwork zones comprise pyrite, pyrrhotite, minor chalcopyrite, and sphalerite. Mineralization occurs disseminated or as quartz-chlorite veins and veinlets with chalcopyrite and pyrite. Sulfide minerals are locally brecciated and recemented. Alteration in the stringer zone consists of abundant quartz, chalcedony, chlorite, and lesser illite and calcite. Some deposits are overlain by Fe-rich and Mn-poor ochre. In many deposits, the stockwork mineralization is ore; other stockworks quite small or are dominantly pyritic (Höy, 1991).

2.4 Massive Sulfides and Ophiolites

It is suggested that many cupriferous massive-sulfide deposits associated with ophiolite complexes are generated in ocean basins at sites of sea-floor spreading. In a complete ophiolitic sequence, the massive-sulfide deposits are related to tholeiitic basalts, which constitute layer 2 of the oceanic crust, and is underlain by coeval dolerite dike swarms and gabbro complexes (layer 3), which in turn overlie ultrabasic rocks or their serpentinized equivalents (upper mantle).

Subsequent to their formation, ophiolites and associated massive-sulfide deposits, as components of oceanic lithosphere, are transported away from ocean rises by means of sea-floor spreading.

When they reach the margins of ocean basins, massive-sulfide deposits are underthrust (along subduction zones) beneath continental margins and island arcs. During subduction, relatively small slabs of oceanic lithosphere may be tectonically emplaced behind or beneath trenches, giving rise to ophiolites, which are subsequently exposed, sometimes as components of mélanges (as in the case of the Karaali mineralization) (Hsü, 1971). In the meantime, some of the deposits are incorporated mechanically into the continental crust as parts of slices of oceanic lithosphere (Coleman, 1971; Dewey and Bird, 1971; Sillitoe, 1972)

Massive-sulfide bodies are situated within the pillow-lava sections of many ophiolites. These sulfide bodies have certain common features, such as, a tendency to be stratabound and to occupy stratigraphic horizons within the volcanic section. The surrounding volcanic rocks have typically been affected by ocean-floor hydrothermal metamorphism and the massive sulfides are found in those rocks that have undergone zeolite- or greenschist-facies metamorphism, under steep thermal gradients (Coleman, 1977). Nearly all of these deposits have well-developed gossans consisting of bright-colored iron oxides, hydroxides, and sulfates which attracted the ancient miners. Remnants of ancient slag heaps are present in many of these massive sulfide mining districts –including the Karaali area- particularly in Cyprus and Oman, and radiocarbon dating of charcoal indicates some of this ancient mining activity extends back to 2500 B.C. (Coleman, 1977).

Table 2-1. VMS deposit types (modified from Evans, 1993).

Type	Volcanic Rocks	Clastic Sedimentary Rocks	Tectonic Environment			Known Age Range
			Depositional Environment	General Conditions	Plate Tectonic Setting	
Kuroko Pb-Zn-Cu:Ag:Au	bimodal suites, tholeiitic basalts, calc-alkaline lavas and pyroclastics	shallow- to medium-depth clastics, few carbonates	explosive volcanism, shallow marine to continental sedimentation	rifting and regional subsidence, caldera formation	ebck-arc rifting	Early Proterozoic Phanerozoic
Cyprus Cu:(Zn):Au	ophiolitic suites Tholeiitic basalts	minor or lacking	deep marine with tholeiitic volcanism	tensional, minor subsidence	oceanic rifting at accreting margin	Phanerozoic
Besshi Cu-Zn:Au	within-plate basalts	continent-derived graywackes and other turbidites	deep marine sedimentation with basaltic volcanism	rifting	epicontinental or back-arc	Early Proterozoic Palaeozoic

CHAPTER 3

REGIONAL GEOLOGY

Turkey is located at the boundary between two megacontinents: Gondwana to the south and Laurasia to the north (Göncüoğlu et al., 1996). During its paleotectonic evolution, the dynamics of these megacontinents played a key role for the development of the major geological features of Turkey. The relative movements of these two resulted in the activation of rift systems forming new oceans and their subsequent closures as a result of collision. The consequences of these processes are the wide distribution of subduction-accretion complexes and ophiolites all across the country, which are consistent with the existence of two Tethyan oceans, Paleotethys and Neo-Tethys, in terms of age and distribution (e.g., Bozkurt and Mittwede, 2001).

Mainly beginning with the work of Şengör and Yılmaz (1981), the Tethyan evolution of Turkey has been a controversial subject for over two decades, and during that period many researchers have contributed to the issue. However, still there is no agreement on the paleogeographic locations and the times of opening and closure of these two oceans. Nevertheless, it is generally accepted that Paleotethys was a Paleozoic-Early Mesozoic ocean, whereas Neo-Tethys was a Mesozoic-Early Tertiary ocean, and that both closed diachronously.

In northern Anatolia the products of Neo-Tethys are represented by continental fragments that are separated by ophiolitic suture belts. From north to south, the order of tectonic zones are Pontide continental fragments, Intra-Pontide suture, Sakarya continent, İzmir-Ankara-Erzincan suture and Central Anatolian Crystalline Complex. The continental fragments have been amalgamated consecutively with the Pan-African, Hercynian and Cimmeride orogenies, and acted as continental

basement during Neo-Tethyan evolution (Tüysüz, 1993). Opening by Early Jurassic rifting of these continental fragments, two new oceans developed, namely the Intra-Pontide Ocean in the north and the İzmir-Ankara-Erzincan Ocean to the south. In the beginning of the Late Cretaceous, the Intra-Pontide Ocean began subducting beneath the Pontide fragment, whereas the İzmir-Ankara-Erzincan Ocean under the Sakarya Continent (Figure 3.1). With the closure of the oceans in the Late Cretaceous, ophiolite obduction and continental collision occurred (Tüysüz, 1993).

The İzmir-Ankara-Erzincan suture is one of the major sutures in Turkey and marks the late Paleozoic-Early Tertiary Tethys Ocean between Laurasia and Gondwana. The İzmir-Ankara-Erzincan suture extends from north of İzmir, eastward to the border with Georgia, whence it continues as the Sevan-Akera suture in the Lesser Caucasus. To the west, the İzmir-Ankara-Erzincan suture probably connects across the Aegean Sea to the Vardar suture. It separates the Sakarya Zone, which constitutes part of the Rhodope-Pontide continental fragment, to the north from the Central Anatolian Crystalline Complex and the various units of the Anatolide-Tauride Block to the south. The İzmir-Ankara-Erzincan suture is represented by offscraped oceanic-crustal material, volcanic seamounts, and trench-fill accretionary prism assemblages that were imbricated with south-vergent faults as a result of the northward-dipping subduction of Neo-Tethys (Şengör and Yılmaz, 1981; Okay and Tüysüz, 1999).

During the northward-dipping subduction of Neo-Tethyan oceanic lithosphere underneath the Sakarya block in the Cretaceous, much of the Neo-Tethyan oceanic crust, volcanic seamounts, and trench fill-accretionary prism assemblages were offscraped and imbricated, yielding many south-vergent thrust faults. Finally, the Sakarya and Kırşehir continental blocks collided at the end of Cretaceous leaving ophiolite-dominated suture zones behind (Şengör and Yılmaz, 1981).

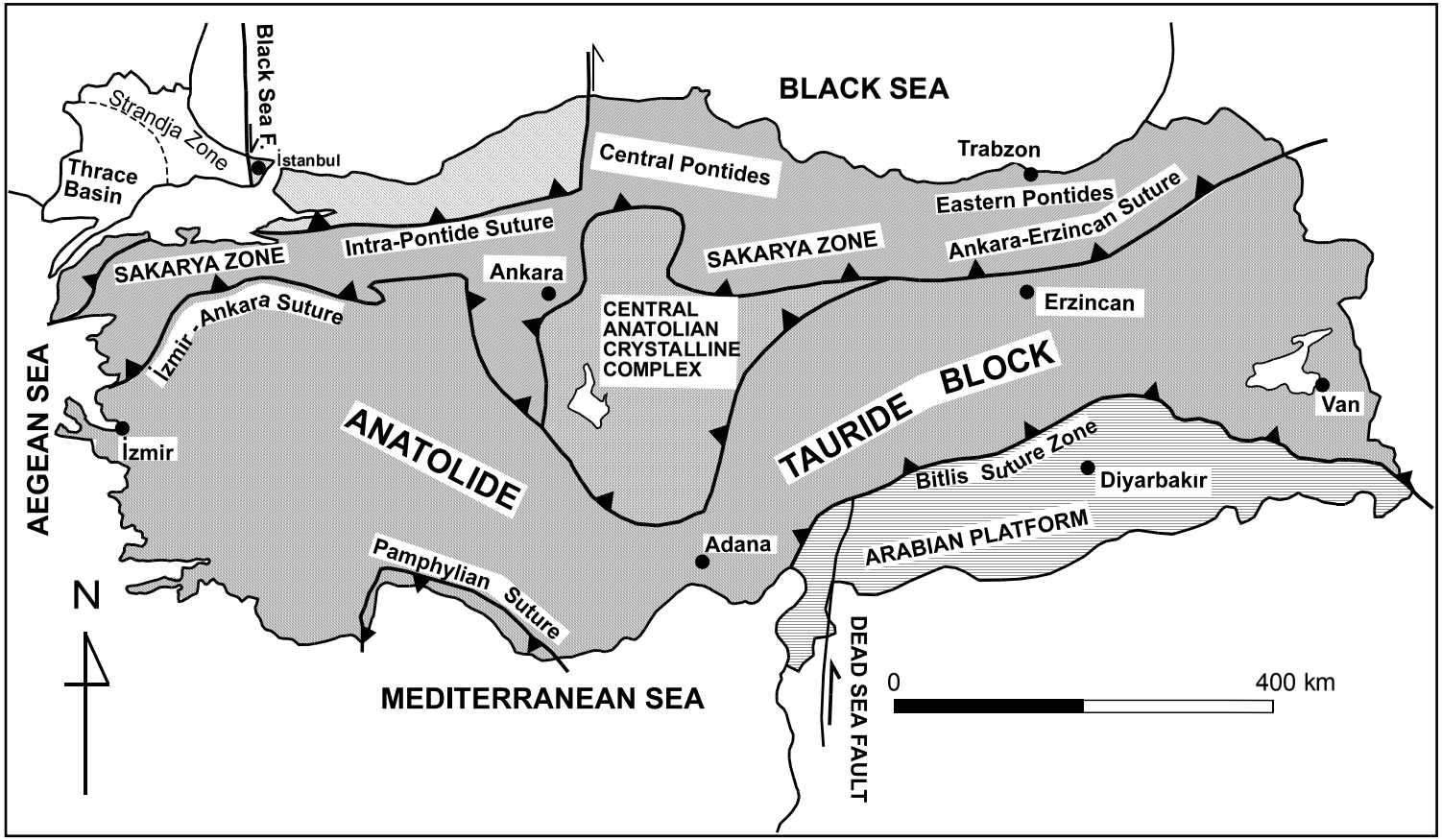

Figure 3-1. Schematic tectonic map of Turkey (modified from Okay and Tüysüz, 1999).

Located on the İzmir-Ankara-Erzincan suture, the geological mosaic of the Ankara region is a reflection of the geological events that occurred during the aforementioned opening and closure of Neo-Tethys.

The geology of the Ankara region displays a wide spectrum of sedimentary, igneous and metamorphic rocks. In earlier studies, such as Bailey and McCallien (1950 and 1953), Boccaletti et al. (1966), Akyürek (1981), Ünalan (1981) and Norman (1984), the main geological units of Ankara region were included in the "Ankara Mélange" term. Subsequently, with more detailed studies, some of these units were excluded from the presumed mélange units. The comprehensive work of Norman (1984) defined many units as parts of the Ankara Mélange and divided the mélange into three subunits. From northwest to southeast, and structurally downsection, these subdivisions are: (1) metamorphic-block mélange; (2) limestone-block mélange; and (3) ophiolitic mélange. Nonetheless, divergent hypotheses emerged soon after. Contrary to the interpretation of Norman (1984), several studies have singled out the Triassic sedimentary and metamorphic units and studied them separately (e.g., Görür et al., 1984; Koçyiğit, 1987 and 1991; Okay and Tüysüz, 1999; Rojay et al., 2001 and 2004).

In the Ankara region, the basement is characterized by a metamorphic sequence of metabasite-phyllite-calc-schist, with mafic to ultramafic lenses metamorphosed in the greenschist facies. The metamorphic assemblage corresponds to the Upper Karakaya Nappe of Koçyiğit (1987). The metamorphic sequence is tectonically overlain by a chaotically deformed Late Triassic series of graywacke, siltstone, basalt and exotic blocks of Carboniferous and Permian neritic limestone. This assemblage is the equivalent of the Lower Karakaya Nappe of Koçyiğit (1987). Contrary to Koçyiğit (1987), in the studies of Akyürek et al. (1984) and Tüysüz et al. (1995), there is no discrimination between the metamorphic sequence and the deformed assemblage. In Akyürek et al. (1984), these are altogether termed the Ankara Group, whereas Tüysüz et al. (1995) named them the Karakaya Unit (Figure 3.2).

Following a marked unconformity, the deformed Triassic assemblage is covered by less-deformed Liassic conglomerate, sandstone and siltstone with ammonitico rosso horizons. Overlying these are the hemipelagic limestones of Late Jurassic-Aptian age, which are preserved locally as small erosional outliers in the region. This clastic group of rocks corresponds to Ankara Group of Koçyiğit (1987) and the Sakarya Unit of Tüysüz et al. (1995). Alternatively, Akyürek et al. (1984) preferred to deal with these units separately, and named the clastic sequence the Hasanoğlan Formation and the carbonates as Akbayır Formation.

With a general approach, Okay and Tüysüz (1999) termed these units the "Sakarya sequence". The Sakarya sequence has been thrust eastward over the Cretaceous subduction-accretion units (Anatolian Complex of Koçyiğit, 1987). This complex is dominated by ophiolitic units derived from the İzmir-Ankara-Erzincan branch of northern Neo-Tethys. The subduction-accretion complex forms a tectonic belt of 5-10-km wide which encircles and radially thrusts the Eocene-Miocene sedimentary rocks of the Çankırı basin forming a large loop (Okay and Tüysüz, 1999). This belt is characterized by a chaotic tectonic mixture of various blocks of different ages, origin, and facies set in an intensely sheared and fine-grained matrix composed mainly of ophiolitic sandstone, shale, pelagic mudstone of Early Campanian age (Koçyiğit, 1991). The ophiolitic belt corresponds to the Anatolian Complex of Koçyiğit (1987) and the Kalecik Unit of Tüysüz et al. (1995).

The Cretaceous subduction-accretion complex can be divided into two distinct thrust sheets: the upper and lower nappes (Tüysüz et al., 1995). The upper nappe is composed of an ophiolitic mélange of ordered slices, whereas the lower nappe is mainly a volcanic assemblage of a Late Cretaceous magmatic belt.

The upper nappe consists of an ophiolitic mélange for which Rojay et al. (2001) informally used the term "North Anatolian Ophiolitic Mélange". This mélange comprises various sized (a few meters to few kilometers) blocks and imbricated tectonic slices of ophiolitic rocks, including serpentinites, gabbros, diabases, pillowed spilites and, epi-ophiolitic sediments, such as pelagic limestones, cherts, pelagic mudstones and flysch-type clastics, including debris flows and continent-

derived blocks. In addition to these lithologies, some continent-derived blocks, such as Upper Jurassic-Lower Cretaceous neritic limestones, metapelitic and metabasic rocks, are also present within the pelagic sediments of the mélange. The lowermost part of the mélange is dominated by oceanic materials, such as ophiolitic and epi-ophiolitic rocks, while the upper part includes continent-derived material (e.g., Rojay et al., 2001 and 2004).

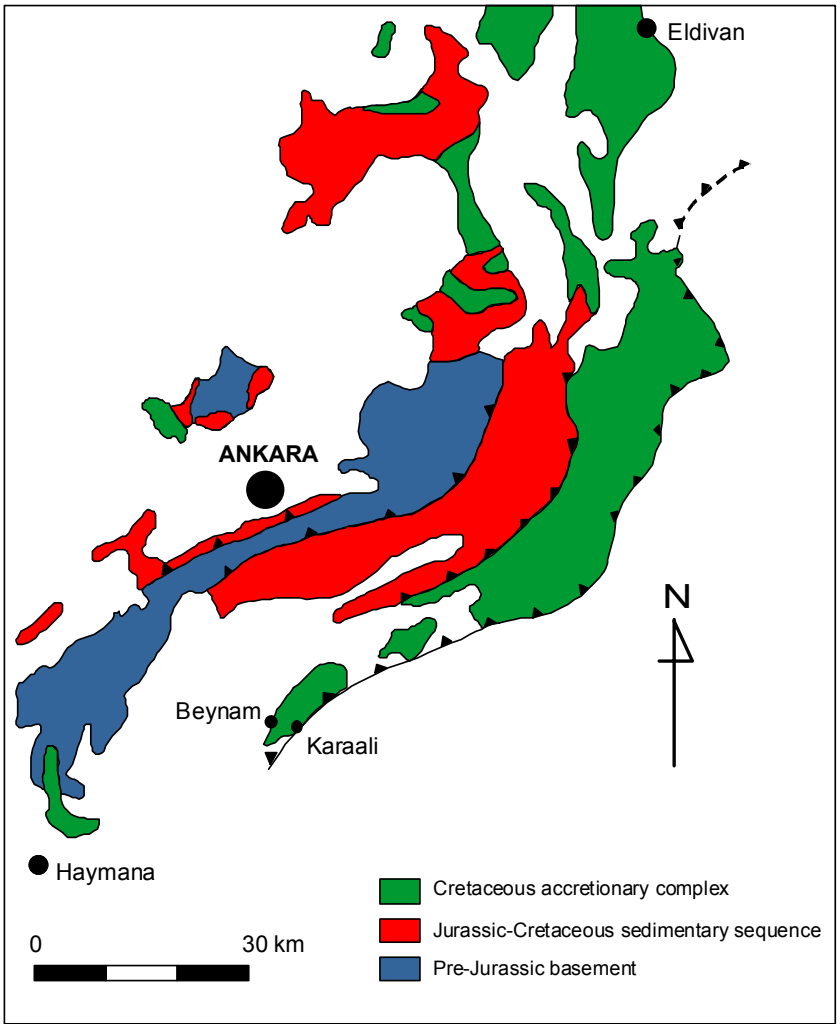

Figure 3-2. Simplified geological map of the Ankara region (modified from Koçyiğit, 1987).

The lower nappe consists of a volcanic and sedimentary association. Structurally, the lower nappe is seen as a tectonic slice between the ophiolitic mélange above, and Upper Paleocene-Oligocene sedimentary rocks of the Çankırı basin at the base. The lower nappe comprises two parts with a more-ordered stratigraphy: a lower part, consisting of volcanics, volcanoclastics, pelagic sediments and ophiolites, and an upper part, consisting of a thick regressive sequence of sandstone, siltstone and shale. The age interval of the lower nappe is Cenomanian to Maastrichtian (Tüysüz et al., 1995; Okay and Tüysüz, 1999).

CHAPTER 4

GEOLOGY OF THE STUDY AREA

4.1 Introduction

The major rock units exposed in the area between Karaali and Beynam villages can be grouped into two: as 1) Jurassic-Cretaceous ocean crustal material; and 2) as the underlying sedimentary sequence, which is also Jurassic-Cretaceous in age (Figures 4.1 and 4.2). These units, overall, are situated within the North Anatolian Ophiolitic Mélange belt (Rojay et al., 2001 and 2004) and belong to the upper nappe of Tüysüz et al. (1995), which is characterized by blocks and tectonic slices of ophiolitic rocks and epi-ophiolitic sediments.

More specifically the map area consists of an ophiolitic megablock which presumably represents a dismembered, tectonically imbricated (partial) ophiolite complex. This megablock is composed of tectonic slivers of highly spilitized pillow and massive basaltic flows, serpentinized peridotite, pelagic limestone, radiolarian chert, gabbro and, to a lesser extent, cross-cutting diabase dikes, from bottom to top. Although they are strongly deformed, these lithologies display an internal pseudostratigraphic order. The imbricate slices laterally extend from northeast to southwest with thicknesses varying from a few meters to one kilometer. Along the thrust zones between different lithologies, meter-thick brecciated zones and hematite-coated, slickensided contacts were observed. This allochthonous ophiolite block covers almost two-thirds (approximately 12 km^2) of the study area and overthrusts a Jurassic-Late Cretaceous sedimentary sequence of bedded clastics and isolated limestone blocks (Figures 4.3 and 4.4).

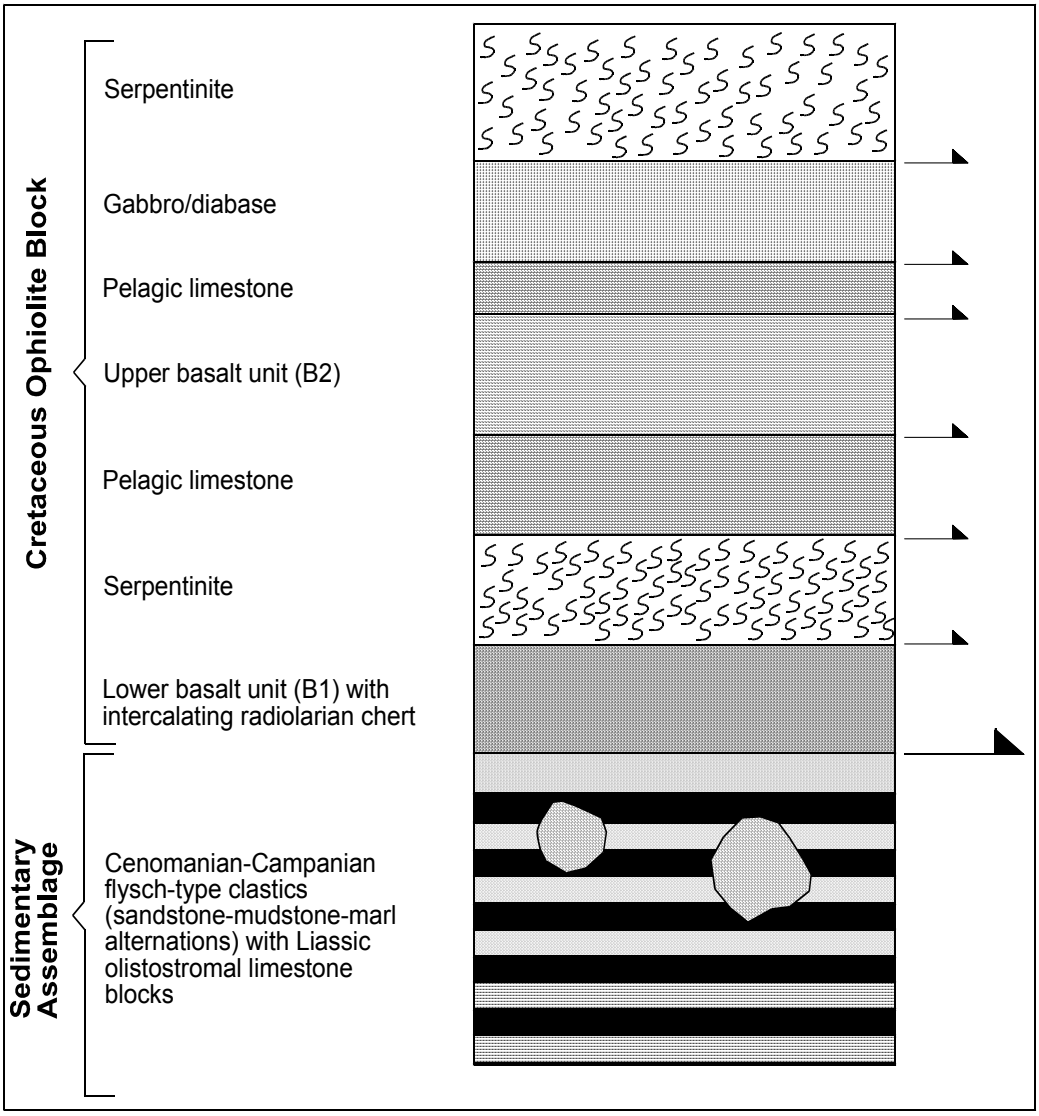

Figure 4-1. Tectonostratigraphic columnar section of the study area (not to scale).

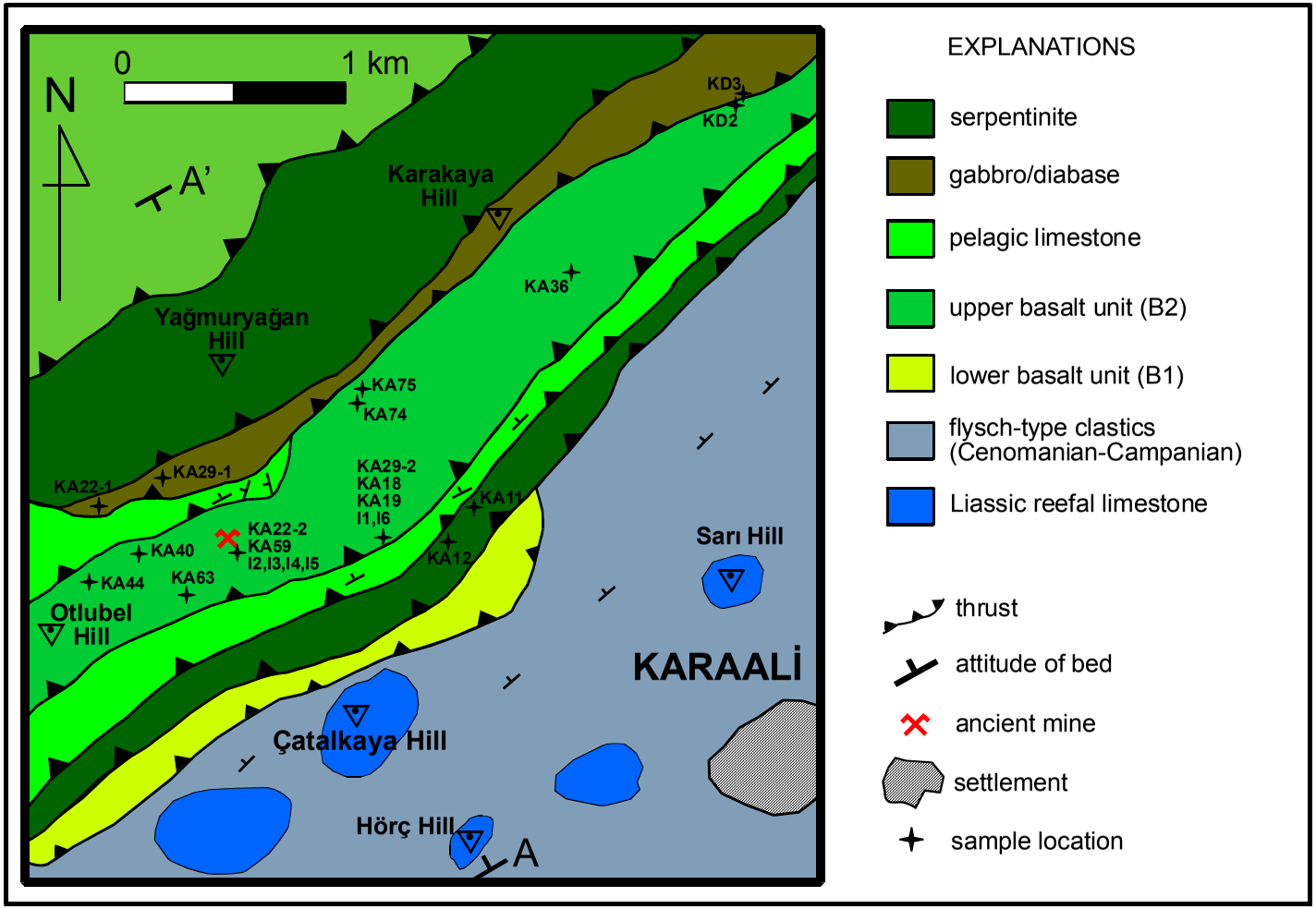

Figure 4-2. Geological map of the study area showing sample locations.

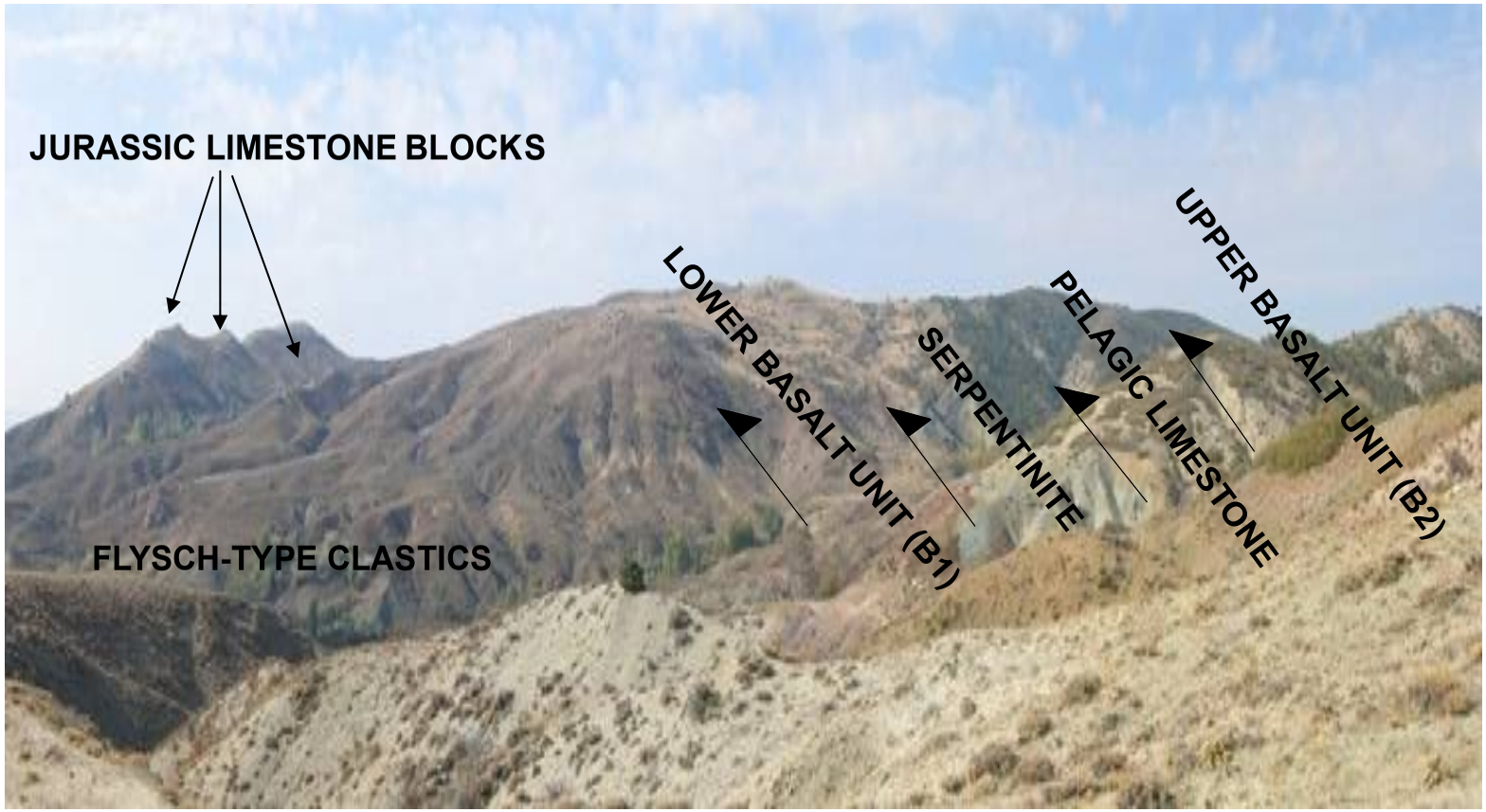

Figure 4-3. General view of the study area from Sarı Hill.

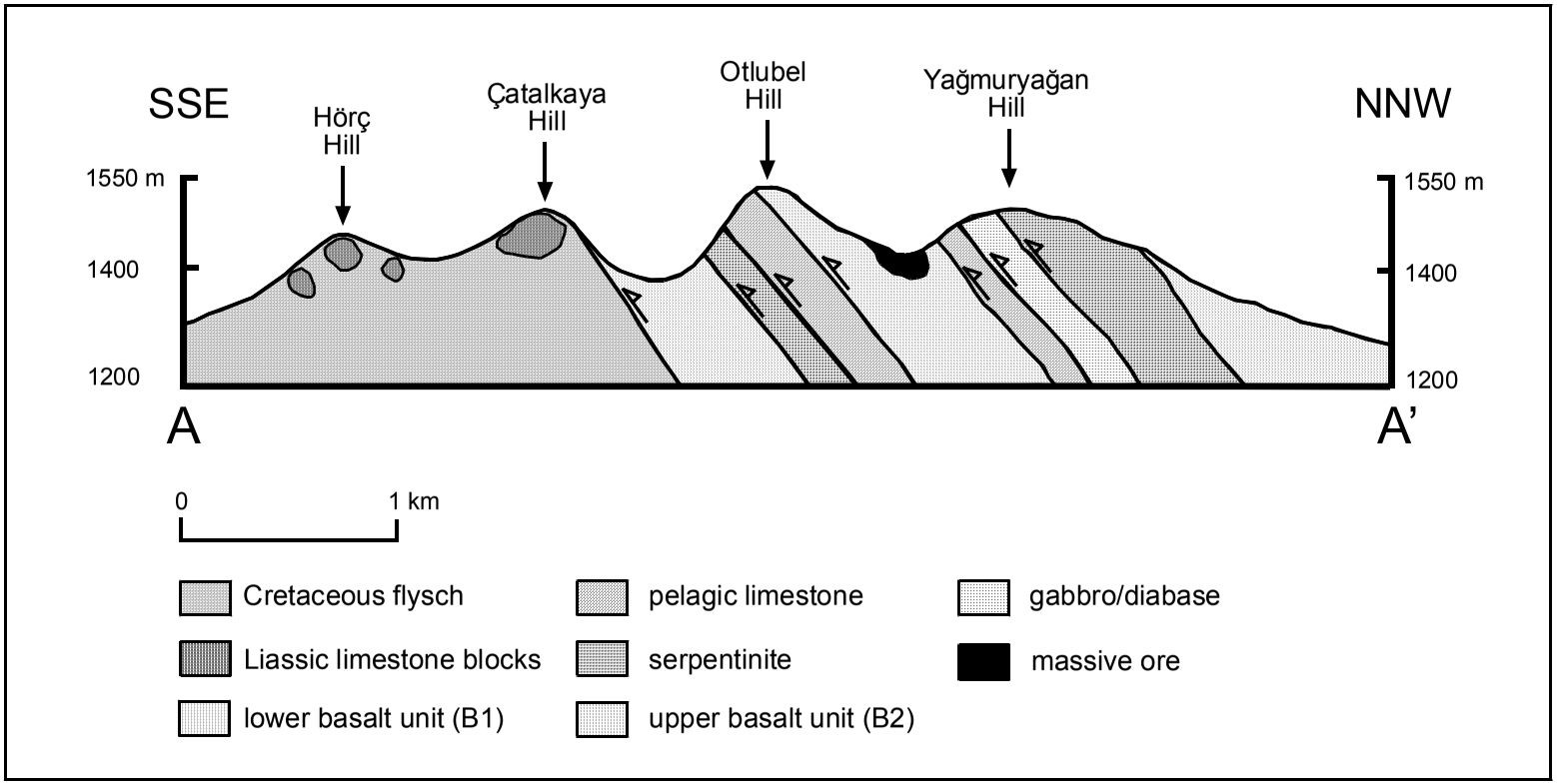

Figure 4-4. Cross-section of the study area.

The emplacement mechanism for these ophiolitic rocks was debris flows and gravity slides, as indicated by numerous previous studies (i.e., Gannser, 1959; Sestini, 1971; Norman, 1984; and Tüysüz et al., 1995).

4.2 Rock Units

4.2.1 Ophiolite Units

The allochthonous ophiolite units in the Karaali area are the focal point of this study. These ophiolitic rocks include serpentinites, pelagic limestones, radiolarian cherts, gabbros with diabase dikes, and pillowed spilites; and all of these lithologies were observed to be related via imbrication. The ophiolite units are not stratigraphically related, yet they display a pseudostratigraphic relation as if there were a specific order to these units from bottom to top.

4.2.1.1 Basalts

Basaltic volcanic rocks are widely exposed in the study area and are the most dominant lithology. Basaltic extrusives are present mostly as spilitized pillow lavas interbedded with massive lava flows. Two different units of spilitized basalts were distinguished in the map area. In the first assemblage, highly spilitized, massive to pillowed basalts are found in association with thin intercalations of radiolarian chert. These lithologies comprise the lowermost tectonic slice of the ophiolite block, and are termed the “lower basalt unit (B1)”. The other basaltic assemblage is more widespread in the study area, appears to occur in association with gabbro and diabase, thrusts over pelagic limestones, and lies structurally higher than the first basaltic assemblage. Consequently, the latter unit will be discussed under the name “upper basalt unit (B2)”. In this second assemblage, the basaltic volcanics also host the massive-sulfide mineralization and, thus indications of hydrothermal alteration are much more evident in outcrops of the upper basalt unit (B2).

4.2.1.1.1 Lower Basalt Unit (B1)

The lower basalt unit forms the lowest tectonic sliver of the ophiolite block in the map area, and is only exposed in a small area down the northeastern foothill of Çatalkaya Hill where it occurs as dark green to black outcrops typically associated with thin (10 to 20 cm), red radiolarian cherts (Figure 4.5). The lower basalt unit consists of massive to pillowed lava flows and is weakly to non-amygdaloidal. Pillows are largely obliterated; however, in a few outcrops well-preserved carbonate material (0.5 to 1 cm thick) around the margins of pillow lobes were identified. Albitization is common in these outcrops, represented by white phenocrysts of feldspar, which range in size from 2 to 4 mm. It is locally folded with the enclosing strata of radiolarian cherts. As the lowermost portion of the ophiolite megablock the lower basalt unit tectonically overlies the sedimentary sequence on the north side of Çatalkaya Hill, and is overthrusted by serpentinites. The same unit was also observed in the northernmost part of the study area as another tectonic slice.

4.2.1.1.2 Upper Basalt Unit (B2)

The upper basalt unit comprises the uppermost tectonic slice of the ophiolite block together with the gabbros and diabase dikes. It overthrusts pelagic limestones and tectonically underlies gabbros.

The upper basalt unit consists of massive to pillowed basalt flows, is intensely altered, and typically green in color due to widespread chloritization. Primary textures are obliterated by alteration. Aphyric basalts show typical amygdaloidal textures. The amygdules are typically filled with calcite. These rocks are albite-rich and, in the least altered samples, large crystals of pyroxene can easily be observed with the naked eye.

Figure 4-5. Strongly spilitized massive basalt with thin intercalations of radiolarian chert on the north side of Çatalkaya Hill.

In a few outcrops, the outer surface of the basalts are covered with thin gypsum coatings. In the vicinity of the ore body, basaltic outcrops are intensely deformed are masked by dense vegetation. In those outcrops, pillow structures are barely preserved. The pillows are well-formed, ellipsoidal to spherical, with diameters ranging from 20 to 50 cm (Figure 4.6). Pillows are enveloped by 0.5-2 cm thick outer rims which are intensely altered due to hydrothermal processes. In contrast, to the pillows of the lower basaltic unit, there is no carbonate infilling material in between the lobes.

The upper basalt unit hosts the massive sulfide mineralization and -around the periphery of the orebody- as a consequence of wall rock alteration, these rocks are physically and chemically transformed into alteration/weathering products such as iron-oxide-rich gossanous material. Apart from chloritization, argillic alteration is also observed in the basaltic volcanic rocks, especially around the sulfide-mineralized quartz veins.

4.2.1.2 Serpentinite

Serpentinite tectonically overlies the lower basalt unit (B2), is widely exposed in the belt that extends from 1 km north of Karaali village towards the southwest, and is best observed 300 m north of Çatalkaya Hill, in the downstream part of Karaboyalık Stream. There, it is underlain by the lower basalt unit and overthrusted by pelagic limestones.

Figure 4-6. Pillow basalts of the upper basalt unit (B2), with intensely chloritized outer rims.

The serpentinites are typically green to dark green with a greasy appearance, and show tectonic fabrics which reflect the plastic deformation they have undergone. Most of the primary mineralogical and textural features of the predecessor peridotites have been obliterated. Locally, granular and porphyritic textures are distinguishable in hand specimen. The serpentinites of the area are quite brittle and highly fractured. Locally, they contain thin chrysotile veins and chromite. The

serpentinites mainly comprise serpentine minerals displaying typical mesh textures. Other than serpentinite minerals, bastite -which is a ferriferous variety of enstatite- has also detected in hand specimen, with its characteristic bronze-like sub-metallic luster on cleavage surfaces. The crystal size of bastite reaches up to 3 cm. At the sheared contacts with the pelagic limestone, talc formation is locally observed.

4.2.1.3 Pelagic Limestone

Serpentinites are tectonically topped by pelagic limestones along thrust planes, with dip angles between 60°-70°. White to light-gray pelagic limestones are quite fine-grained, almost micritic. They are moderately bedded, with bedding thicknesses varying between 20 and 30 cm. The limestone beds dip towards the northeast with angles of around 30°. However, locally deformed and tilted limestone beds display varying dip angles and directions. Especially at the serpentinite contact, the dip of the limestone beds reaches up to a maximum of 70°, which is conformable to that of the thrust plane (Figure 4.7). Brecciation of the limestones is also observed at this contact (Figure 4.8). Pelagic limestone also occurs as a lens within the upper basalt unit, 200 m northeast of the main massive-sulfide orebody.

Pelagic limestones consist of organism fragments and also include some sparry calcite infillings. According to Tüysüz et al. (1995), the following fossils have been distinguished in the pelagic limestones of this ophiolitic mélange:

Globotruncana lapparenti Brotzen, *Globotruncana group* Lapparenti, *Rosita fornicata (*Plummer), *Globotruncana arca* (Cushman), *Praeglobotruncana* sp., *Rugoglobotruncana* sp.

As indicated by the paleontological data, an age interval of Campanian-Maastrichtian was ascribed by Tüysüz et al. (1995) for the pelagic limestone unit within the ophiolite block.

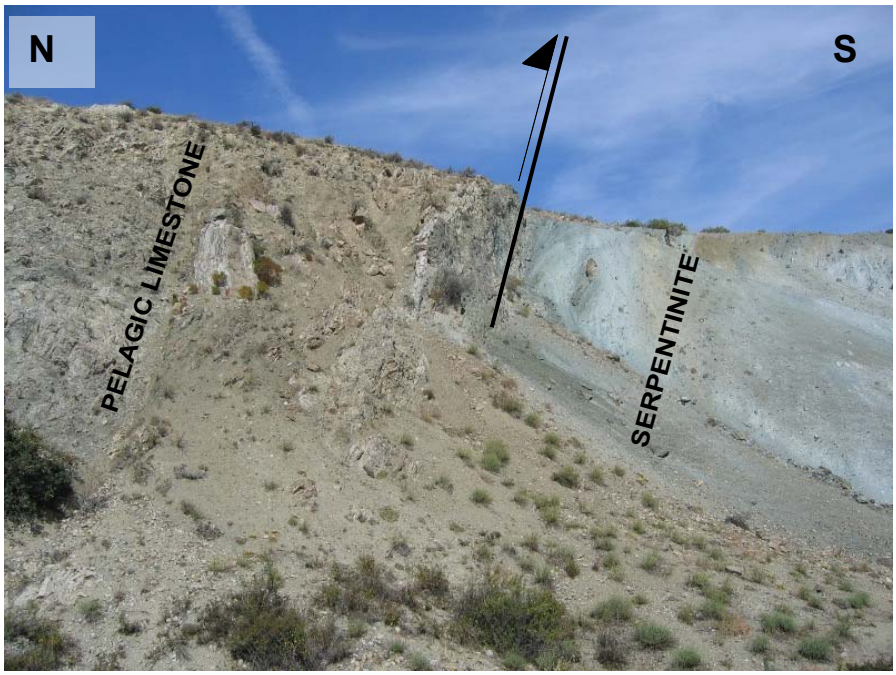

Figure 4-7. Tectonic contact between serpentinite and overlying pelagic limestone in the Elmalı Stream.

Figure 4-8. Brecciated limestone exposure at the tectonic contact between serpentinite and pelagic limestone.

4.2.1.4 Gabbro and Diabase

Above the spilitized pillow basalts, intrusive mafic rocks are exposed. The thickness of this sequence is only around 30 m, and outcrops of the gabbro-diabase unit are scarce. This unit is best observed in Karanlık Stream to the northeast of and to the south of Yağmuryağan Hill. This assemblage thrusts over altered basalts of the upper basalt unit.

This unit comprises gabbros and cross-cutting diabase dikes. The gabbros are dark green, and the crystal sizes of the gabbros vary within the sequence. Both fine- and coarse-grained varieties occur in the study area. Coarse-grained gabbros are most readily distinguished by their large pyroxene crystals. White bands of feldspars were observed locally.

Similar to the basaltic volcanics, the gabbros were significantly influenced by ocean-floor metamorphism. Green color, indicative of chloritic alteration, is common to all of the gabbros. On the other hand, scarce diabase dikes that cut the gabbros are also dark green and are finer-grained than the gabbros.

4.2.2 Sedimentary Sequence

The sedimentary sequence comprises clastic and non-clastic sedimentary units of Jurassic-Cretaceous age. Alternating clastic units display a flysch character and neritic limestone blocks are embedded in this flysch matrix. The sedimentary package is, as a whole, tectonically overlain by the ophiolite megablock.

4.2.2.1 Flysch-type Clastics

The lowermost part of the observed sedimentary sequence is dominated by an assemblage of flysch-type clastics (mainly distal turbidites), including debris-flows and continent-derived blocks. The blocks within this assemblage are argillaceous limestones, which are generally situated on topographic highs.

The flysch-type clastic deposits consist of thick, alternating sandstone-marl assemblages which, up section, gradually pass into alternating sandstone and mudstones. The sandstones are yellowish-brown, poorly-sorted, sub-angular to sub-rounded, and grain-supported; while the mudstones and marls (Figure 4.9) are red and gray, respectively. The sandstones are poorly cemented and non-bedded, whereas the red mudstones are thinly bedded. Within the sequence, dip directions and angles are variable. Especially at the contact with the lower basalt unit, dip direction and angles are consistent with that of the thrust plane. The alternating clastic sediments are tectonically overlain by the lower basalt unit on the north side of Çatalkaya Hill.

The limestone blocks embedded into this unit are yellow. They are massive, mud-supported and consist of clay-sized particles.

Figure 4-9. Gray marl forming the lower horizons of the flysch sequence.

The clastic-sedimentary assemblage corresponds to the Kocatepe Member of Akyürek et al. (1996) and the Irmak Formation of Norman (1972), while the pelagic limestones topping the section correspond to the Günalan Formation of Akyürek et al. (1996). According to Akyürek et al. (1996), the fossil assemblage of these limestones is:

Praeglobotruncana stephani (Gandolfi), *Rotaliopora apenninica* (Renz), *Hedbergella* sp., *Ticinella* sp., *Cuneolina* sp., *Texturlariella* sp., *Valvulammina* sp.

This assemblage of fossils indicates an age interval of Cenomanian-Campanian for the clastic-sedimentary units (Akyürek et al., 1996).

4.2.2.2 Jurassic Limestones

Atop the clastic-dominated assemblage rest olistostromal blocks of massive limestone. Limestone blocks have mainly been identified at Hörç Hill, Çatalkaya Hill and Elgazi Hill, all situated in the southernmost part of the study area. The unit extends towards Günalan village to the southwest. The large limestone blocks (10-100 m) typically are exposed at the highest elevations (Figure 4.10).

The limestones are white to gray, massive and non-bedded, and fractured. The base of the limestones contains erosional features. These rocks are sparitic and contain significant amounts of mollusk, coral and algae fossils. These rocks correspond to the Hörç Limestone Member of Akyürek et al. (1996). According to that study these limestones are Liassic in age, with the observed fossils as follows:

Involutina liassica (Jones), *Aulotortus* gr. *gaschei* (Koehn-Zaninettive Bronimann), *Aulotortus* gr. s*inousus* (Weynschenk), *Maychina* cf. *termieri* Hottinger, *Vidaline* sp., *Trochammina* sp., *Glomospira* sp., *Nauticulina* sp., *Trocholina* sp., *Spirillina* sp., *Frandicularia* sp., *Nadosariidae, Opthalmidiidae, Miliolidae, Doustominiade, Thaumatoporella* sp., *Cayeuxia piae* Frollo.

Figure 4-10. General appearance of a huge Jurassic limestone block at Sarı Hill.

4.3 Karaali Fe-Cu Sulfide Occurrence

4.3.1 Deposit Morphology and Characteristics

As mentioned above, the basic and ultrabasic rocks of the Karaali area represent a dismembered ophiolite, with imbricate slices trending ENE-WSW. These rocks are exposed in a linear belt, as steeply inclined narrow sheets, ranging from a few kilometers to tens of kilometers in length.

Similar to some other ophiolite-associated massive-sulfide deposits of Eastern Mediterranean region (i.e., Troodos and Oman), the abandoned mine in the Beynam Forest seems to have been operated in Byzantine times. According to a C^{14} age determination from charcoal engulfed in fragment of Karaali slag, the history of mining in the region extends back to ~950 yr B.P (W.E. Sharp and S.K. Mittwede, unpublished data). Since then the majority of the ore has apparently been extracted, and only the remnants of the old mine and a slag heap (Figure

4.11) in Karaali village have survived to date. Today, there is no evidence of subsequent mining activities and the mine entrances are totally collapsed.

Figure 4-11. Slag heap in Karaali village.

The massive sulfides are hosted by altered pillow basalts within the ophiolite sequence between Beynam and Karaali villages. Basaltic flow rocks have layering, with alternating pillowed and massive layers. Morphologically, the sulfide ores can be divided into 1) massive-sulfide ores that are present as a concordant lens, and 2) discordant, veinlet-disseminated/vein-type sulfide minerals associated with quartz.

The massive-sulfide lens is located approximately 250 m northeast of Otlubel Hill, in the upstream part of Karaboyalık Stream (Figure 4.12). The massive-sulfide

orebody mainly consists of pyrite and lesser chalcopyrite, with minor bornite, covellite and quartz. This assemblage is restricted to a mound-shaped zone 50-m long and 30-m wide, and bounded by an iron cap on the east. This horizon is characterized by an assemblage of iron oxides that were previously a part of the massive-sulfide orebody. Limonite is the major constituent of this horizon. Additionally, some parts of this assemblage experienced a more advanced style of leaching yielding a totally disintegrated mass of goethite.

Structurally below this zone, quartz veins have intruded along small faults and brecciated zones into the spilitized pillow basalts. These veins are best exposed 500 m east of the main orebody and can be followed over a distance of approximately 100 m. In general, the veins strike parallel to the main fault zone (N80°E) with very steep dips to the south.

Pyrite is the predominant sulfide mineral phase in the veins, with subordinate chalcopyrite. Some minute crystals of sphalerite are observed in a few cases within this zone. Instead of a homogeneous distribution, the sulfide minerals are found disseminated along these veins, and their abundance is significantly lower than that of a typical stockwork zone. Apart from the primary sulfide minerals, patches of malachite are observed locally in these veins, indicating a supergene oxidation event. The mineralized veins have an average thickness of 10 m, with quartz veins at the center and surrounding lavas which are hydrothermally altered into chlorite, sericite and kaolinite. These hydrothermally altered rocks gradually pass into adjacent host rocks that are distinguished by background low-temperature alteration (i.e., albitization, chloritization, epidotization and carbonitization).

In addition, another set of quartz veins is observed along Karanlık Stream which strikes N70°E and dips southward. The length of the major vein is about 500 m. Contrary to the veins in Karaboyalık Stream, the sulfide mineralization is poor in the Karanlık Stream veins.

4.3.2 Structural Control

There is strong evidence that the massive-sulfide mineralization of Karaali is structurally controlled. The structural framework of the study area is spatially associated with a system of northeast-trending shear zones. These shear zones seem to be the dominant, ore-controlling structures. The host rocks adjacent to these zones are intensely sheared and hydrothermally altered (silicified, sericitized, and kaolinitized) (Figure 4.12).

The massive-sulfide mineralization appears to be developed as fault-hosted, steeply dipping vein-like bodies of veinlet-disseminated and vein-type ore mineralization and an overlying massive-sulfide lens. The main sulfide orebody is a northeast trending elongate mound of massive sulfides with abundant pyrite and chalcopyrite. East of this zone, in the downstream part of Karaboyalık Stream, there is a set of quartz veins which are strongly associated with sulfide mineralization. These veins are restricted to a 10-meter thick zone around which there is a zone of marked hydrothermal alteration. In the vicinity of these sulfide-bearing quartz veins, the intensity of alteration is much more evident than in any other section of the study area. These veins are trend N80°E direction and steeply dip towards the northwest, with dips around 70°. The sulfide-mineral assemblage of the quartz veins is similar to that of the main ore body, with predominant pyrite and chalcopyrite. Additionally, sphalerite has been observed in lesser quantities. In addition to these, the sulfide-bearing quartz veins within Karanlık Stream at the northeastern end of the study area have orientations similar to those in Karanlık Stream. Conversely, another group of quartz veins were identified north of the main ore body. These trend N80°W and completely lack sulfide minerals.

Thus, it is clear that the trends of mineralized veins are consistent with the trends of the major faults, whereas the quartz veins trending in different directions are totally devoid of sulfide mineralization. The structural aspects of the deposit clearly demonstrate a structural control on the sulfide mineralization.

Figure 4-12. Late-stage argillic alteration of gossanized basalt outcrop proximal to the sulfide-bearing quartz veins within Karaboyalık Stream.

CHAPTER 5

PETROGRAPHY

5.1 Introduction

The field characteristics of the rock units of the study area were discussed in the previous chapter. This chapter presents the petrographic features of these rock units obtained via detailed microscope studies. As mentioned in the preceding chapters, massive-sulfide mineralization near Karaali is associated with ophiolitic units, more specifically, with altered pillow basalts. Therefore, only the petrographic evaluation of the mafic and ultramafic rocks (basalts, gabbros and serpentinites) adjacent to the mineralized rocks is dealt with in this section.

A total of 62 samples out of the 112 collected rock samples from the study area were investigated under the polarized microscope. Additionally, 15 polished sections were studied under reflected microscope, for the identification of ore minerals and in order to ascertain the textural relationships among these minerals. Thin and polished sections were prepared in the thin-section preparation laboratory in the Geological Engineering Department of Middle East Technical University. Additionally, photomicrographs of polished blocks were taken at the Mineral Research Institute (MTA) of Turkey using a LEICA DMLP transmitted-reflected light polarizing microscope.

The studied rock units will be discussed in terms of their crystallinity, granularity, fabric, mineral assemblages and alteration products. Modal percentages of the minerals are based on visual estimates.

5.2 Basalts

The Karaali basalts are green to dark green, and are most readily distinguished by the large amounts of vesicles and amygdules. Most of the samples are intensely altered as a consequence of hydrothermal processes. The least-altered samples are differentiated from their pervasively altered counterparts by their dark green to black colors. Owing to widespread alteration, primary textural relationships are typically obliterated. The studied samples are hypocrystalline, aphyric to porphyritic with phenocrysts in small quantities and are equigranular in some cases. Phenocrysts are generally 1 to 2 mm in size.

Primary and secondary mineral assemblages were determined via microscopic studies. Primary mineral phases in the basalt samples are calcic-plagioclase and clinopyroxene. Of these, plagioclase feldspar is widespread in the samples whereas clinopyroxene is present in relatively lesser amounts. In most cases, the primary mafic mineral assemblage is strongly overprinted by secondary mineral assemblages. Secondary minerals, such as albite, chlorite, calcite, quartz and epidote, are found in significant amounts along with minor sericite, actinolite and green pleochroic hornblende, which are also of secondary origin. Apart from these, the Karaali basalts consist of accessory titanite, apatite and opaque minerals.

Of these aforementioned minerals, mentioned above, the phenocrysts are clinopyroxene, plagioclase and green pleochroic hornblende, which vary in size between 1 and 2 mm. The groundmass consists of 0.2-0.7-mm crystals of the same minerals, plus quartz and chlorite.

Plagioclase is randomly distributed as euhedral to subhedral microcrysts (less than 1 mm in length) with rare phenocrysts, ranging from 1 to 2 mm in size; it is colorless and found in significant amounts (up to 60 modal percent). Typically plagioclase microliths are albitic in composition. However, in a few samples plagioclase feldspars of An_{50} composition are present. Thus, it is concluded that the plagioclases were originally labradoritic before pervasive albitization of the

basalts (Figure 5.1). Thin albite microliths are the main constituents of the groundmass in the Karaali basalts (Figure 5.2). In some cases, albite phenocrysts are replaced by sericite. Lath-shaped plagioclase microliths are typically subparallel in arrangements, displaying trachytic texture. Less commonly, these lath-shaped microliths in the groundmass exhibit variolitic texture with divergent, fan-like arrangements. The interstices between these microcrysts are mainly occupied by groundmass material or secondary minerals, especially quartz, calcite and chlorite. Despite intense alteration, albite and polysynthetic twinnings are preserved locally. A brown cloudy appearance, in plagioclase crystals –a consequence of kaolinization- was observed under plane polarized light. Also, plagioclase crystals have been, in many cases, replaced by calcite and, locally, by sericite. However, albitization can be regarded as the most prominent type of alteration in plagioclases. Accordingly, the basalts can be regarded as “spilitic” basalts.

Clinopyroxene is typically present as microcrysts, occurring intergranularly to the plagioclase microliths, yet seldom-preserved clinopyroxene phenocrysts were also observed in many samples (Figures 5.3 and 5.4). However, the majority of these phenocrysts are deformed, and occur as medium-grained, subhedral to anhedral, colorless to pale-green crystals. Where unbroken/undeformed, the size of the phenocrysts reaches 2 mm. The abundance of clinopyroxene phenocrysts was determined approximately as approximately 5 modal percent. On the basis of its optical characteristics, clinopyroxene in the basalt samples is augite. Along their cleavage planes the clinopyroxenes are partially or completely uralitized, and in the later stages are typically transformed into actinolite, chlorite and epidote. In some cases, patches of green, pleochroic hornblende developed along the margins of clinopyroxene crystals.

Chlorite is generally the most abundant alteration mineral in the basalt samples. It occurs mainly in the groundmass but in places replaces clinopyroxene, and elsewhere occurs in amygdules, typically associated with epidote, calcite and quartz.

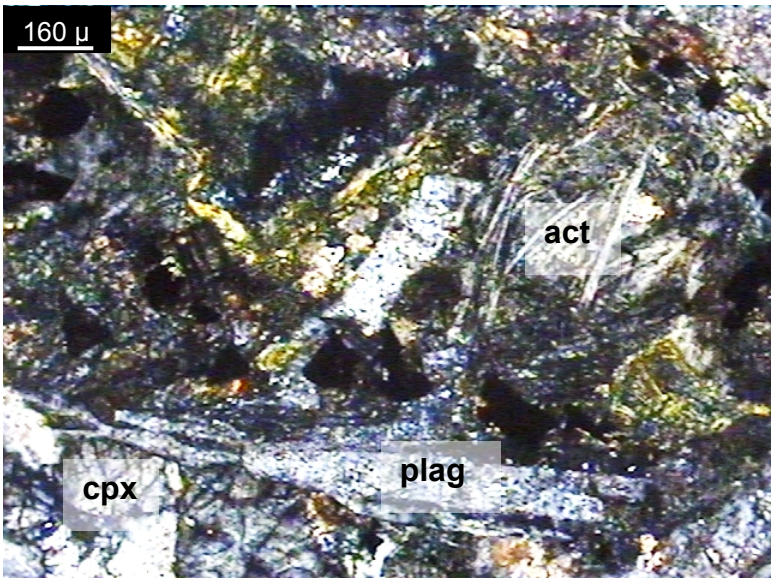

Figure 5-1. Photomicrograph of altered basalt showing the general appearance with seldom preserved labradoritic plagioclase (plag) laths surrounded by clinopyroxene (cpx) and secondary mineral assemblages, consisting mainly of chlorite (green) and thin fibers of actinolite (act) (Sample KA22-1, x10, XPL).

Figure 5-2. Photomicrograph of basalt showing the general appearance of intense spilitization with randomly distributed, unoriented plagioclase microliths in the groundmass associated with altered mafic minerals (Sample KA93, x4, XPL).

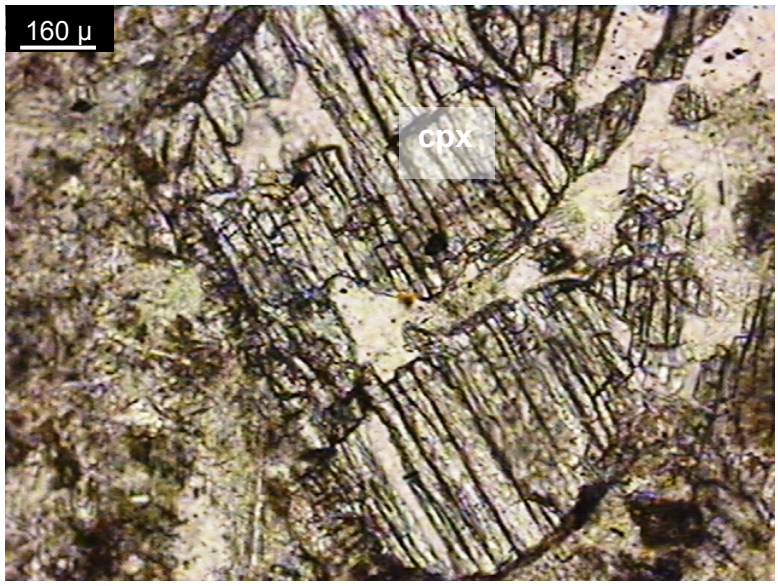

Figure 5-3. Photomicrograph of basalt showing a clinopyroxene (cpx) phenocryst with epidotized outer rim embedded in chlorite-rich groundmass material (Sample KA75, x10, PPL).

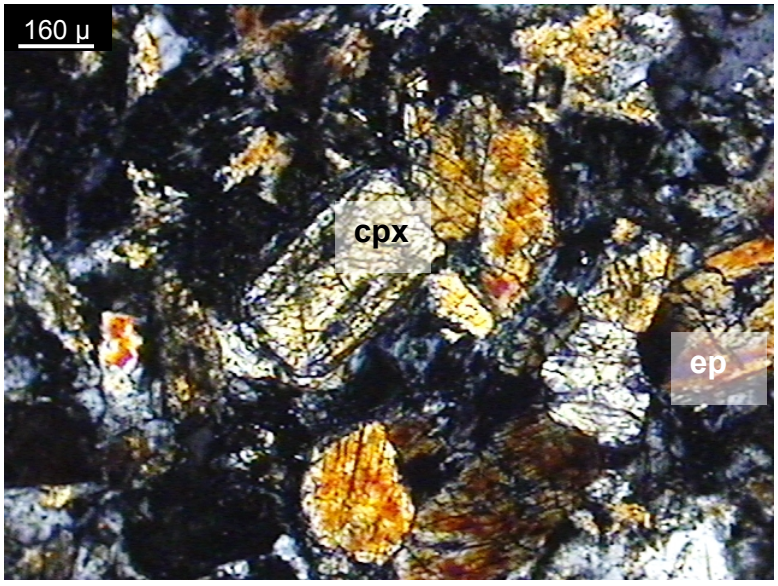

Figure 5-4. Photomicrograph of basalt showing replacement of anhedral to euhedral clinopyroxene (cpx) phenocrysts with epidote (ep) (Sample KA75, x10, XPL).

The chlorite is generally yellowish green or pale green and somewhat pleochroic. Chlorites in some of sections exhibit strong Berlin-blue interference colors. This characteristic property implies that they are probably penninite. Crystal sizes of the chlorite varies on the basis of the mineral that chlorite has replaced.

Around the peripheries of amygdules, thin rims of chlorite surround the infilling material (calcite or quartz), indicating that chlorite is replaced by either calcite or quartz in the later stages of hydrothermal alteration.

Colorless to pale-green epidote appears in thin sections as subhedral to anhedral, small to large grains (Figure 5.5). Fine-grained epidote crystals are either randomly distributed throughout the sections or are found in aggregates displaying a characteristic glomeroporphyritic texture. A green variety of epidote is observed within the amygdules in association with quartz and/or calcite (Figure 5.6). Unlike the fine-grained epidote crystals, this type of epidote is significantly larger in crystal size and has a sheaf-like appearance with very high birefringence. Looking at the intergranular relationship of crystals in amygdules, it can be stated that epidote is replaced partially by calcite, which would later be replaced by quartz.

Quartz is another randomly distributed secondary-mineral phase in the basalts. It is colorless and anhedral in thin sections. In general, there are two types of quartz occurrences. Coarse-grained quartz crystals are widely distributed in amygdules, these are usually found in association with calcite and epidote, and observed as the material replacing coarse calcite crystals within the amygdules (Figure 5.7). Fine-grained quartz crystals are generally distributed throughout the groundmass and also occur in some veinlets (Figure 5.8). Secondary quartz occupies the interstices between plagioclase grains and, locally, partially replaces them. Some of the quartz crystals show undulose extinction.

As with quartz crystals, calcite crystals are secondary in origin and make up a significant proportion of the sections. Colorless calcite crystals can easily be distinguished by their typical perfect cleavage and extreme birefringence.

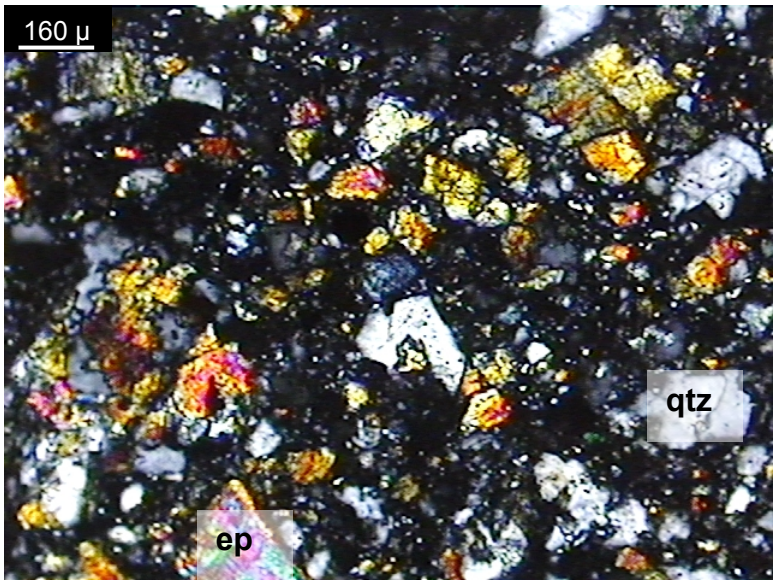

Figure 5-5. Photomicrograph of a basalt sample showing complete alteration of primary mineral phases to quartz (qtz) and epidote (ep) (Sample KA36, x10, XPL).

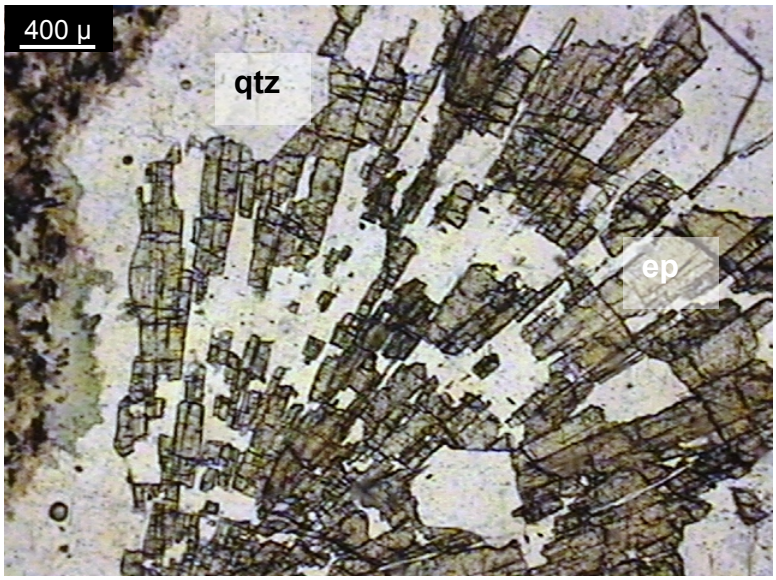

Figure 5-6. Photomicrograph of an amydaloidal basalt showing relict poikilitic texture in an amygdule where a large quartz (qtz) oikocryst encloses a deformed epidote (ep) grain (Sample KA47, x4, PPL).

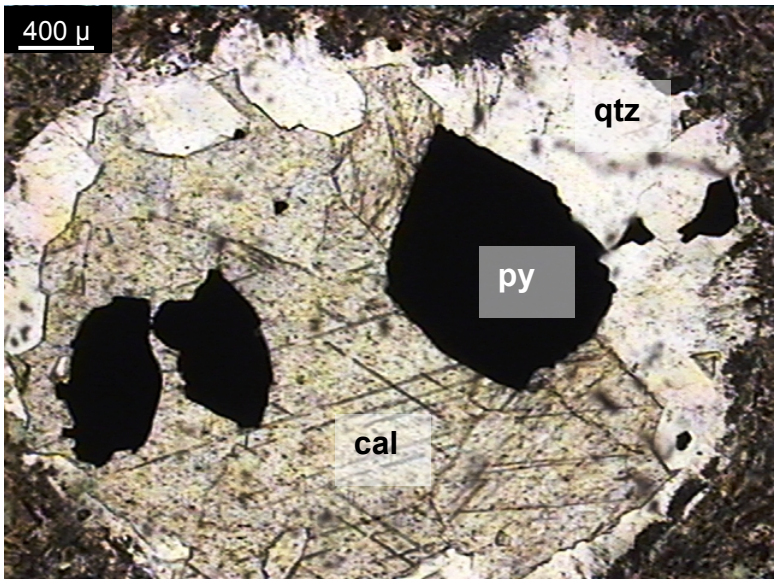

Figure 5-7. Photomicrograph of an amygdaloidal basalt sample. The amygdule is occupied by large crystals of quartz (qtz), calcite (cal) and pyrite (py) (Sample KD2, x4, XPL).

Figure 5-8. Photomicrograph of hydrothermally altered basalt showing both fine- and coarse-grained secondary quartz (qtz) occurrences as the infilling material in veinlets. The groundmass is composed of fine microliths of albite (Sample KA66, x4, XPL). (cal: calcite)

Crystals range in size from medium to coarse and, again, like quartz occur both in amygdules and in groundmass. In many sections calcite comprises a great proportion of the groundmass, and large calcite crystals occur widely as an infilling material in amygdules. Calcite generally replaces epidote and some plagioclase phenocrysts. Also some of the veinlets are occupied mainly by calcite.

In the late stages of hydrothermal alteration, calcite crystals, especially the ones in amygdules, were replaced by quartz crystals. On the other hand, within the quartz-sulfide veins in the basaltic lavas, euhedral dolomite rather than calcite is the major carbonate mineral. Colorless dolomite is characterized by higher refractive indices than calcite and has a typical cloudy appearance.

Clinopyroxene is partially altered to colorless or pale-green actinolite and green pleochroic hornblende. Actinolite occurs as thin, prismatic crystals of fine- to medium-grain size, and many actinolite crystals show weak pleochroism. In a similar manner, green pleochroic hornblende, which is secondary in origin, occurs as patches along relict clinopyroxene crystals. Hornblende is generally anhedral and occurs as 0.1 to 0.3 mm crystals.

Titanite is the dominant accessory phase in the Karaali basalts and it is distinguished by its very high relief. Yellowish to brown titanite crystals are euhedral to anhedral. Another accessory phase in the basalt samples is colorless apatite, which occurs as small, elongated wedge-shaped crystals.

Zeolite minerals locally fill amygdules in the basalts; they are colorless and occur as anhedral crystals forming clusters that fill the amygdules completely. The zeolite crystals display radiating habit to some extent (Figure 5.9).

Other than these rock forming minerals, the Karaali basalts also contain opaque minerals. In the vicinity of the mine site, basalt samples contain large pyrite crystals, especially in their amygdules. Pyrite grains in the basalts are euhedral to subhedral and are 2-3 mm in size. Similarly, hematite is widespread in the basalt samples around the massive-sulfide orebody.

Red hematite mainly occupies veinlets and occurs mainly in association with quartz and pyrite. It seems that pyrite and hematite were incorporated into the basalts in the later stages of hydrothermal alteration, together with quartz.

In the vicinity of the main mineralized zone, the basalt outcrops exhibit traces of argillic alteration, mainly in the form of kaolinitization. Microscopic study of the samples from this zone reveals that basalts with late-stage argillic alteration are devoid of primary mineral phases and a general cloudy appearance under plane polarized light dominates the thin sections of the argillically altered samples (Figure 5.10).

5.3 Gabbros

The green to dark-green gabbros are phaneritic. There are two varieties of gabbro: coarse- and fine-grained. The fine-grained gabbros carry the signs of hydrothermal alteration and typically are in green color, whereas the coarse-grained gabbros are relatively unaltered, and are olive-green or dark-green in color, with white bands of feldspars. The primary and secondary mineral assemblages of the gabbros are somewhat similar to the basalts, with plagioclase and clinopyroxene as the primary mineral phases, and chlorite, calcite, actinolite, and hornblende, with little quartz and prehnite, as the secondary mineral phases (Figures 5.11 and 5.12). Also observed are opaque minerals, accessory Titanite and spinel. Compared to the basalts, the degree of hydrothermal alteration is relatively lower in the coarse-grained gabbros, as reflected by the higher abundances of primary minerals.

Plagioclase is the major primary mineral phase in the gabbros. Colorless plagioclase phenocrysts are present as euhedral to subhedral crystals, and range in size from a few millimeters up to 1 cm. The average grain size is about 2 mm. Generally, the gabbros consist of 40-50 modal percent plagioclase. The interstices between large plagioclase laths are usually occupied by coarse-grained clinopyroxenes and, in some cases, by secondary amphiboles. Plagioclase phenocrysts display well-developed Carlsbad and albite twins.

Figure 5-9. Photomicrograph of basalt sample with zeolite (zeo) minerals filling the amygdules. Minerals with anomalous blue interference color are penninite. The groundmass is composed of fine albite microliths and high-birefringence epidote minerals (Sample KA34, x4, XPL).

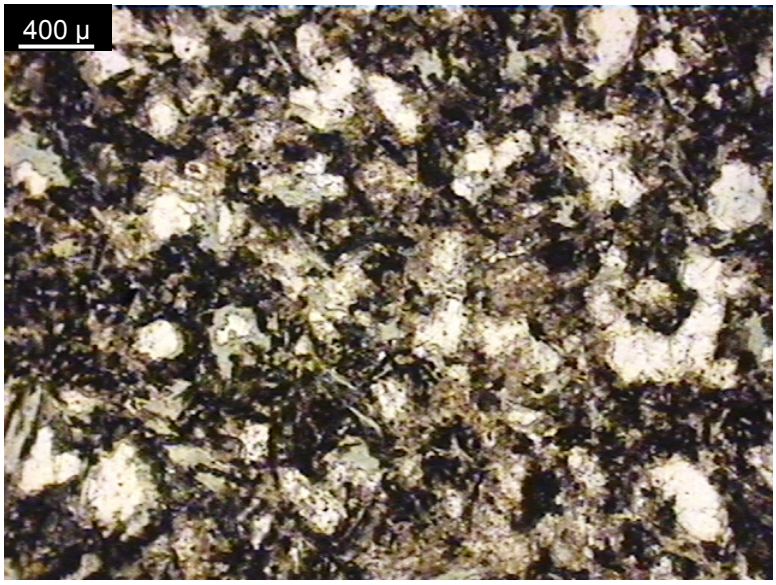

Figure 5-10. Photomicrograph showing intense argillic alteration of a basalt sample. Dark-brown cloudy appearance is caused from kaolinitization. White phenocrysts are quartz crystals, green crystals are chlorite, and opaque minerals are fine pyrite grains (Sample KA47, x4, PPL).

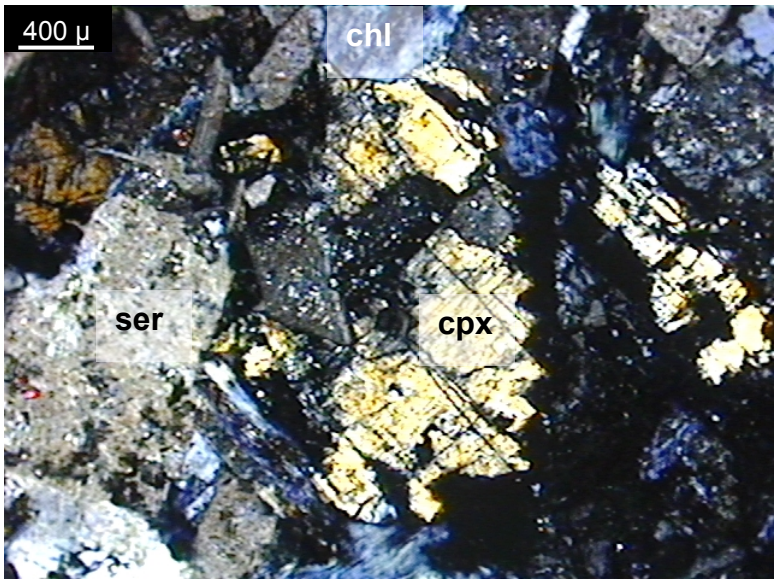

Figure 5-11. Photomicrograph of a coarse-grained gabbro sample. Relict clinopyroxene (cpx) at the center is surrounded by sericite (ser) and chlorite (chl) (Sample KD3, x4, XPL).

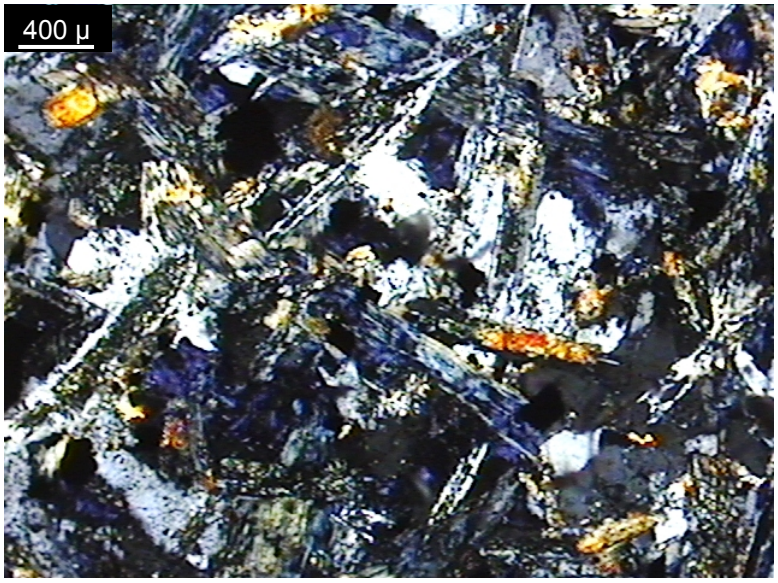

Figure 5-12. Photomicrograph of a fine-grained gabbro sample showing laths of altered, randomly-oriented plagioclase crystals. Interstices are filled with secondary quartz (white) and chlorite (blue) (Sample KA41, x4, XPL).

The compositions of plagioclases were determined by the Michel-Levy method. For this purpose, several samples were analyzed and many plagioclase crystals were measured using the extinction angles of albite twins. According to this method, the maximum extinction angle between albite twins is between 27° and 30°, indicating that these plagioclase feldspars are of labradoritic (An_{50} to An_{55}) composition (Figure 5.13). Plagioclase in the gabbros remain relatively unaltered compared to the plagioclase in the basalts. However, in many sections, replacement of plagioclase by chlorite, sericite, calcite, and less commonly by saussurite is analogous to the basalts.

Clinopyroxene is randomly distributed throughout the groundmass but is more abundant as phenocrysts; it comprises approximately 20 modal percent of the gabbro samples. Pale clinopyroxene crystals are subhedral to anhedral and display subtle greenish pleochroism. The extinction angles of the clinopyroxenes range from 37° to 44° and, similar to the basalt samples, the gabbros are characterized by augitic clinopyroxenes. Crystals of clinopyroxene show well developed intergranular textures with plagioclase phenocrysts within them. Additionally, with plagioclase crystals, the clinopyroxenes form equigranular textures. Alteration in clinopyroxenes is prominent, with the most typical alteration styles being uralitization and chloritization. Most augites were pseudomorphed by chlorite. Under cross-polarized light, chlorite crystals are observed with an anomalous Berlin-blue color that is typical of “penninite”.

Secondary, magnesian hornblende is seldom found in the Karaali gabbros. It is green pleochroic and anhedral. In only a few samples hornblende crystals were recognized as relict, and these are closely associated with clinopyroxene crystals where observed. Formation of hornblende is mainly due to the uralitization of primary pyroxene crystals. A notable feature of hornblende is its replacement of secondary chlorite. Other than secondary hornblende, actinolite is also present in these sections; it is colorless to pale green and occurs as fibrous crystals.

Calcite and quartz are typically found together, but the overall abundance of quartz is much lower than that of calcite. Colorless calcite crystals are subhedral

to anhedral, and they are distinguished by perfect cleavage and strong interference colors. On the other hand, subhedral quartz crystals are colorless in thin section.

Prehnite is scarce in the gabbros, occurring as isolated crystals. It is characterized by long, somewhat prismatic or tabular crystals which are medium-grained, colorless, display radial alignments. Prehnite crystals have low birefringence with pale yellow to gray interference colors.

In the gabbros, pyrite, hematite and spinel are the opaque phases. As in the case of the basalts, gabbros contain minor amounts of opaque minerals. Relatively fresh, coarse-grained gabbros consist of euhedral to subhedral pyrite grains around 3 mm in size.

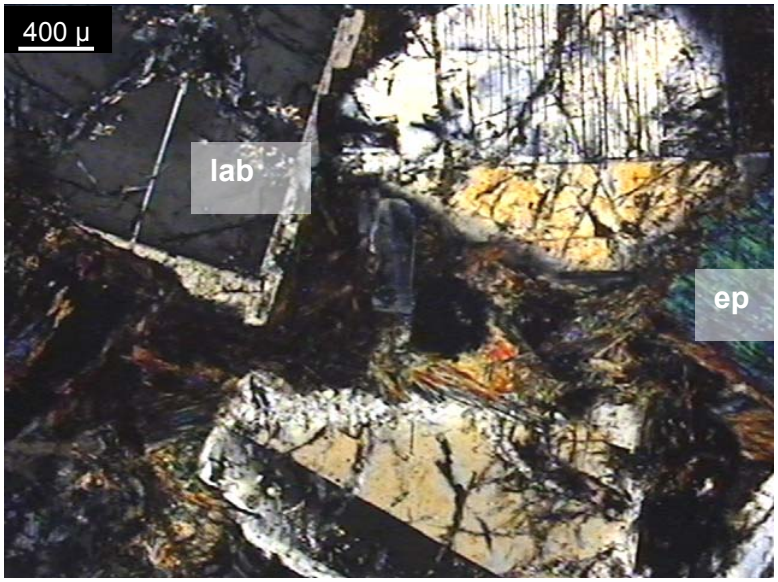

Figure 5-13. Photomicrograph of a coarse-grained gabbro sample showing labradorite (lab) phenocrysts with typical Carlsbad and albite twins. Interstices between labradorite crystals are occupied by epidote (ep) grains (Sample KA29, x4, XPL).

Abundant spinel grains are present in the gabbro samples of Karaali. Some spinel grains are euhedral, however, most are angular. Locally the crystal sizes reach up to 5 mm, but average crystal size is around 3 mm. They are usually opaque or, rarely, translucent, and are reddish brown and dark brown (Figure 5.14).

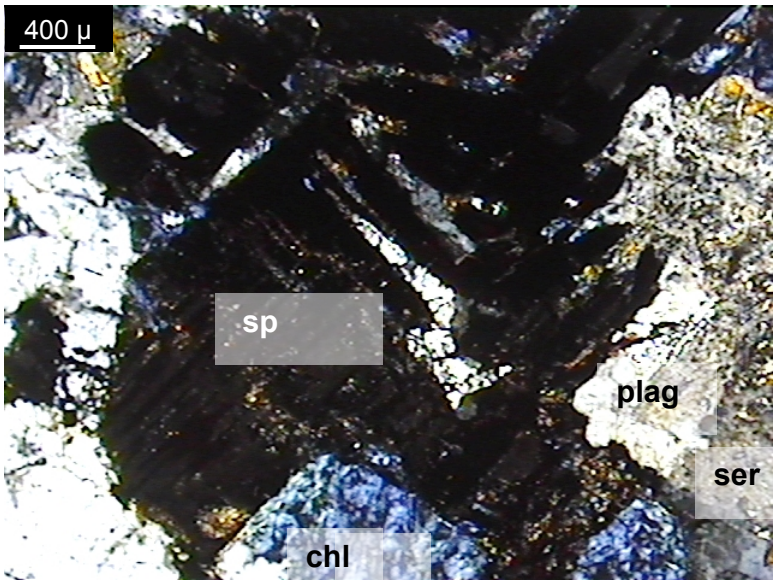

Figure 5-14. Photomicrograph of a gabbro sample with a large spinel (sp) grain surrounded by sericite (ser) and chloritized plagioclase (plag) crystals (Sample KA47, x4, PPL).

5.4 Serpentinites

Formerly ultramafic rocks, the serpentinites still retain some petrographic features of their precursors. Despite the presence of some primary mafic minerals, the degree of serpentinization is so high that these rocks should be regarded as serpentinites. In hand specimen, the serpentinites are dark green in color with a greasy feel and appearance. Thin chrysotile veins crosscut the serpentinites and large crystals of bastite are notable features of some specimens. On some outer surfaces, talc formation occurs locally.

O'Hanley (1996) defined three types of serpentinite textures: (1) pseudomorphic (preserve the textural features of the protolith); (2) nonpseudomorphic (do not preserve the textural features of the protolith; and (3) transitional (preserve some of the textural features of the protolith).

Petrographically, the serpentinite is composed mainly of lizardite (see Appendix A for results of XRD analysis) and lesser orthopyroxene, clinopyroxene, bastite, chrysotile, hematite and chromite. Serpentinites from Karaali partly preserve the original textures of the protolith peridotites and are characterized by both pseudomorphic and non-pseudomorphic textures. Primary textures preserved in serpentinites are generally granular, poikilitic and porphyritic textures caused mainly by the relationships between primary mineral phases, such as olivine, orthopyroxene and clinopyroxene, with or without serpentine minerals. The typical pseudomorphic textures in the Karaali serpentinites are mesh textures, ribbon textures and pseudomorphic bastites. The mesh texture was produced prior to deformation by alteration of a parental peridotite.

In serpentinites, large crystals (1-2 mm) of orthopyroxene are preserved in many cases. Orthopyroxene is usually colorless, but due to subtle serpentinization, some phenocrysts are yellow and yellowish green. The clinopyroxene is distinguished by parallel extinction and weak, pinkish pleochroism. Orthopyroxenes are partly pseudomorphed by bastite, a variety of enstatite (Figure 5.15).

Clinopyroxene is not as abundant as orthopyroxene. It is most readily distinguished by its relatively high interference colors. In thin section, clinopyroxene is preserved within mesh-textured serpentine. The earliest clinopyroxene phenocrysts are fractured and later altered to serpentinite along grain boundaries and fractures. Consequently, small clinopyroxene grains are observed as small grains forming the core of meshes, while serpentine forms the rims. Apart from this, there are two additional types of mesh texture. One is distinguished by the presence of serpentine minerals both in the cores and rims of

the meshes, while in the other rims are altered to bastite and cores are made up of clinopyroxene grains.

Lizardite, the main serpentinite mineral, is colorless in thin section. It displays typical mesh texture with polygonal meshes enclosing cores of weakly birefringent serpentine minerals (Figure 5.16). Additionally, ribbon texture in which ribbons of lizardite display planar fabrics in the form of anastomosing arrays, are widespread (Figure 5.17).

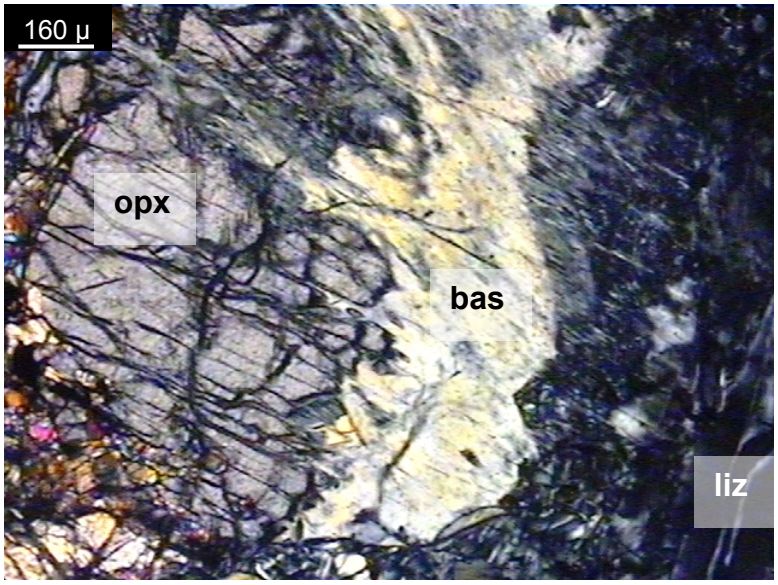

Figure 5-15. Photomicrograph of serpentinite showing partial replacement of gray orthopyroxene (opx) phenocryst -on the left- by black lizardite (liz) on the far right. The white to light gray transitional zone is bastite (bas) and the highly birefringent minerals on the far left are clinopyroxenes (Sample SP1, x10, XPL).

Two major vein generations were observed in the serpentinites: (1) white cross-fiber chrysotile veins, and (2) very thin hematite veins, both present in varying proportions. In the first type of veins, chrysotile is the chief infilling material and the thicknesses range from less than 1 mm to 2 mm.

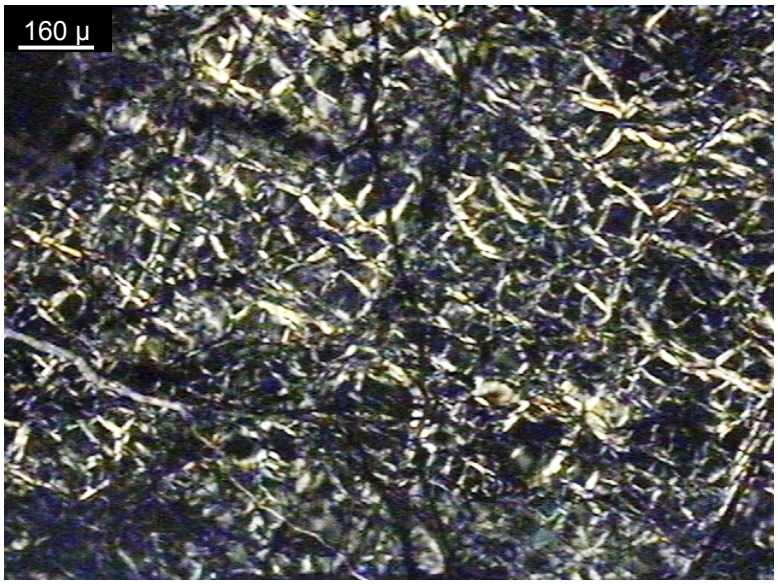

Figure 5-16. Photomicrograph of serpentinite showing typical mesh texture consisting of lizardite in the mesh rims and orthopyroxene in the mesh centers (Sample SP1, x10, XPL).

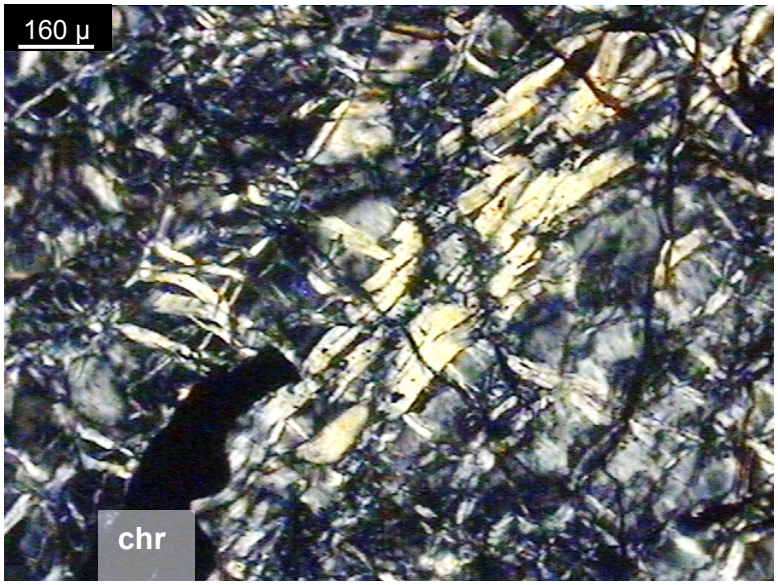

Figure 5-17. Photomicrograph of serpentinite with ribbon texture. Ribbons of bastite (white) and lizardite (dirty white to gray) are oriented from upper right to lower left and crosscut by thin veinlets of hematite (reddish brown) (Sample SP1, x10, XPL). (chr: chromite)

Along the vein boundaries, signs of serpentinization are more evident. Adjacent minerals are strongly serpentinized. In the second type of veins, hematite is the infilling material. Very narrow, anastomosing hematite veinlets are widespread; these cut the last penetrative fabric and seem have formed in the latest stage.

Apart from hematite, chromite is the other opaque mineral phase. Anhedral aggregates of chromite are randomly distributed in the sections. Although they are mainly opaque, dark brown haloes are typically developed around chromite grains (Figure 5.18).

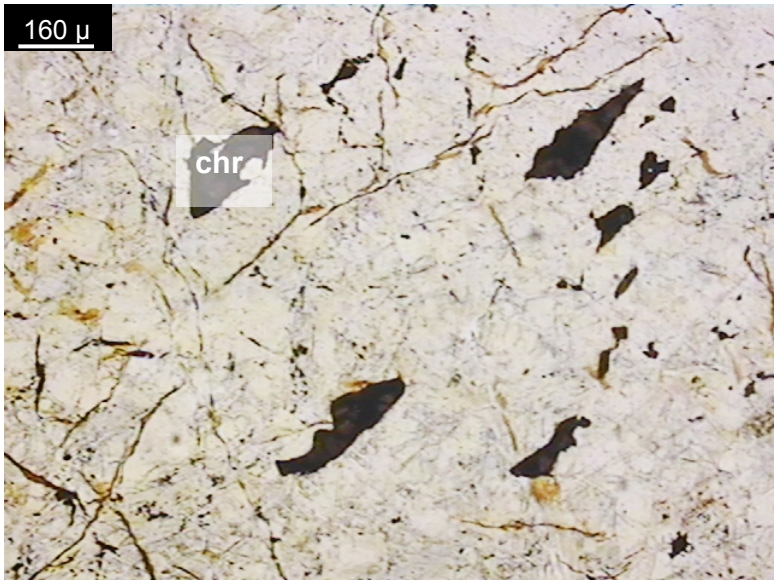

Figure 5-18. Photomicrograph of serpentinite with tectonized chromite (chr) grains scattered throughout serpentinite minerals (white areas in the background). Cross-cutting veinlets are hematite (Sample SP1, x10, XPL).

5.5 Ore mineralogy

Sulfide minerals in the Karaali district are invariably hosted by the incipiently metamorphosed and hydrothermally altered basaltic volcanics. Textural characteristics of the ore minerals range from disseminated through clustered

massive-sulfide lenses, to vein-type. The Karaali Fe-Cu sulfide ores have a simple sulfide ore mineralogy comprising a pyrite-chalcopyrite blend with minor bornite and covellite. Sphalerite has only been observed in vein-type mineralizations.

Polished sections of massive, disseminated and vein-type ore samples show simple textural relationships. The massive-sulfide lens in the basaltic volcanics is pyrite-dominated. Chalcopyrite partially replaces disseminated to massive pyrite. Bornite and covellite occur as replacements of chalcopyrite; however, they are very minor, even in the massive ore body. Secondary quartz essentially fills the interstices within the massive-sulfide ore body. Almost all sulfide minerals appear to be overprinted by deformational fabrics and are, in places, brecciated.

In rocks with disseminated sulfide mineralization, sulfide minerals are present as fine-grained (1-3 mm) rounded aggregates enclosed in primary silicate or secondary alteration minerals.

Pyrite is the principal ore mineral in the Karaali deposit. It occurs as irregular pods and veins in quartz associated chalcopyrite and minor bornite and covellite. It is found as anhedral to euhedral crystals with crystal sizes that reach up to 2 mm. Locally, pyrite inclusions occur in chalcopyrite grains. Pyrite crystals are intensely deformed. Deformational ore textures subsequent to tectonic processes have been reported from different cases of base-metal sulfide mineralization around the world (Stanton, 1972; Craig and Vaughan, 1981; McClay and Ellis, 1984; Kuşçu and Erler, 1994, 1999 and 2002).

Pyrite crystals from the Karaali massive sulfide orebody have undergone intense deformation, and deformational textures have been well observed during ore-microscopic studies. In general, the pyrites display evidence of cataclastic deformation rather than plastic deformation. Cataclastic textures are mainly due to mechanical effects caused by pressure. Pyrite grains in both the main orebody and in the vein-type disseminated ores are strongly fractured (Figure 5.19). These fractures were subsequently filled by interstitial quartz crystals. In most sections

the pyrite crystals show partial alteration to limonite along fracture zones which developed as a result of deformation.

Chalcopyrite is the principal copper mineral of the Karaali massive-sulfide deposit and typically replaces pyrite in the district (Figures 5.20 and 5.21). Where observed, chalcopyrite is cataclastically deformed –similar to pyrite- and partly replaced by bornite and chalcopyrite.

Bornite and covellite have been identified only in a few cases in the study area. Purple bornite and blue covellite generally occur as replacements minerals of chalcopyrite. In the sulfide-bearing veins, malachite and secondary hematite formation occurred subsequent to the alteration/weathering of sulfide minerals. Isolated grains of malachite occur locally within the quartz veins.

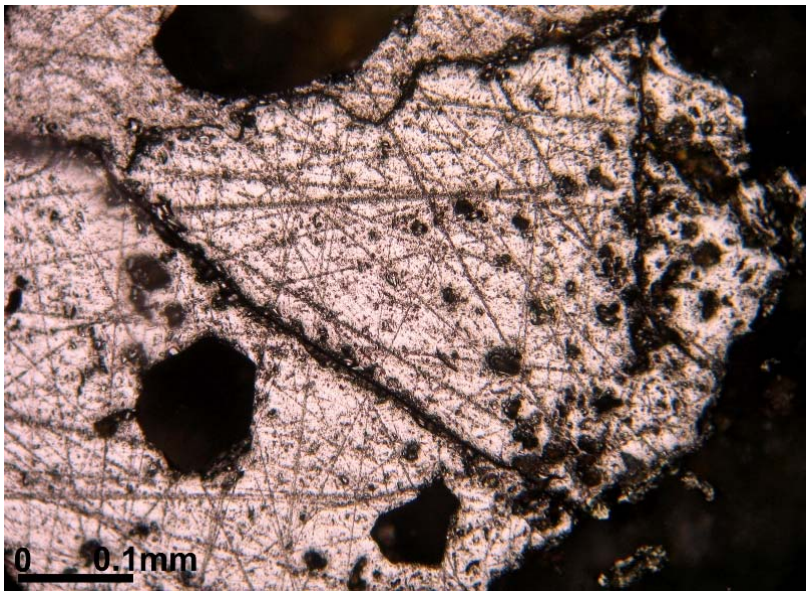

Figure 5-19. Photomicrograph of massive ore showing a highly fractured pyrite, a result of strong mechanical deformation (Sample KA79).

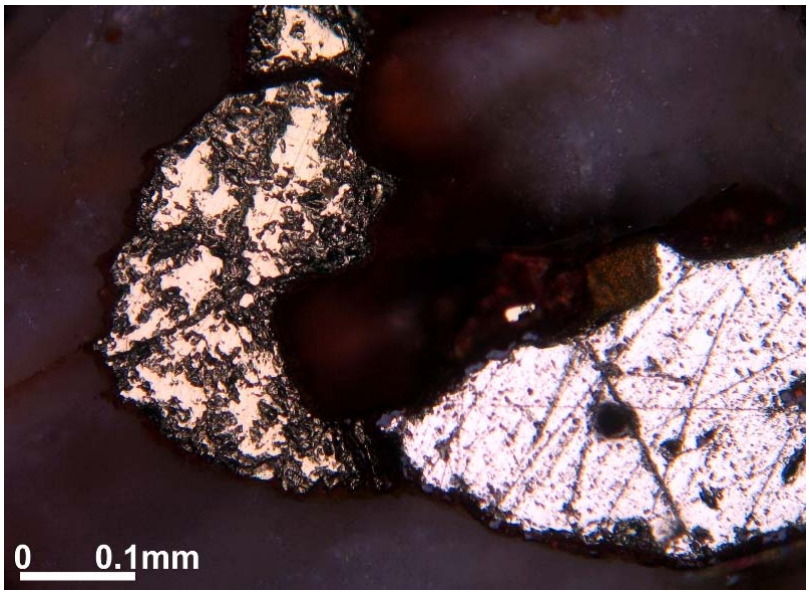

Figure 5-20. Photomicrograph of a mineralized quartz vein showing an association of pyrite (light yellow) and chalcopyrite (yellow). Outer rim of the pyrite grain is limonitized (Sample KA97).

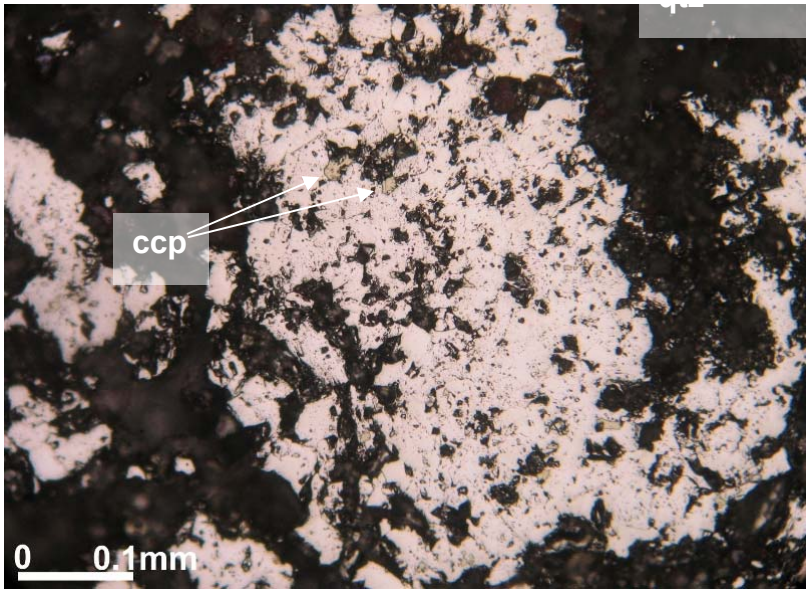

Figure 5-21. Photomicrograph of massive ore showing small inclusions of chalcopyrite (ccp) within pyrite (light yellow) crystals. Interstices within sulfide minerals are filled with quartz (qtz) (Sample KA22-2).

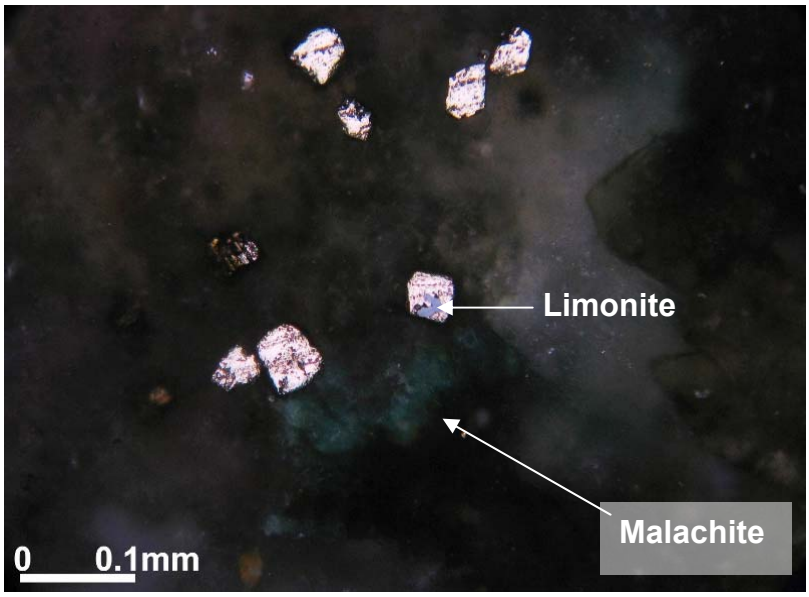

Figure 5-22. Photomicrograph of mineralized quartz vein showing euhedral to subhedral crystals of pyrite partially replaced by limonite and surrounded by patches of green malachite (Sample KA97).

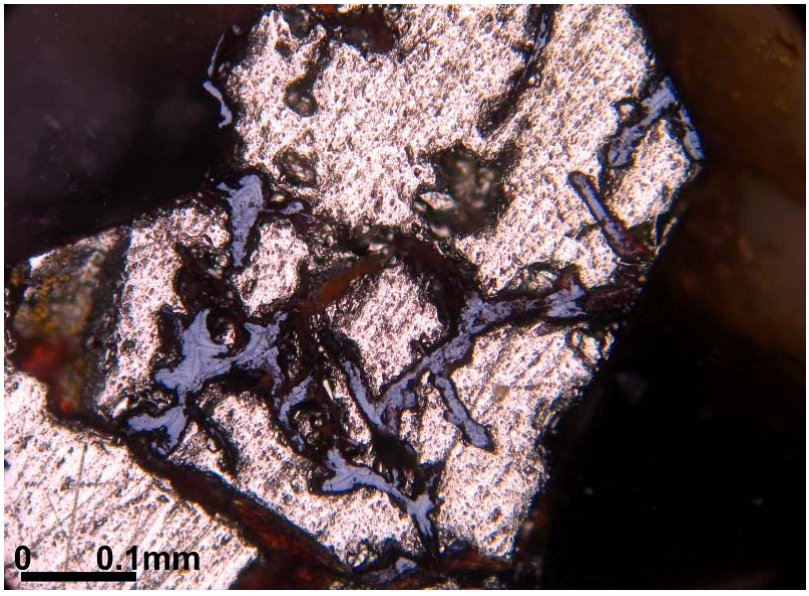

Figure 5-23. Photomicrograph of disseminated ore showing limonitization of pyrite along fracture zones (Sample KA97).

CHAPTER 6

GEOCHEMISTRY

6.1 Introduction

In the previous sections, the field and petrographical characteristics of the rocks of Karaali area were investigated. Geochemical signatures of the basic rocks are used in order to support the outcome of field and petrographic studies. Through use of geochemistry, available geological information can be interpreted more accurately. The chemical composition of a rock may reflect either the magma source from which it was derived or subsequent events that the rock has experienced. The main use of geochemical data is to determine rock type and tectonic settings. Whole-rock analyses were carried out on eighteen samples from the ophiolitic fragment located in the Karaali area. Selection of these samples was made upon their degree (or lack thereof) of alteration. On the basis of petrographic studies, least-altered samples were determined, and eight basaltic and three gabbroic rock samples were chosen. In addition to those, two serpentinite and five ore-bearing samples were selected for whole-rock analyses. Of the five ore-bearing samples, two are massive-ore samples, two of them are vein-type, and one is a disseminated ore-bearing sample. Results of whole-rock geochemical analyses of the basalt and gabbro samples are given in Table 1 (see Appendix A for a complete listing of the samples).

In this chapter, the major- and trace-element geochemistry of eight basaltic and three gabbroic samples will be evaluated using variation and discrimination diagrams. Further interpretations and discussion related to the petrogenesis of the Karaali basic rocks will be presented in the Discussion chapter, including comparisons with some other ophiolite-hosted massive-sulfide deposits, namely the Troodos and Küre deposits.

Table 6-1. Major-, trace- and rare-earth-element abundances of basic rock samples from Karaali.

Sample no.	KA 22-1	KA 29-1	KD 3	KA 36	KA 40	KA 44	KA 46	KA 63	KA 74	KA 75	KD 2
	G	G	G	B	B	B	B	B	B	B	B
SiO_2 (wt.%)	48.32	51.19	52.16	53.73	52.82	54.07	54.42	52.51	57.13	51.37	50.99
Al_2O_3	14.83	18.41	15.71	13.81	11.83	11.81	14.91	13.83	14.37	13.08	13.69
$Fe_2O_{3(T)}$*	7.01	6.22	12.04	7.8	9.42	7.43	7.39	7.47	8.4	7.82	7.52
MgO	5.84	6.42	6.64	9.35	10.97	10.42	7.56	9.86	6.24	9.54	8.41
CaO	12.33	11.1	4.87	5.85	7.85	9.18	7.6	7.0	4.95	12.51	8.05
Na_2O	4.73	2.49	3.0	3.04	3.23	1.99	2.93	3.18	3.9	0.09	3.28
K_2O	0.26	0.22	0.19	0.07	0.05	0.07	0.28	0.04	0.1	0.04	0.06
TiO_2	1.08	0.25	0.44	0.24	0.19	0.17	0.25	0.19	0.49	0.19	0.24
P_2O_5	0.11	0.01	0.03	0.02	0.02	0.01	0.01	0.01	0.03	0.01	0.02
MnO	0.14	0.07	0.15	0.08	0.11	0.12	0.1	0.14	0.1	0.14	0.12
Cr_2O_3	0.037	0.019	0.024	0.075	0.115	0.127	0.029	0.06	0.019	0.12	0.041
LOI	5.1	3.5	4.5	5.8	3.2	4.5	4.4	5.6	4.1	5.1	7.4
SUM	99.82	99.9	99.76	99.89	99.83	99.92	99.89	99.88	99.84	100.01	99.84
Ni (ppm)	128.5	8.6	29.6	69.2	53.5	105.9	28.9	98.7	36.8	122.6	63
Sc	37	37	42	47	48	45	44	46	34	42	43
Mo	2.0	1.9	3.3	1.8	1.7	2.4	1.2	1.7	3.0	4.1	2.5
Cu	51.4	7.9	1196	156.4	504.4	46.3	5.4	52.9	195	97	80.8
Pb	1.0	<.1.0	0.2	0.8	0.4	1.7	0.2	2.6	0.3	1.2	0.5
Zn	60	4	48	55	14	41	10	95	54	61	61
As	1.5	<.5	1	1.7	1.1	1.7	0.6	12.8	2.9	1.5	0.8
Cd	0.4	<.1	<.1	<.1	<.1	<.1	<.1	0.1	<.1	<.1	<.1
Sb	0.1	<.1	0.1	0.1	0.1	0.3	0.1	0.1	0.2	0.3	0.2
Ag	0.1	<.1	0.1	<.1	<.1	<.1	<.1	<.1	0.1	<.1	<.1
Au**	2.0	0.5	3.8	1.7	<.5	1.0	<.5	8.6	1.2	2.4	<.5
Hg	0.01	0.07	<.01	<.01	<.01	<.01	<.01	0.02	<.01	<.01	0.01
Se	<.5	<.5	0.6	<.5	<.5	<.5	<.5	<.5	<.5	<.5	<.5

G: gabbro, B: basalt; *$Fe_2O_{3(T)}$= total Fe, ** in ppb

Table 6-1. (cont'd)

Sample no.	KA 22-1	KA 29-1	KD 3	KA 36	KA 40	KA 44	KA 46	KA 63	KA 74	KA 75	KD 2
	G	G	G	B	B	B	B	B	B	B	B
Ba (ppm)	45.6	40.8	19.1	34.7	7.1	15.9	73.4	23.5	22.2	5.8	20.9
Be	<1	<1	<1	<1	<1	<1	<1	<1	<1	1	1
Co	74.1	30.6	40	34.1	35.7	34.7	34	24.1	28.9	33.9	29.3
Cs	0.2	1.1	0.1	<.1	<.1	0.1	0.4	<.1	0.2	<.1	<.1
Ga	11.9	14	14.3	11.1	9.2	9.7	10.1	11.4	11.5	10.6	11.3
Hf	2.1	<.5	<.5	<.5	<.5	<.5	<.5	<.5	0.7	<.5	<.5
Nb	2.4	0.9	0.6	0.8	<.5	0.7	0.8	0.7	1.0	0.7	0.6
Rb	3.9	4.8	3.3	1.3	0.9	1.4	4.0	0.7	2.1	<.5	1.0
Sr	149.9	246.4	111.4	117.9	34.6	117.7	243.1	71.5	87.6	18.3	123.1
Ta	0.2	<.1	<.1	<.1	<.1	<.1	<.1	<.1	<.1	<.1	<.1
Th	0.2	0.3	0.4	0.2	0.3	0.1	0.4	0.2	0.2	0.1	0.2
U	2.9	<.1	<.1	<.1	<.1	0.2	0.2	0.1	0.1	<.1	<.1
V	247	283	256	268	230	225	292	242	260	233	241
W	0.5	0.3	0.4	0.3	0.2	0.3	0.6	0.9	0.6	0.5	0.2
Zr	58.6	7.3	15.1	7.4	5.0	4.7	7.7	6.4	18.2	6.8	6.1
Y	27.1	7.0	11.8	7.7	6.1	5.4	7.8	7.3	12.2	7.0	7.1
La	3.9	1.1	1.2	0.9	0.7	0.6	1.1	0.8	1.3	0.6	0.8
Ce	10.8	1.9	2.8	1.6	1.3	1.0	2.1	1.6	3.1	1.4	1.4
Pr	1.62	0.19	0.41	0.19	0.15	0.11	0.24	0.15	0.44	0.15	0.16
Nd	8.2	0.7	2.5	0.7	0.7	<.4	1.2	0.7	2.4	0.6	1.1
Sm	3.0	0.3	0.9	0.3	0.3	0.3	0.3	0.3	0.8	0.3	0.4
Eu	1.06	0.18	0.34	0.12	0.13	0.12	0.17	0.15	0.34	0.12	0.19
Gd	3.95	0.68	1.35	0.65	0.58	0.47	0.74	0.58	1.54	0.57	0.7
Tb	0.78	0.16	0.31	0.17	0.13	0.12	0.15	0.14	0.31	0.14	0.14
Dy	4.42	1.03	1.92	1.12	1.03	0.76	1.06	1.1	1.9	0.92	1.04
Ho	0.96	0.27	0.43	0.3	0.22	0.2	0.27	0.25	0.45	0.25	0.26
Er	2.87	0.78	1.25	0.81	0.7	0.65	0.89	0.86	1.39	0.74	0.78
Tm	0.4	0.14	0.19	0.13	0.11	0.11	0.13	0.15	0.21	0.12	0.14
Yb	2.46	0.8	1.23	0.87	0.74	0.67	0.93	0.97	1.33	0.79	0.85
Lu	0.41	0.15	0.22	0.14	0.14	0.1	0.16	0.16	0.23	0.16	0.17

G: gabbro, B: basalt

In the general context of the current study, the genesis of the Karaali massive-sulfide mineralization is chiefly considered. Thus, sulfur-isotope analyses were carried out in order to determine the origin of the sulfur present in the orebody as sulfides. Including massive and vein-type mineralizations, six ore-bearing samples were selected from the deposit and analyzed for their $\delta^{34}S$ contents. The sulfur-isotope abundances of selected samples will be presented in this chapter, and a comparison with similar deposit types will be included in "Discussion" chapter.

6.2 Analytical Methods

For whole-rock geochemical analysis, a total of 18 samples were powdered to 200 mesh in the Geological Engineering Department of Middle East Technical University, and analyzed in the ACME Analytical Laboratories Ltd. in Vancouver, Canada. Major-oxide and trace-element abundances were reported from 0.2 g samples analyzed by ICP-emission spectrometry following $LiBO_2$ fusion and dilute nitric-acid digestion. Loss on ignition (LOI) is by weight difference after ignition at 1000°C. Rare-earth and refractory elements were determined by ICP mass spectrometry following $LiBO_2$ fusion and nitric-acid digestion of 0.2 g samples (same decomposition as major and trace elements). In addition, separate 0.5 g splits were digested in aqua regia and analyzed by ICP-Mass spectrometry to acquire the precious- and base-metal values.

For sulfur-isotope analysis six ore-bearing samples were initially powdered to 200 mesh in the Geological Engineering Department of Middle East Technical University, and submitted to Activation Laboratories Ltd. in Ontario, Canada. In brief, pure $BaSO_4$ and pure sulfide samples are combusted to SO_2 gas under a $\sim 10^{-3}$ torr of vacuum. The SO_2 is inlet directly from the vacuum line to the ion source of a VG 602 Isotope Ratio Mass Spectrometer (Ueda, 1986). Quantitative combustion to SO_2 is achieved by mixing 5 mg of sample with 100 mgs of a V_2O_5 and SiO_2 mixture (1:1). The reaction is carried out at 950˚C for 7 minutes in a quartz-glass reaction tube. Pure copper turnings are used as a catalyst to ensure conversion of SO_3 to SO_2. Internal lab standards ($SeaWater_{BaSO4}$ and $Fisher_{BaSO4}$

are run at the beginning and end of each set of samples (typically 25) and are used to normalize the data as well as to correct for any instrumental drift. All results are reported in the per mil notation relative to the international CDT (Canon Diablo Troilite) standard. Precision and reproducibility using this technique is typically better than 0.2 per mil (n = 10 internal lab standards) (Ueda, 1986).

Fluid-inclusion studies were performed in the Geological Engineering Department of İstanbul University. The petrography of fluid-inclusion assemblages was first examined at low magnifications using a standard Leica DMLP polarized microscope. Microthermometric analysis was carried out using a calibrated Linkam THMG-600 stage which is suitable for heating work to 600°C and freezing work to -196°C. Heating/freezing temperatures can be controlled either manually or using Linksys-32 DV software. Accuracy in the measurements is ± 0.2°C for freezing, ± 0.2°C for heating between 0-100°C, and ± 0.4°C for heating between 100-350°C, according to Linkam FI standards. The analyses were performed on selected crystals of dolomite that were prepared as 150-200 μm thick doubly polished wafers.

6.3 Geochemistry of the Karaali Basic Rocks

6.3.1 Major Elements

6.3.1.1 Element Mobility

Over the last few decades much work has been carried out concerning the use of major and trace elements in characterization of igneous rocks and for discrimination of their tectonic settings. The pioneering studies of Miyashiro (1974 and 1975), Pearce (1975, 1976) and Pearce et al. (1977) emphasized the importance of major oxides for geochemical characterization of basaltic rocks and produced some major oxide-based discrimination diagrams. However, the outcome of these studies gives trustworthy approaches *only* if the considered samples are fresh or only slightly altered. The term “element mobility” mainly

expresses the chemical changes which take place in rock after its formation, usually through interaction with a fluid. It is known that secondary processes such as weathering, diagenesis, metamorphism and hydrothermal alteration can alter major- and trace- element distributions in a rock; if they are used incorrectly, misinterpretations on the origin the rock become unavoidable. As a result, to better understand the origin of rocks that were subjected to secondary processes, it is necessary to use elements that have been relatively immobile, and thus preserve a geochemical signature of the protolith (Rollinson, 1993).

As Shervais (1982) noted, the relations between ophiolites and adjacent terranes are generally tectonic, and because low-temperature hydrothermal alteration and metamorphism are ubiquitous in ophiolite complexes, major-element geochemistry is not definitive of origin in most cases. Some researchers noted this disadvantage of some elements (mainly major elements) and tried to eliminate the consequences of element mobility by examining the behavior of specific elements under the conditions of weathering, metamorphism or hydrothermal alteration. The early studies of Cann (1970), Pearce and Cann (1971 and 1973), Hart et al. (1974), Pearce (1975), Pearce and Norry (1979), Winchester and Floyd (1975) and Wood (1980) proposed the use of relatively immobile elements as discriminants of ophiolite petrogenesis. These attempts seemed to be successful for many differentiated basic rocks, and immobile elements began to be used conventionally as petrogenetic indicators. These diagrams are based on empirical observations that there are systematic chemical differences in the source characteristics of basic magmas erupted in different tectonic settings. Thus, the concentrations and ratios of selected elements can be used to distinguish among these tectonic settings (Gorton and Schandl, 2000).

Element mobility may also be detected using bivariate diagrams which are generally used to display variation among samples in order to identify trends. Bivariate diagrams in which oxides are plotted against SiO_2 or MgO are often called Harker diagrams. Normally the oxide which shows the greatest range in the data set would be selected and, in basic rocks, this oxide might be MgO. MgO-

based Harker diagrams are most appropriate for rock series that include abundant mafic members (Rollinson, 1993). Harker diagrams are useful for investigation of the origin of differences in chemical composition between members of a rock series, presumed to represent stages in the evolution of a magma (Wilcox, 1979). Scattered trends on Harker diagrams may also be a useful indicator of element mobility in the rock and elucidate its conditions of weathering, alteration or metamorphism. Studies of basaltic rocks have documented well that Ti, Al, and P are generally immobile, whereas Ca and Na are almost always mobile (Rollinson, 1993).

In this study, in order to understand the overall trends and possible genetic relationships, a series of Harker diagrams were plotted. Selected major- and trace-element Harker diagrams are shown in Figures 6.1 and 6.2. On these diagrams, MgO was used as a differentiation index since the samples lie compositionally in a basic range. Linear correlations of Al_2O_3, TiO_2, P_2O_5 and $Fe_2O_{3(T)}$ against MgO are noteworthy. In general Al_2O_3, and P_2O_5 display negative correlations with MgO, whereas TiO_2 and $Fe_2O_{3(T)}$ values are restricted in a narrow range. MgO versus SiO_2, CaO, Na_2O, K_2O plots have scattered distributions. In particular, the scattered trends displayed by alkalis and Ca are to be expected due to the sensitivity of these elements to hydrothermal alteration and ocean-floor metamorphism (Figure 6.1). In a series of Harker diagrams, selected trace elements were plotted against MgO (Figure 6.2). In these diagrams, only Ni displays positive trends with MgO content while Zr, Y, La and Ce contents decrease with increasing MgO. Plots of relatively mobile elements such as Rb, Sr, and Ba give scattered distributions against MgO as in the case of mobile major elements.

As the Harker diagrams indicate, SiO_2 contents of the Karaali basalts have a wide range of distribution (between 51 and 57 wt %). The basaltic rocks seem to be slightly enriched in SiO_2 possibly due to accommodation of secondary quartz in amygdules. Low MgO concentrations are typical, mostly between 8-11 wt %. In addition, the basalts have low K_2O (0.04-0.10 wt %), CaO (5-9 wt %), TiO_2 (0.17-

0.49 wt %) and P_2O_5 (0.01-0.03 wt %) contents. The depletion of CaO can be attributed to widespread albitization of the basalts. The alteration of Ca-rich plagioclase feldspars (i.e, labradorite) to Na-rich plagioclase feldspars of albitic composition is the major cause of this depletion. High Na_2O contents (around 2.71 wt %) of basalt samples also support this suggestion.

The gabbros, on the other hand, are slightly depleted in SiO_2 (48-52 wt %) and MgO (5.8-6.6 wt %) compared to the basalts, whereas their Al_2O_3, Fe_2O_3, CaO, Na_2O, K_2O, TiO_2 and P_2O_5 contents are considerably higher than those of the basalts.

The main reason for these differences is probably related to decreasing degree of ocean-floor metamorphism and hydrothermal alteration with depth. The examination of trace elements will likely be enlightening with regard to understanding the compositional dissimilarities between basalt and gabbro samples.

The major-element composition of basaltic rocks from Karaali and selected tectonic settings are given in Table 6.2 for comparison. In general, basalt samples from Karaali are slightly depleted in most of the major elements, such as Ti, Fe, Mn, Ca, K and P, as compared to mid-ocean ridge basalts, island-arc tholeiites, and island-arc calc-alkaline basalts. Generally, ocean-island basalts from Hawaii seem far more enriched in these major elements, so there is a huge difference between the major-element composition of the Karaali basalts and ocean-island basalts. According to this table, the Karaali basalts appear slightly enriched in SiO_2 relative to basalts from mid-ocean ridges and island-arcs, and Hawaiian alkali and tholeiitic basalts. Relatively immobile major-oxides contents (TiO_2 and P_2O_5) are consistent with those of island-arc tholeiitic basalts (IATB), whereas oxides of Ca and Na, which are alteration sensitive, are closer to mid-ocean ridge basalts (MORB) abundances. However, as pointed out above, the use of major-element geochemistry cannot elucidate the origin of the Karaali basalts because of low-temperature alteration and metamorphism.

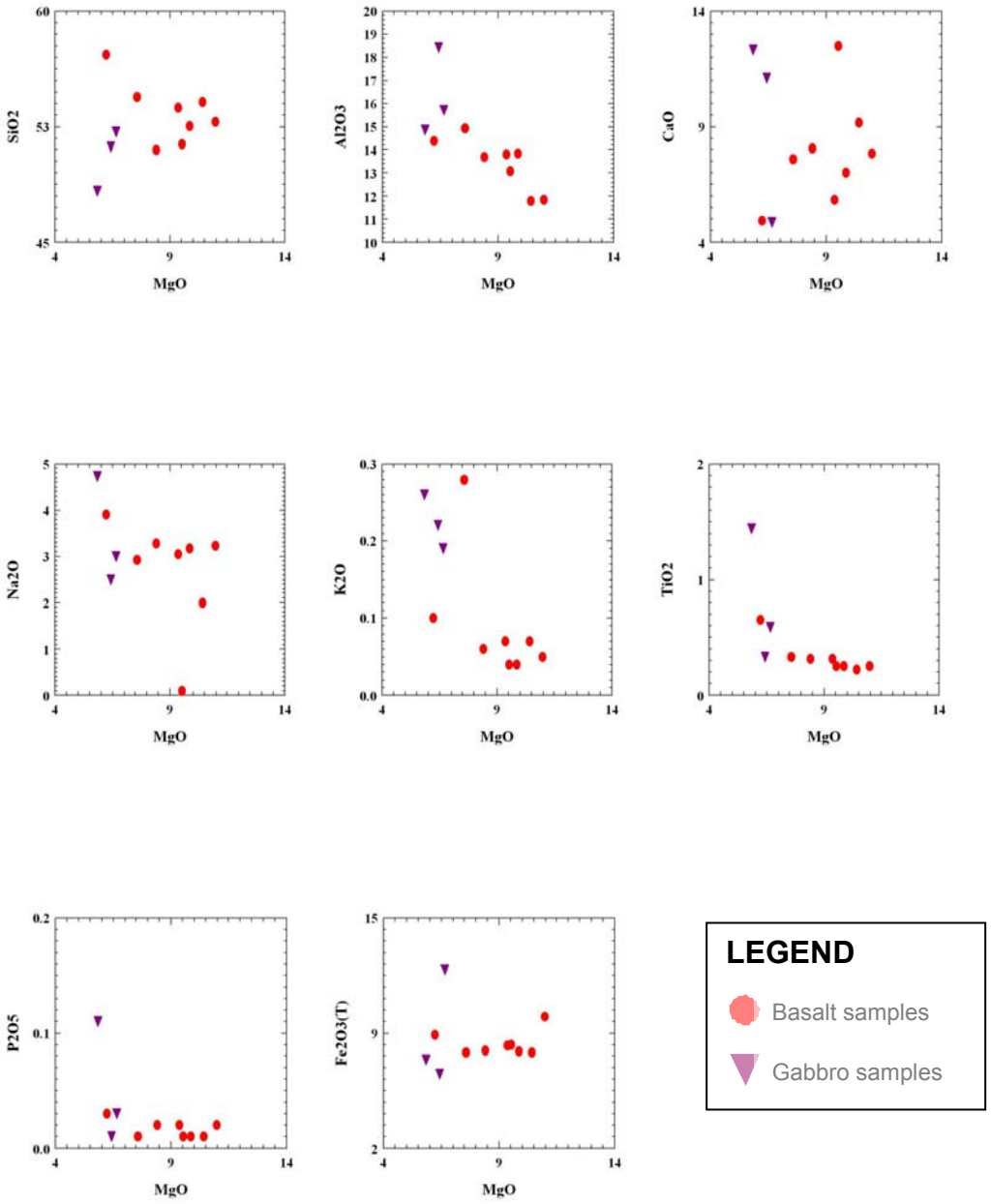

Figure 6-1. Harker diagrams for the major elements in the Karaali basic rocks.

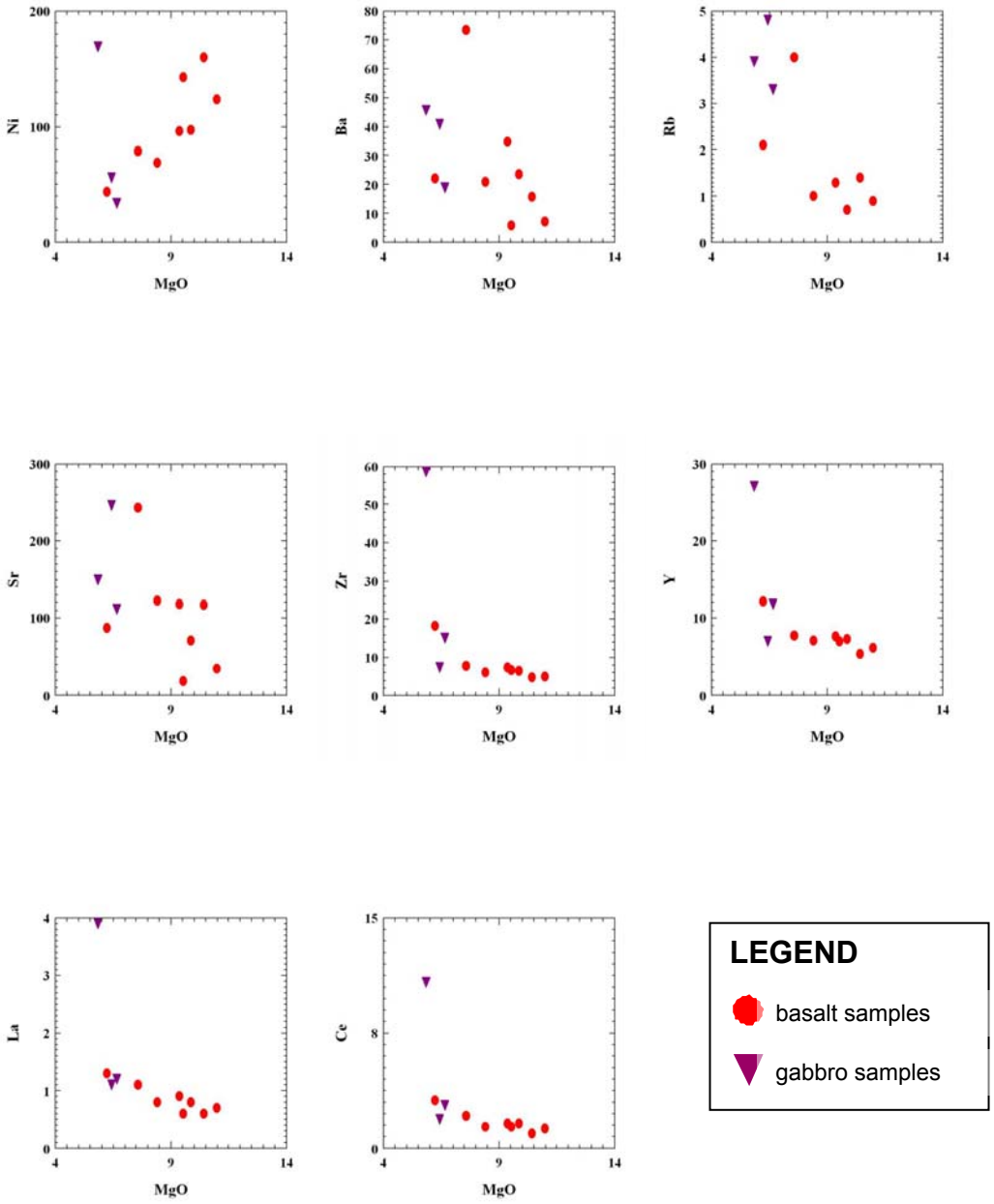

Figure 6-2. Harker diagrams for the selected trace elements in the Karaali basic rocks.

Table 6-2. Comparison of major-element compositions of Karaali basaltic rocks with mid-ocean ridge and oceanic islands.

	average Karaali basalts	average Atlantic MORB[a]	island-arc tholeiite[b]	island-arc calc-alkaline basalt[b]	Hawaiian alkali basalt[c]	Hawaiian tholeiite[d]
wt. %						
SiO_2	**53.38**	50.67	49.20	49.40	44.50	49.20
TiO_2	**0.25**	1.28	0.52	0.70	2.15	2.57
Al_2O_3	**13.42**	15.45	15.30	13.29	14.01	12.77
$Fe_2O_{3(T)}$	**7.91**	9.67	9.00	10.15	12.51	11.40
MnO	**0.11**	0.15	0.18	0.20	0.19	0.17
MgO	**9.04**	9.05	10.1	10.44	10.12	10.00
CaO	**7.87**	11.72	13.00	12.22	10.63	10.75
Na_2O	**2.71**	2.51	1.51	2.16	2.47	2.12
K_2O	**0.09**	0.15	0.17	1.08	0.53	0.51
P_2O_5	**0.02**	0.20	0.06	0.20	0.42	0.25

Data sources: [a]Best, 1982; [b]Perfit et al., 1982; [c]Clague and Frey, 1982; [d]Hughes, 1982

6.3.2 Trace and Rare-Earth Elements

6.3.2.1 Rock Classification Diagrams

As mentioned in previous sections, the studied rock units have undergone intense low-temperature ocean-floor metamorphism and hydrothermal alteration. Consequently, many of the primary mineralogical and geochemical characteristics of these ophiolitic rocks are no longer available and, in order to avoid erroneous results, it is incumbent on us to use of immobile elements instead of relatively mobile elements and major oxides.

The basic rock samples from the ophiolite suite of the Karaali area have been plotted onto different geochemical rock classification diagrams. On the

Zr/TiO_2*0.0001 versus Nb/Y diagram of Winchester and Floyd (1977), the Karaali samples plot in subalkaline-basalt field (Figure 6.3).

Another diagram used for rock classification is the Winchester and Floyd (1977) diagram in which SiO_2 values are plotted against Zr/TiO_2*0.0001 values. In this diagram, the majority of samples are concentrated in the subalkaline-basalt field, but a few of them fall across the andesite field (Figure 6.4). However the use of this diagram may be inappropriate since the samples have undergone hydrothermal alteration, including silicification.

On the total alkali (Na_2O+K_2O) versus SiO_2 diagram (Figure 6.5a), most of the basalts and gabbros plot in the subalkaline field. Total alkali concentrations range from 2 to 6 weight percent, with the exception of one sample (KA75). This sample has an obvious deficiency of total alkalis and actually demonstrates that the total alkali concentrations of the mafic rocks collected from the Karaali area were open to and profoundly changed by hydrothermal alteration. One gabbro sample (KA22-1) falls in the alkaline field. The remaining samples plot in the subalkaline field. However, the use of the Irvine and Baragar (1971) diagram may be inappropriate since it employs major oxides, (which can seriously be affected by alteration), as the main variables.

Another diagram used for alkaline-subalkaline discrimination of samples is the Zr versus P_2O_5 diagram of Floyd and Winchester (1975). When P_2O_5 and Zr concentrations of the Karaali samples are plotted, it is seen that the results are quite similar to the previous diagram (Figure 6.5b). All samples plot at the far left of the diagram, in the tholeiitic basalt field, with their very low concentrations of P_2O_5 and Zr (P_2O_5; 0.01 to 0.12 weight % and Zr; 5 to 98 ppm). Therefore, it is understood that basalt and gabbro samples from the Karaali area are of subalkaline character.

For further subdivision of these subalkaline basic rock samples, they were plotted on AFM diagram in which total alkalis-FeO(t)-MgO are utilized (Figure 6.5c).

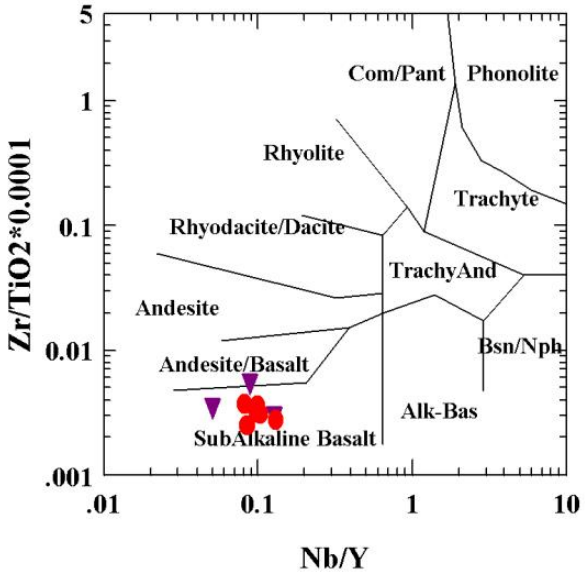

Figure 6-3. Nb/Y versus Zr/TiO2 diagram indicating the magma type of the basalt and gabbro samples (after Winchester and Floyd, 1977). (Symbols as in Figure 6.1)

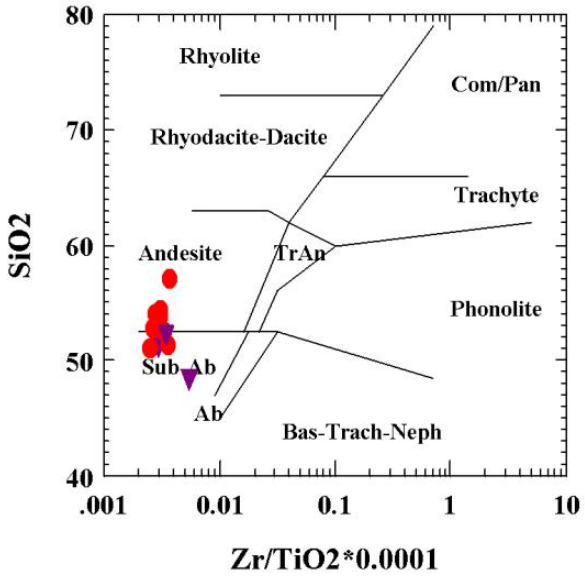

Figure 6-4. Zr/TiO2 versus SiO2 diagram of Winchester and Floyd (1977) showing the composition of basic rocks of the Karaali area. (Symbols same as in Figure 6.1)

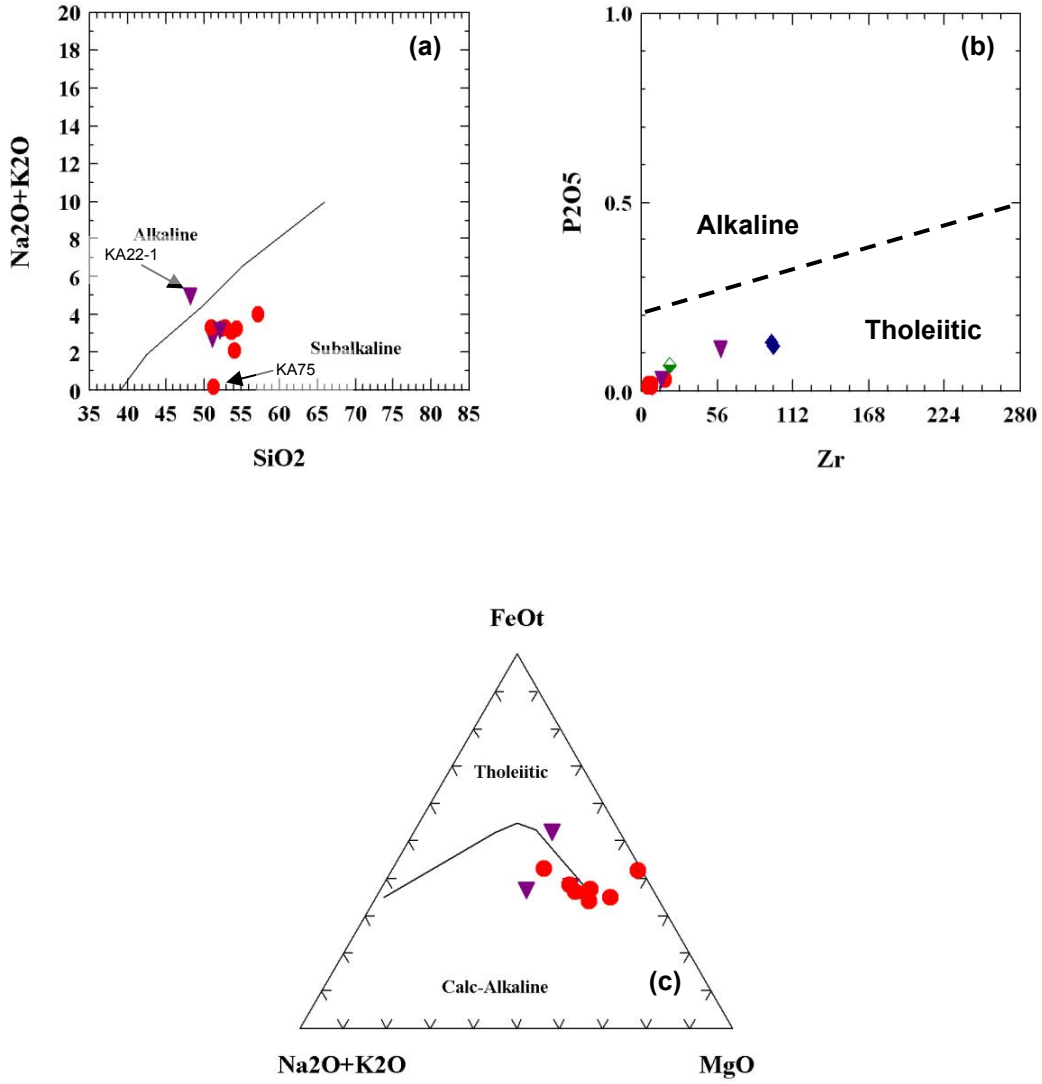

Figure 6-5. Alkalinity diagrams for the Karaali basalts. (a) Total alkali (Na2O+K2O) versus SiO_2 diagram of Irvine and Baragar (1971) classifying alkaline and subalkaline nature of basic rocks, (b) P_2O_5 versus Zr diagram of the basalt and gabbro samples (after Floyd and Winchester, 1975), showing the fields of oceanic and tholeiitic basalts, and (c) Total alkali (Na_2O+K_2O)-FeO(t)-MgO diagram of Irvine and Baragar (1971) discriminating between calc-alkaline and tholeiitic nature of basic rocks. (Symbols as in Figure 6.1)

In this diagram, the samples are usually distributed along the calc-alkaline-tholeiitic discrimination line. As noted above, sample KA75 is grossly depleted in total alkalis and plots in the tholeiitic field. One gabbro sample (KA22-1) plots in the calc-alkaline field. The remaining samples plot slightly above or below the discrimination line. However, hydrothermally altered samples are scattered, most probably due to alkali depletion and/or Mg-Fe enrichment.

6.3.2.2 Tectonic-Setting Discrimination Diagrams

Most conventionally used tectonic setting discrimination diagrams employ specific trace and rare-earth elements due to element mobility which, of course, mainly influences the major elements. The most widely used trace and rare-earth elements in tectonomagmatic discrimination diagrams are Ti, Cr, Zr, Sr, Nb, Y, Th, Ta and Hf.

As presented in Table 6.1 above, the Karaali basic rocks are significantly depleted in some of these elements, including Zr, Ta and Hf. Among these, Ta and Hf are below the detection limits and, thus, tectonic discrimination diagrams of these elements cannot be employed, whereas Zr values in some diagrams may give unusual distributions.

6.3.2.2.1 Ti versus Zr

Both Ti and Zr are truly immobile and also indicative of the differentiation stage of the magma. Accordingly, they are useful for showing the extent of differentiation. The Ti versus Zr plot of Pearce (1982) is used to discriminate between volcanic-arc, mid-ocean ridge and within-plate basalts. When the basalt and gabbro samples from Karaali region are plotted on the Ti versus Zr diagram of Pearce and Cann (1973) they mainly fall in or near the low-potassium tholeiite (LKT) field with very low Ti and Zr concentrations (Figure 6.6). Only one gabbro sample (KA22-1) plots in the field for both low-potassium tholeiites (LKT) and ocean-floor basalts (OFB).

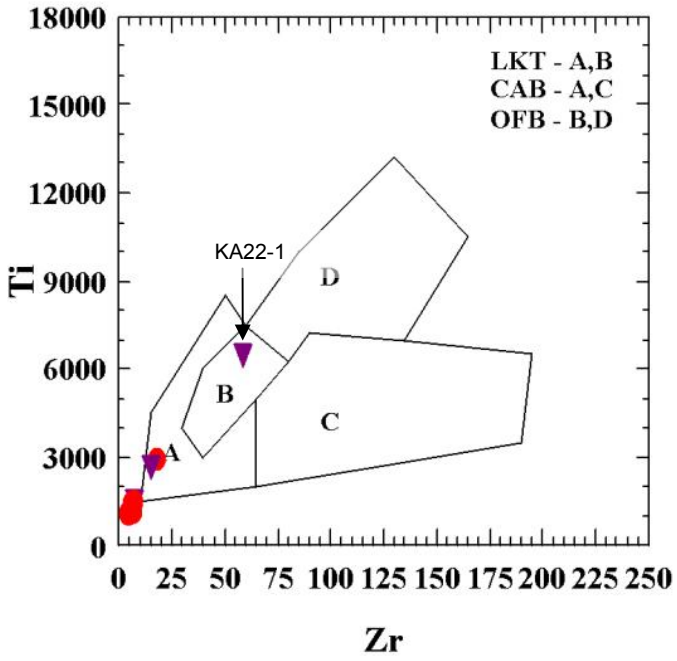

Figure 6-6. Zr versus Ti discrimination diagram of the Karaali basalts and gabbros showing the fields of low-potassium tholeiites, calc-alkaline basalts and ocean floor basalts (Pearce and Cann, 1973). (Symbols as in Figure 6.1)

6.3.2.2.2 Ti/100-Zr-Y*3

On the basis of Ti, Zr and Y contents of the basalts, Pearce and Cann (1973) introduced another tectonomagmatic discrimination diagram. With this diagram ocean-floor basalts (OFB), island-arc tholeiites (IAT) calc-alkaline basalts (CAB) and within-plate basalts (WPB) can be differentiated. In this diagram, within-plate basalts (WPB) are mainly distinguished from plate-margin basalts with their relatively higher Ti/Y and Zr/Y ratios.

On the Ti/100-Zr-Y*3 diagram, the basic rocks of the Karaali area are scattered across island-arc tholeiites (IAT) field (Figure 6.7a). The Karaali samples are characterized by low concentrations of Zr/Y against Zr content and plot in or near the island-arc tholeiites (IAT) field.

6.3.2.2.3 Ti/100-Zr-Sr/2

Pearce and Cann (1973) also proposed another tectonomagmatic discrimination diagram in which Sr is used as an additional parameter, along with Ti and Zr. Geochemically, Sr is more open to the effects of metamorphism or alteration and thus is relatively mobile compared to Ti and Zr, as noted by those authors.

The Ti/100-Zr-Sr/2 plot of Pearce and Cann (1973) discriminates well between ocean-floor basalts (OFB), island-arc tholeiites (IAT) and calc-alkaline basalts (CAB). This diagram is based on subduction-mobile elements and used to separate mid-ocean ridge and supra-subduction zone magmas, but it is alteration sensitive (Pearce, 2003).

The Ti/100-Zr-Sr/2 discrimination diagram for the studied basic rocks from the Karaali area is given in Figure 6.7b. In this plot, gabbro sample KA22-1 and basalt sample KA75 are located in ocean-floor basalts (OFB) field. The remaining samples are mainly distributed in or near the island-arc tholeiites (IAT) field.

6.3.2.2.4 Ti versus V

According to Shervais (1982), most transition metals are immobile during alteration and metamorphism with the exception of Ti and V; these elements are compatible and moderately to strongly partitioned into refractory residual phases during partial melting and into early-liquidus mafic phases during crystallization. As a result, plots of V against Ti (a commonly used discriminator) can be used for the discrimination of tectonomagmatic setting due to the differing geochemical behavior of V in different tectonic settings. This diagram accepts the fact that subduction-related lavas have lower Ti contents than mid-ocean ridge basalts (MORB) at a given V content. Important in this Shervais (1982) plot is the sensitivity of V to oxygen fugacity; it is found more in higher oxidation states of 4+ and 5+ relative to common 3+ state under hydrous subduction conditions. As a result, subduction-zone lavas have higher V concentrations than those under anhydrous mid-ocean ridge conditions. Thus, subduction-related lavas have

higher V and lower Ti contents than mid-ocean ridge basalts (MORB) (Pearce, 2003).

In the Ti versus V plot of Shervais (1982) volcanic rocks from modern island arcs (IAT) have Ti/V ratios of ≤20, whereas mid-ocean ridge basalts (MORB) and continental flood basalts (CFB) have Ti/V ratios of about 20-50 and alkaline rocks have Ti/V generally >50.

Most of the samples from the Karaali area obviously fall above the Ti/V=10 discrimination line, with low Ti concentrations, indicating an arc origin for these rocks (Figure 6.7c). Only one gabbro sample (KA22-1) has a Ti/V ratio between 20 and 50.

6.3.2.2.5 Zr/4-Nb*2-Y

As in the case of many of the tectonomagmatic discrimination diagrams mentioned above, the Zr/4-Nb*2-Y diagram of Meschede (1986) also utilizes relatively immobile elements. Different from the Ti-Zr-Y and Ti-Z-Sr diagrams of Pearce and Cann (1973), this diagram also discriminates between different mid-ocean ridge basalt (MORB) types -as normal-type MORB (N-MORB) and enriched-type MORB (E-MORB). Enriched-type MORB is also known as plume-type MORB (P-MORB). The main geochemical difference between these two types of mid-ocean ridge basalts is their different enrichment levels of incompatible trace elements. Enriched-type mid-ocean ridge basalts are, as their name implies, enriched in incompatible trace elements.

When the basic rocks of the Karaali area are plotted on the Zr/4-Nb*2-Y diagram of Meschede (1986), all samples fall into the fields for normal-type mid-ocean ridge basalts (N-MORB) and volcanic-arc basalts (VAB) (Figure 6.7d). However, in the diagram of Meschede (1986), there is a major overlap of normal-type mid-ocean ridge basalts (N-MORB) and volcanic-arc basalts (VAB), and this situation causes some uncertainties about the origin of samples distributed in this field.

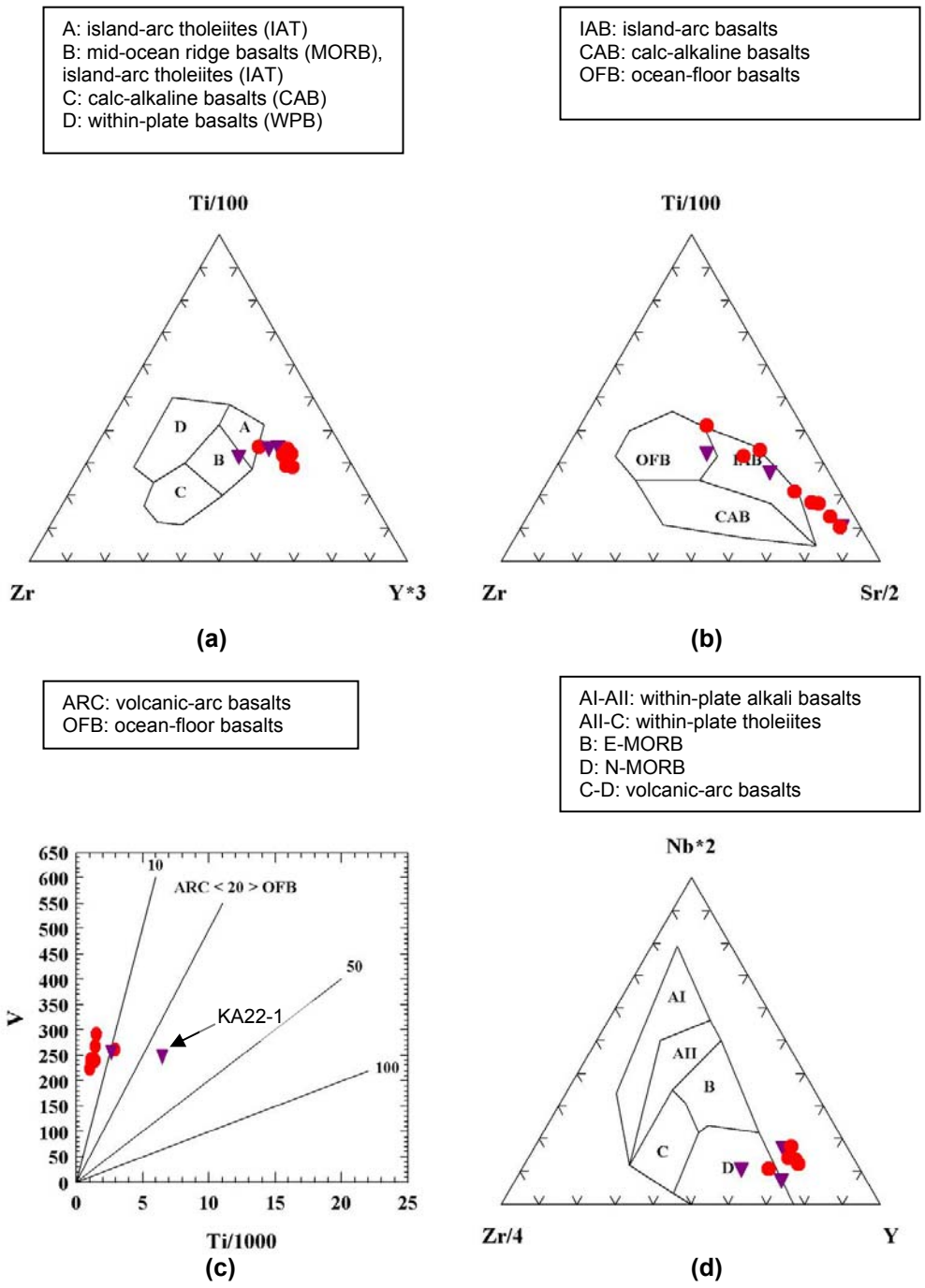

Figure 6-7. Selected tectonic discrimination diagrams of (a) Ti/100-Zr-Y*3 (after Pearce and Cann, 1973), (b) Ti/100-Zr-Sr/2 (Pearce and Cann, 1973), (c) Ti/1000 versus V (after Shervais, 1982) and (d) Nb*2-Zr/4-Y (after Meschede, 1986). (Symbols as in Figure 6.1)

A comparison of average of the selected trace-element composition of the Karaali basalts with selected tectonic settings is shown in Table 6.3. The assessment of trace-element compositions will provide a more confident approach to the origin of the Karaali basalts than major-oxide compositions. On the whole, the Karaali basalts are depleted in most trace elements as compared to N-type and E-type mid-ocean ridge basalts, island-arc tholeiitic basalts, island-arc calc-alkaline basalts and ocean-island basalts.

Relatively mobile elements such as Rb and Ba in the Karaali basalts are comparable to N-type mid-ocean ridge basalt values. As shown in the Harker plots, these two elements give scattered distributions against MgO, indicative of their susceptibility to secondary processes that modify the chemical composition of rocks. Thus, any concluding remark regarding the tectonomagmatic significance of these elements will be incorrect. When relatively immobile, high-field-strength (HFS) elements such as La, Y, Ce, Zr, Ti and Nb are taken into consideration, the Karaali basalts are seen to have strong arc-related affinities. The Karaali basalts usually display depleted trends in these elements but elemental abundances are analogous to the incompatible, immobile trace- and rare-earth element signature of island-arc tholeiitic basalts.

In most cases, the correlation of trace elements alone does not give any idea about the original tectonic setting of rocks. Geochemical imprints of secondary processes, both on major and trace elements, may mislead researchers. In order to minimize the effects of fractionation, the ratios of incompatible elements have been utilized. In this way, the character of the mantle source can be delineated, thus avoiding any interference of weathering, metamorphism or alteration.

Th is an essential element in the discrimination of subduction zones. It is generally enriched in all arc lavas, and so is mobilized in subduction zones, but is immobile until temperatures close to melting temperatures are reached. Pearce et al. (1984) reported that, during weathering and metamorphism, most elements enriched in supra-subduction zone ophiolites are mobile except Th. As a result, a ratio such as Nb/Th can be particularly useful, since these two elements behave consistently

in oceanic supra-subduction zone basalts, but behave independently in the subduction environment. Piercey et al. (2003) noted that island-arc tholeiitic magmas are characterized by distinctive negative Nb anomalies relative to Th, and by typical Nb/Th ratios between 1.8 and 5.2. Similarly, the Karaali basalts have an average of Nb/Th ratio around 3.8, which is much lower than both N-type and E-type mid-ocean ridge basalts as well as ocean-island basalts. On the other hand, the average value of 3.8 correlates well to that island-arc tholeiites.

Another useful pair of trace elements, Ce and Sr, behave similarly in MORB but, because of their differing mobilities in aqueous fluids, behave very differently in volcanic-arc basalts. Volcanic-arc basalts show enrichment in Sr relative to Ce, whereas in mid-ocean ridge basalts (MORB) Ce and Sr have very similar concentrations. The Ce/Sr ratio is therefore a useful discriminant between MORB and volcanic-arc basalts. The relative enrichment of Sr to Ce in the Karaali basalts is reflected by very low (around 0.017) Ce/Sr, similar to island-arc tholeiitic basalts.

Similar to the Nb/Th ratio, the Th/Ta ratio is principally used for the identification of subduction-related magmas. Subduction-related lavas have enriched Th relative to Ta. In addition, Yb is assumed to be immobile in an aqueous fluid and to behave as an incompatible element (and so the ratio of the two incompatible elements will remain unchanged) during partial melting and fractional crystallization. Furthermore, the same assumption is valid for the Ta/Yb ratio. Combined Ta/Yb and Th/Yb ratios are widely used in the discrimination of volcanic-arc basalts, mid-ocean ridge basalts and within-plate basalts (Pearce, 1982, postulated a well-known diagram using these ratio pairs). Volcanic-arc basalts are characterized by relatively higher Th/Yb ratios (between ~0.1 and ~1.0) and lower Ta/Yb (between 0.01 and 0.10) than mid-ocean ridge basalts and intraplate basalts.

Table 6-3. Comparison of selected trace-element composition of Karaali basaltic rocks with mid-ocean ridge and island-arc and oceanic island basalts.

	average of Karaali basalts	**N-type MORB[a]**	**E-type MORB[a]**	**island-arc tholeiites[a]**	**island-arc calc-alkaline basalts[a]**	**ocean-island basalts[b]**
Rb	**1.6**	1.0	3.9	4.6	14.0	31.0
Ba	**25**	12	68	110	300	350
K	**737**	1060	1920	3240	8640	12000
Nb	**0.8**	3.1	8.1	0.7	1.4	48.0
La	**0.85**	3.0	6.3	1.3	10	37.0
Ce	**1.7**	9.0	15.0	3.7	23.0	80.0
Sr	**102**	124	180	200	550	660
Nd	**1.1**	7.7	9.0	3.4	13.0	38.5
Zr	**8**	85	75	22	40	280
Sm	**0.4**	2.8	2.5	1.2	2.9	10.0
Ti	**1499**	9300	8060	3000	4650	17200
Y	**8**	29	22	12	15	29
Th	**0.21**	0.20	0.55	0.25	1.10	4.00
U	**0.15**	0.10	0.18	0.10	0.36	1.02
Ce/Sr	**0.017**	0.072	0.083	0.018	0.042	0.120
Nb/U	**5**	31	45	7	4	47
Nb/Th	**3.8**	15.5	14.7	2.8	1.3	12.0

Data sources: [a]Sun (1980), [b]Sun and McDonough (1989)

The Karaali basalts have Th/Yb ratios around 0.22 and Yb concentrations around 0.9 ppm. Unfortunately, Ta abundances are very low in the Karaali basalts (below the detection limit of 0.1 ppm); however, considering that Ta concentrations are lower than 0.1 ppm, the Ta/Yb ratios for the Karaali basalts have must be within the interval of 0-0.11, indicating an island-arc setting affinity.

6.3.2.2.6 Multi-element Variation Diagrams

One way of determining the tectonic setting of the studied basic rocks is to compare their trace- and rare-earth-element variations. The systematic variation in trace and rare-earth elements is best illustrated by plotting the log of the relative abundances. The use of relative abundances of elements is a must because of the Oddo-Harkins effect. According to the Oddo-Harkins effect, elements with even atomic numbers have higher concentrations as compared to those of neighboring odd-numbered elements (Wilson, 1989). Relative abundances are calculated by dividing the concentration of each element by its concentration in a set of normalizing values. This operation is called “normalizing” and eliminates effects related to nuclear stability, producing a smooth pattern.

In order to determine the tectonic setting of the Karaali basalts and gabbros, trace-element abundances of these samples were plotted on MORB-normalized multi-variation diagrams together with reference values from selected tectonic settings (Figure 6.8a and 6.8b).

At first glance, all of the basalts samples display selective enrichment in large-ion lithophile elements (LILE) such as Sr, K, Ba and Rb (all LIL elements) relative to high-field-strength elements (HFSE). As compared to mid-ocean ridge basalts (MORB), the abundances of both large-ion lithophile elements and high-field-strength elements (HFSE) are slightly depleted, around ratios of 1/2 for large-ion lithophile elements (LILE) and 1/10 for the latter. The samples, as a whole, exhibit spiked patterns for the large-ion lithophile elements, with a significant trough from Th towards Nb.

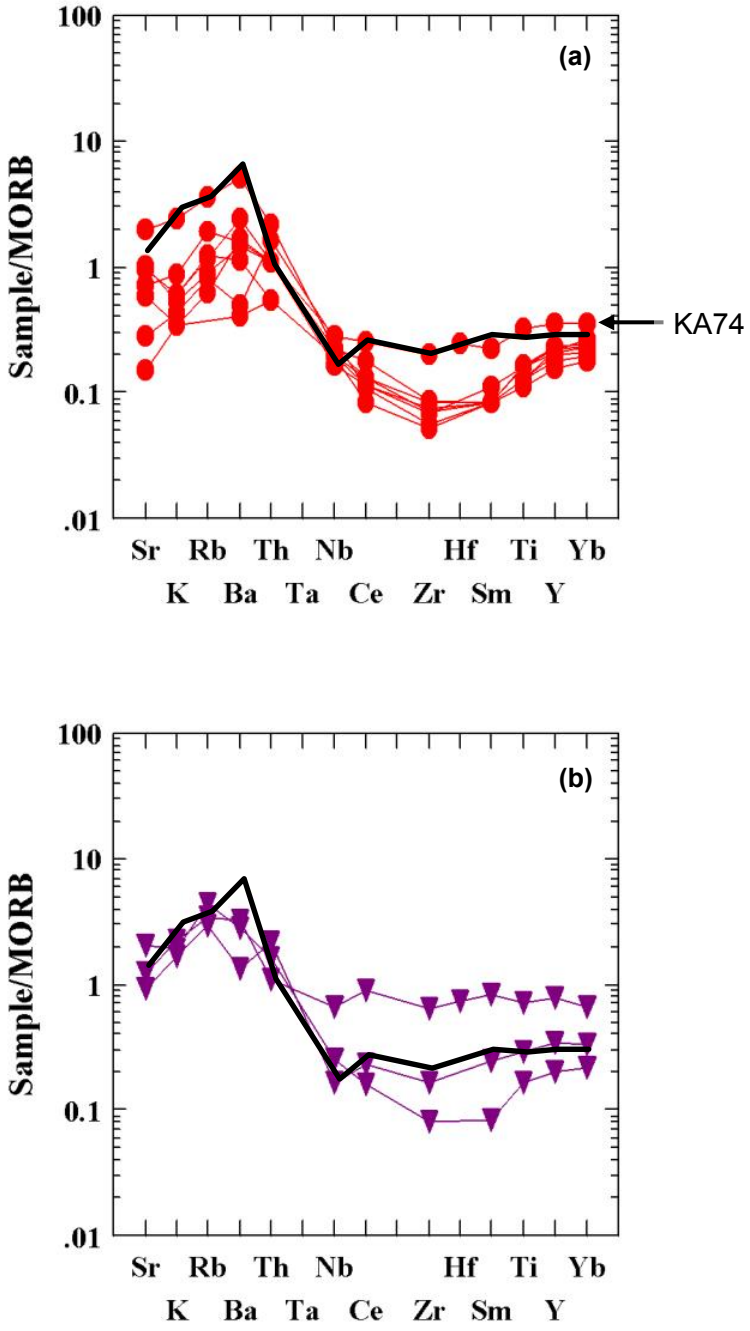

Figure 6-8. MORB-normalized multi-element spider diagram of (a) basalt and (b) gabbro samples. Black line indicates the island-arc tholeiite values of Sun (1980). Normalizing values are from Pearce (1982). (Symbols as in Figure 6.1)

Retention of Nb and Ta in subduction zones is a well-known phenomenon which is typical of arc-related magma generation (Pearce, 2003). Additionally, for high-field-strength (HFS) elements, the abundances of these samples reflect a flat trend or slightly depleted patterns. Karaali gabbro samples plotted on the same MORB-normalized spider diagram show similar geochemical trends.

A comparison between analyzed samples and typical island-arc tholeiitic magmas show that the Karaali basalts and gabbros resemble island-arc tholeiites, with their relative enrichment/depletion of selected trace elements. In general, comparatively altered samples have lower abundances of large-ion lithophile elements (LILE), whereas relatively unaltered samples have enrichment levels similar to island-arc tholeiites.

6.3.2.2.7 Rare-Earth-Element Variation Diagrams

Because the rare-earth-elements are highly insoluble and immobile, rare-earth-element patterns often remain unchanged during secondary processes such as metamorphism or alteration. Hence rare-earth-element patterns can provide information on the premetamorphic history of a rock (White, 2005). If the alteration conditions of both basaltic and gabbroic rocks of the Karaali area are considered, the use of rare-earth elements for obtaining more reliable results is seen to be inevitable. The most common reference standard to which rare-earth-element concentrations are normalized is chondritic meteorites, which are assumed to be relatively unfractionated samples of the solar system dating from the original nucleosynthesis (Rollinson, 1993).

In general, rare-earth-element patterns for island-arc basalts show a wide spectrum from light-REE-depleted, to flat, to strongly light-REE enriched. These broadly correspond to the major subdivisions between the different magma series based on K_2O content. Island-arc tholeiitic basalts are typically depleted in light-REE relative to calc-alkaline basalts. In general, the relative magnitudes of the Sr, K and Ba spikes appear to correlate with the degree of light-REE enrichment.

Typical N-type MORB has unfractionated heavy-REE abundances and is strongly depleted in light REE. Primitive basalts have REE concentrations of 10 times chondrite or less, whereas extremely differentiated basalts may contain up to 50 times chondrite. In contrast, P-type MORB shows relatively little tendency for light-REE depletion and, in some instances, are light-REE enriched. On the other hand, the REE patterns of oceanic-island basalts are characterized by varying degrees of light-REE enrichment relative to the heavy REE (Wilson, 1989).

Study of the chondrite-normalized rare-earth-element diagrams of the Karaali samples show that all samples display quite similar patterns (Figure 6.9a and 6.9b). All samples have rather flat profiles, some with slight depletions in light REE. The majority of the Karaali basalts and gabbros are selectively depleted in light rare-earth elements (LREE) relative to heavy rare-earth elements (HREE). These samples have quite similar light rare-earth-element (LREE) abundances, but their heavy rare-earth-element (HREE) concentrations are 4 to 5 times chondrite. Among these, unaltered basalt sample KA-74 and gabbro sample KD-3 are distinguished by their higher degrees of enrichment (4 times and 6 times chondrite for light- and heavy rare earth elements, respectively). The rare-earth-element plots of these samples have characteristics of normal-type mid-ocean ridge basalts (N-MORB).

6.3.3 Isotope Geochemistry

Stable-isotope geochemistry uses the natural abundance patterns of different isotopes of elements to determine how earth materials are formed and modified in their environmental settings. Elements such as H, C, N, O, and S exist in a variety of oxidation states, or form a wide variety of compounds, or are important constituents of naturally occurring solids and fluids. Thus, they are often the main constituents of geologically important fluids, affording a means of directly measuring both the fluids and the effects of fluid-rock interaction.

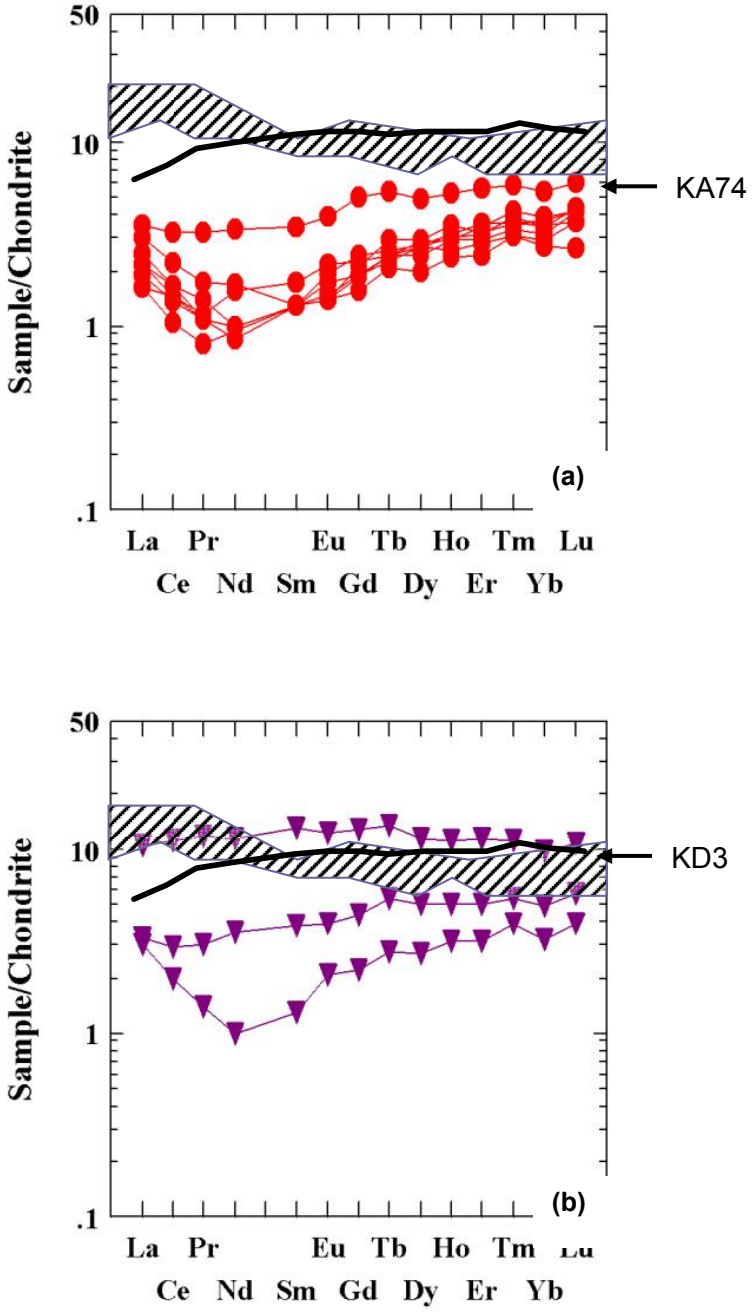

Figure 6-9. Chondrite-normalized REE distribution patterns of the Karaali (a) basalts and (b) gabbros. Black line indicates the N-MORB values of Sun and McDonough (1989). Dashed areas represent island-arc tholeiites (Wilson, 1989). Normalizing values are from Sun and McDonough (1989). (Symbols as in Figure 6.1)

In addition, stable isotopes are used as tracers to determine the source of an element, temperature of formation of a compound, or the reaction mechanism of a geological process (Rollinson, 1993).

Stable-isotope-ratio variations are typically in the parts per thousand to parts per hundred range, and are most conveniently and commonly presented as permil deviations, δ, from some standard. The standard for sulfur isotopes is the Canon Diablo Troilite (CDT) (White, 2005).

The earth's mantle is one of the two major sulfur reservoirs, and has a $\delta^{34}S$ of ~0 in which sulfur is primarily present in reduced form. The other major reservoir of sulfur is seawater, which has a $\delta^{34}S$ of +20 (for modern seawater) and in which sulfur is present as SO_4^{-2}. Sulfur in sedimentary, metamorphic, and igneous rocks of the continental crust may have $\delta^{34}S$ values that are either both greater and smaller than these values (Figure 6.10). All of these can be sources of sulfide in ores, and further fractionation may occur during transport and deposition of sulfides. Thus the sulfur-isotope geochemistry of sulfide ores is remarkably complex (White, 2005).

Sulfides have formed in a variety of environments under very different conditions. Consequently, they comprise an important part of base-metal ores. Sulfur can commonly occur in five different valence states in the Earth. These are +6, +4, 0, -1 and -2 valence states, and each of these valence states can form numerous compounds through isotopic fractionation. Finally, sulfur is important in biological processes, and in fractionations in biologically mediated oxidations in abiotic equivalents (White, 2005).

6.3.3.1 Sulfur-Isotopic Data from Hydrothermal Deposits

Knowledge of the distribution and isotopic composition of sulfur in oceanic and ophiolitic crust is important to understanding the role that submarine hydrothermal systems play in the cycling of sulfur in the oceans through geologic time. One of the most comprehensive works on the systematics of sulfur isotopes is the study

of Ohmoto and Rye (1979). This study provides a broad review of both theoretical aspects and applications of sulfur-isotope studies to a variety of deposits. In most cases, sulfur isotopes have been used for determination of temperature and the mechanism of sulfide deposition, as well as the origin of sulfur in these deposits.

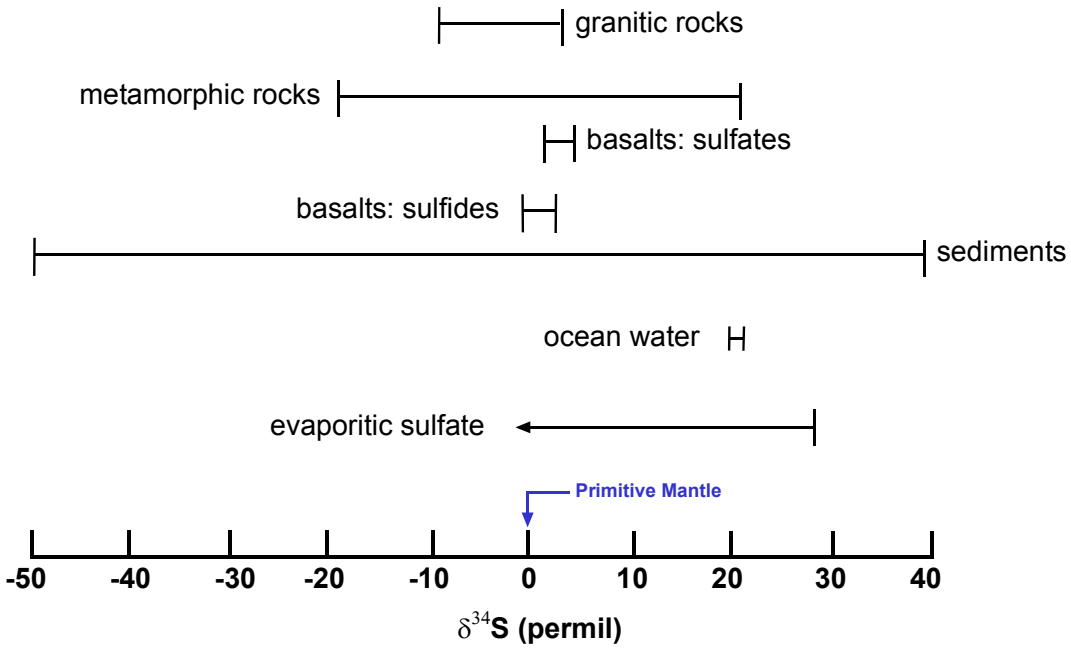

Figure 6-10. $\delta^{34}S$ abundances in various geologic materials (modified from Hoefs, 1987).

Ohmoto and Rye (1979) interpreted the source of sulfur in ore deposits according to their discrete $\delta^{34}S$ values. For example, ore deposits with $\delta^{34}S$ values near 0‰ were interpreted to have formed from magmatic fluids, whereas deposits in which $\delta^{34}S$ values were variable (e.g., more than 10‰) were interpreted as biogenic.

The same study suggested that the origin of sulfur in hydrothermal ore deposits, which is usually fixed as sulfide and/or sulfate minerals, can be (1) an igneous source and/or (2) a seawater source. The former includes (a) sulfur carried in

magmatic fluids and (b) sulfur obtained by leaching of sulfur-bearing minerals in igneous rocks.

Seawater sulfur is found as aqueous sulfates and may be incorporated into sulfide deposits through various paths. In environments near the earth's surface, *in situ* reduction of sulfate to H_2S by sulfur-reducing bacteria generates sedimentary sulfides. These sedimentary sulfides may then be leached by hydrothermal fluids, or they may be replaced by other sulfide minerals when encountered by metal-carrying brines. Reduction of aqueous sulfates to aqueous sulfides can also take place non-bacterially at elevated temperatures. Therefore, sulfate-bearing seawater, "sulfate-rich" connate water, or meteoric waters bearing sulfate dissolved from marine evaporates can evolve into sulfide-bearing hydrothermal fluids (Ohmoto and Rye, 1979).

There are several mechanisms of sulfur-isotope fractionation past record of an ore fluid. Isotopic fractionation may take place (1) at the source of sulfur, such as during separation of fluids from a magma, or during leaching of sulfides; (2) during the evolutionary history of hydrothermal fluids involving reduction of seawater sulfate; (3) during cooling of hydrothermal fluids; and (4) during precipitation or replacement of minerals (Ohmoto and Rye, 1979).

The sulfur-isotopic compositions of massive-sulfide deposits typically display relatively narrow ranges. Generally individual ore types (massive or disseminated) display much narrower isotopic ranges than deposits consisting of different ore types. Most massive-sulfide deposits have sulfide compositions that are either very close to zero per mil, -the composition of primary standard Canon Diablo Troilite (CDT), -or else are enriched in ^{34}S (Franklin et al., 1981).

Massive-sulfide deposits that occur in volcanic rocks are generally thought to be related to submarine volcanism and formed at or near the seawater-rock interface. The $\delta^{34}S$ values of sulfides in these deposits are typically positive, except for the very late stages of mineralization in some deposits, such as the Kuroko deposits (Ohmoto and Rye, 1979). Sangster (1968) examined the isotopic signature of a

number of Kuroko-type deposits and noted that the average $\delta^{34}S$ values of sulfides in each deposit were approximately 17‰, lower than the $\delta^{34}S$ value of the contemporaneous seawater, and suggested that the sulfides in this type of deposit formed by mixture of magmatic sulfur and H_2S (or HS^-) produced by bacterial reduction of seawater sulfate.

6.3.3.2 Source of Sulfur

From Karaali, six samples were analyzed-four of which belong to the zone of main the massive orebody and two that are representative of the vein-type mineralization. The sulfur-isotopic compositions of the Karaali massive sulfides seem to be restricted in a narrow range (between 1.9 and 6.8 per mil) (Table 6.4).

Table 6-4. Sulfur-isotopic data from ore-bearing samples from Karaali.

Sample no.	Mineral	Description	S (%)	$\delta^{34}S$(‰) (CDT)
I-1	pyrite	vein-type ore	2.3	4.5
I-2	pyrite	massive pyrite ore	53	1.9
I-3	pyrite	massive pyrite ore	40	5.1
I-4	pyrite	massive pyrite ore	48	2.2
I-5	pyrite	massive pyrite ore	56	2.4
I-6	pyrite	vein-type ore	1.7	6.8

Vein-type ores have greater $\delta^{34}S$ values (average 5.6 per mil) relative to the $\delta^{34}S$ values of massive ores (average 2.9 per mil). The $\delta^{34}S$ values of sulfide in the massive and vein-type ores of Karaali average about 3.7‰, and these values are very close to those of sulfide deposits from modern mid-ocean ridges, which average around +3‰. Sulfide deposits of the East Pacific Rise are a good example of such present-day seafloor sulfide deposits, and previous studies (e.g., Arnold and Sheppard, 1981; Styrt et al., 1981; Shanks and Seyfried, 1987; Bowers, 1989) have shown that there is a strong contribution of magmatic sulfur,

as much as 90%, with little contribution from reduced seawater sulfate (Figure 6.11). Therefore, the sulfur-isotope data strongly suggest that the source of sulfur for the Karaali ores was a mixture of magmatic-sulfide sulfur leached from the volcanic host rocks during hydrothermal convection processes -and of seawater-derived sulfur. However, since the $\delta^{34}S$ values are much closer to that of magmatic sulfur in basic igneous rocks, it is suggested that this was the dominant sulfur source.

6.4 Fluid Inclusions

6.4.1.1 Introduction

A fluid inclusion is a cavity, with or without negative crystal faces, containing one or two fluid phases (L), a gas phase (V) and possibly one or more minute crystals (S), in a host crystal. Fluid inclusions are widely used in geological applications, including mineral deposits studies since they are almost ubiquitous in geologic samples (Roedder, 1984).

Via the use of fluid-inclusion investigations in mineral-deposits studies, the temperature of formation of an ore deposit, pressure conditions, and the composition and density of the ore-bearing fluids can be determined (Roedder, 1984).

On the basis of their origin, fluid inclusions can be divided into three main groups: primary, secondary and pseudosecondary. Primary inclusions form during primary crystal growth, often along growth zones. Secondary inclusions are the result of the healing of fractures formed at some time later than the crystal growth. On the other hand, pseudosecondary inclusions form during the healing of fractures formed during crystal growth (Roedder, 1984).

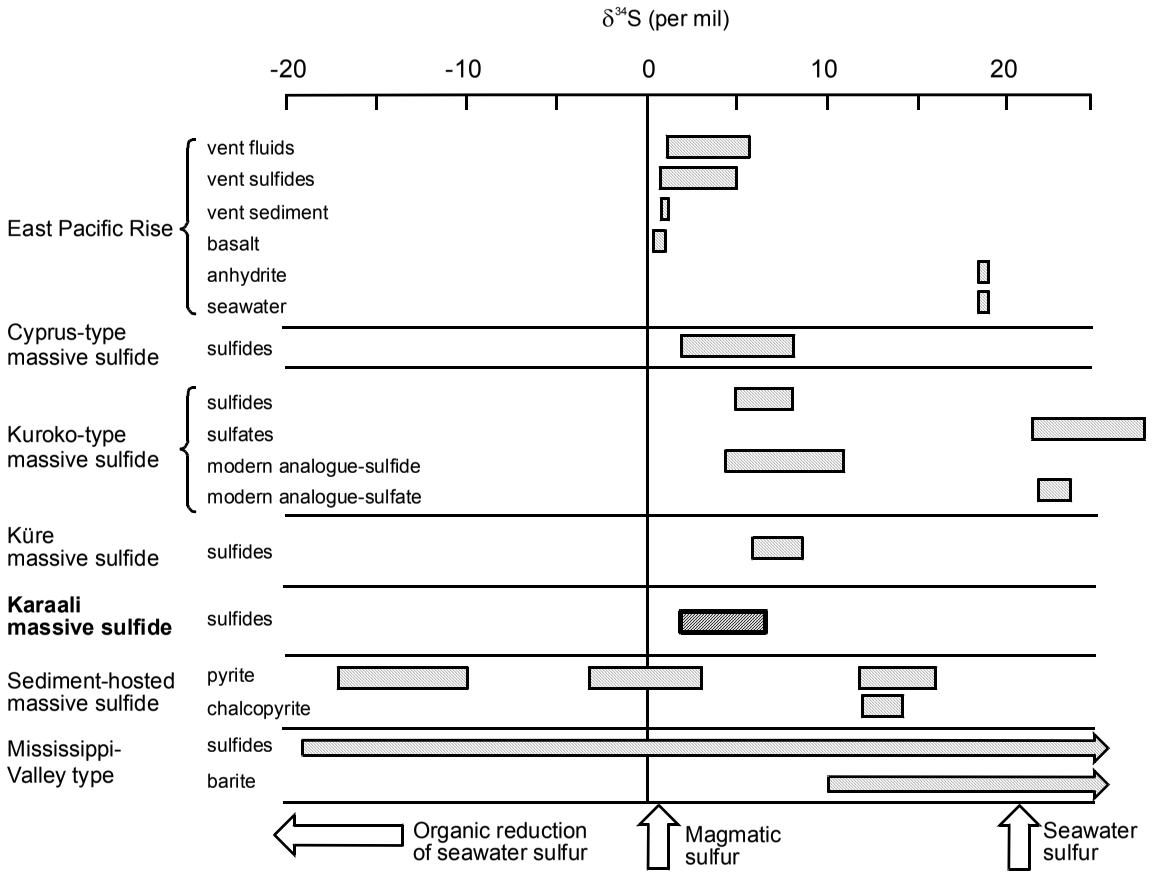

Figure 6-11. $\delta^{34}S$ values for sulfur-bearing minerals in massive-sulfide deposits (modified from Rollinson, 1993; data for the Küre massive sulfides is from Erler et al., 1994).

Several attempts have been made by different authors to classify fluid inclusions, and the Sheppard et al. (1985) classification of fluid inclusions on the basis of their compositions is one of the most conventional of all classification systems:

1. Single-phase (L),
2. Two-phase inclusions (L+V), containing liquid phase with minor gas phase,
3. Two-phase inclusions (V+L), gas phase and liquid phase with the amount of the gas phase more than 50% of the inclusion,
4. Single-phase (V),
5. Multi-phase (S+L±V),
6. Immiscible two-phase (L1+L2±V).

6.4.1.2 Microthermometric analysis

Petrographic examination of vein-mineralized samples from Karaali revealed that the sulfide-bearing quartz veins consist of the main sulfide phases pyrite, and chalcopyrite, with minor sphalerite. Other than early stage coarse-grained quartz, the samples also contain significant amounts of dolomite and late-stage microcrystalline quartz. On the basis of petrographic studies, sphalerite and coarse-grained quartz seem to be syngenetic with the formation of quartz-sulfide stockworks, whereas dolomite and microcrystalline quartz are products of another hydrothermal event. Fluid inclusions within the quartz crystals are mostly secondary or pseudosecondary whereas dolomite crystals contain well-developed primary inclusions together with secondary inclusions. Consequently, microthermometric measurements were performed using only dolomite crystals for the estimation of the temperature conditions of a late-stage hydrothermal event.

Dolomite in the sulfide-bearing quartz veins of Karaali contains both single-phase and two-phase inclusions. The single-phase inclusions consist of gas phase (Type 4), while the two-phase inclusions are composed of liquid and gas (L+V) (Type 2). In the majority of inclusions, the gas phase is mobile at room temperature. Samples contain both primary and secondary inclusions. Primary inclusions are two-phase, whereas single-phase inclusions are observed in the form of

secondary inclusions mainly developed along fractures in the crystals. Homogenization-temperature measurements were obtained from the primary fluid inclusions. Homogenization in the inclusions occurred in the liquid phase, and the gas phase generally occupies 3-5% volume of the inclusions. Inclusion sizes vary between 8 and 25μm.

Dolomite in the sulfide-bearing quartz veins of Karaali contains primary Type 2 (L+V) fluid inclusions with low Th values (83-103.5°C) as well as secondary Type 4 (G) inclusions. The average homogenization temperature from the dolomites is 92.1°C, indicative of a low-temperature crystallization environment (Figures 6.12a, 6.12b, 6.13 and Table 6.5).

When three samples (KA-101, KA-102 and KA-104) are examined separately on the basis of homogenization temperature of the inclusions, it can be suggested that the dolomite crystals in these samples crystallized under the same environmental conditions.

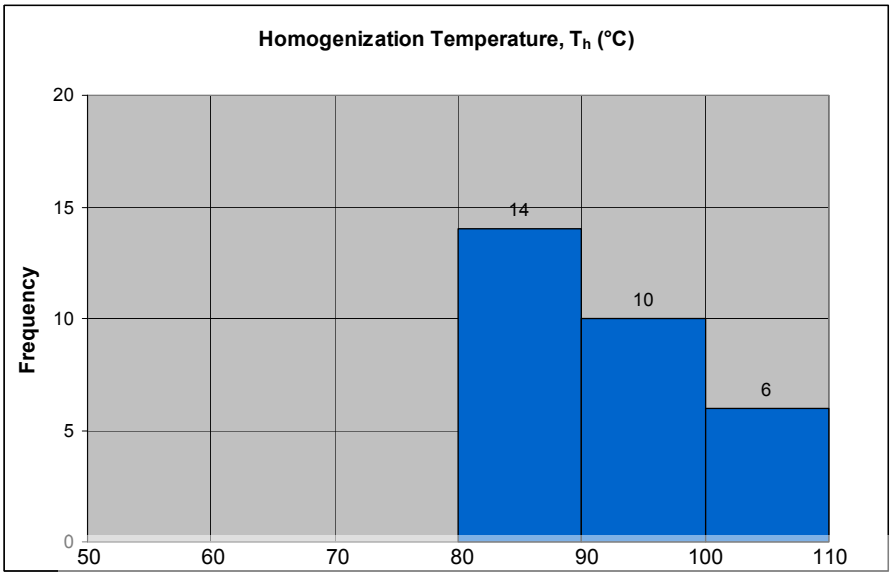

Figure 6-12. Scatter diagram showing the distribution of microthermometric data obtained from dolomites in samples KA-101, KA-102 and KA-104 with respect to homogenization temperature (Th).

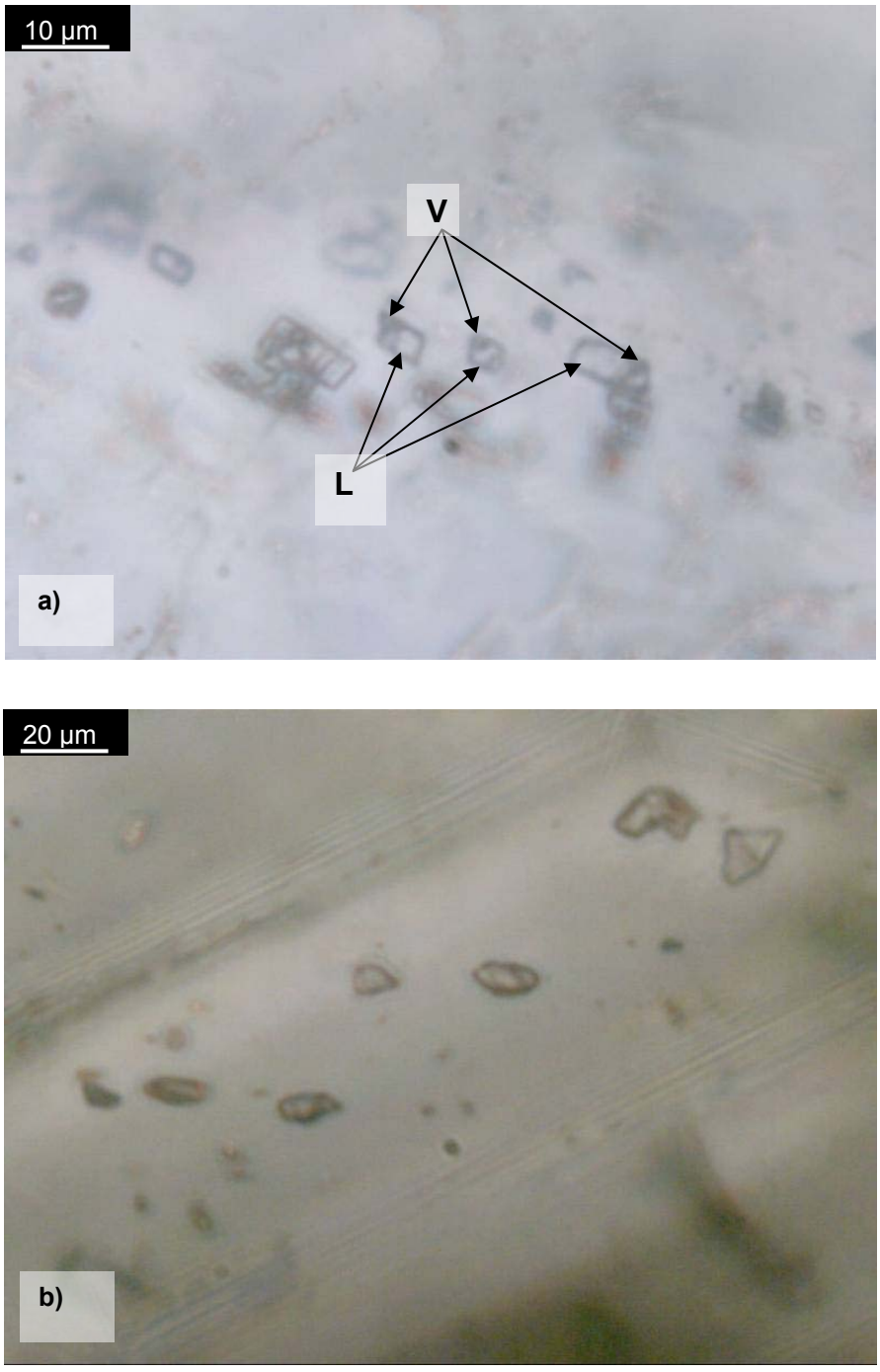

Figure 6-13. Photomicrographs of (a) primary, two-phase (L+V) (Sample KA-101) and (b) primary, single phase (V) (Sample KA-102) inclusions in dolomite crystals.

Table 6-5. Fluid-inclusion data from selected dolomite crystals.

Sample no.	Inclusion no.	Mineral	Type	Homogenization Temperature, T_h(°C)
KA101	1	dolomite	primary	83.6
KA101	2	dolomite	primary	102.7
KA101	3	dolomite	primary	82.7
KA101	4	dolomite	primary	83.5
KA101	5	dolomite	primary	83
KA101	6	dolomite	primary	84.7
KA101	7	dolomite	primary	86.4
KA101	8	dolomite	primary	93.2
KA101	9	dolomite	primary	90.5
KA101	10	dolomite	primary	89.7
KA101	11	dolomite	primary	97
KA102	1	dolomite	primary	97.4
KA102	2	dolomite	primary	88
KA102	3	dolomite	primary	96
KA102	4	dolomite	primary	89.8
KA102	5	dolomite	primary	101
KA102	6	dolomite	primary	87
KA104	1	dolomite	primary	93
KA104	2	dolomite	primary	89.9
KA104	3	dolomite	primary	91
KA104	4	dolomite	primary	83
KA104	5	dolomite	primary	84.6
KA104	6	dolomite	primary	101.2
KA104	7	dolomite	primary	90.4
KA104	8	dolomite	primary	88.6
KA104	9	dolomite	primary	98
KA104	10	dolomite	primary	98
KA104	11	dolomite	primary	102
KA104	12	dolomite	primary	103.5
KA104	13	dolomite	primary	103.5
AVERAGE				**92.1**

The minimum homogenization temperature obtained from sample KA-101 is 82.7°C whereas the maximum homogenization temperature is 102.7°C. The average of the homogenization temperatures from KA-101 is 88.8°C. In sample KA-102, the minimum homogenization temperature acquired from the primary inclusions in the dolomite crystals is 87°C while the maximum recorded is 101°C with an average of 93.2°C. Finally, sample KA-104 gave minimum and maximum homogenization temperatures of 83 and 103.5°C, respectively with an average of 94.4°C.

CHAPTER 7

DISCUSSION & CONCLUSIONS

7.1 Field Geological Constraints

The Fe-Cu sulfide mineralization in the vicinity of Karaali village developed within a partially preserved, strongly dismembered and, significantly imbricated ophiolitic megablock. The megablock belongs to an ophiolitic mélange belt signifying a suture zone, namely the İzmir-Ankara-Erzincan Suture Zone, which was developed during the closure of Neo-Tethys.

Regional tectonic activity that occurred between the time of formation of the ocean- crustal material and the time of closure of Neo-Tethys had a strong influence on the present tectonic position and the internal structure of the ophiolite block that lies between Karaali and Beynam villages.

The imbricate slices were thrust southerly over one another, partially preserving the ophiolite's internal structure, and producing a pseudostratigraphy in which basaltic lavas (lower basalt unit, B1) underlie slices of serpentinite and pelagic limestone. These tectonic slivers are overlain by another zone of massive and pillowed basaltic lavas (upper basalt unit, B2) and, finally, at the top, by gabbro and diabase. Along tectonic contacts the rocks are highly deformed and sheared, locally forming well-developed slickensided or brecciated zones.

One striking feature of the ophiolitic assemblage at Karaali is its lack of sheeted dikes. Although it has been both physically and chemically modified, the Karaali ophiolitic block should retain at least a remnant of the sheeted dikes if any were present originally. However; neither in the Karaali area nor in the other localities

where ophiolitic fragments are partially/completely preserved (i.e., Eldivan), is there any evidence of a well-developed sheeted dike complex.

The upper basalt unit (B2) is the most widespread lithology within the ophiolitic block, and it is the unit that hosts the massive-sulfide mineralization. Sulfide mineralization is confined to a narrow zone within the altered and deformed lava outcrops. A mound-shaped massive sulfide lens is located in this zone. This lens is approximately 50 m long and 30 m wide and surrounded by a zone of intensive leaching. Mineralization in the sulfide lens consists mainly of pyrite with lesser amounts of chalcopyrite, secondary hematite and subordinate bornite and covellite. Apart from the massive-sulfide lens, anastomosing, sulfide-bearing quartz veins are found in the area as vein-type and veinlet/disseminated mineralization. The veins are mainly filled with fine to coarse crystals of quartz, and the mineral paragenesis is almost as same within the massive sulfide lens.

The distribution of sulfide mineralization in the Karaali region is controlled by the main structural features of the host and adjacent rocks. Fault-hosted veins have strikes conformable to the general trend of the thrust zones that separate the various ophiolitic rocks. Two vein-type sulfide occurrences have been identified in the study area to date: a 10-m-thick alteration zone within Karaboyalık Stream, and a poorly mineralized vein-type occurrence in Karanlık Stream, both of which strike N80°E. Just to the north of the main massive-sulfide orebody another set of quartz veins with strikes of N80°W are devoid of any ore minerals; this evidence supports the theory of structural control of the mineralization.

An important geological factor that influence of the development and preservation of massive-sulfide mineralization at Karaali is the mélange character of the host and adjacent rock assemblages. Since mélanges are the products of strong tectonic processes, the primary features (both chemical and physical) of the lithologies within a mélange are significantly modified. Accordingly, metallic mineralization hosted by mélanges reflects the overprints of the associated tectonic processes.

Laznicka (1985) investigated the major mineralization styles within various mélanges and genetically classified them as: (1) relict mineralization formed outside the mélange and unchanged during the process of incorporation (except for a dismemberment); (2) relict mineralization, modified after incorporation into mélange; (3) mineralization newly formed within a mélange, largely by internal processes; (4) mineralization formed within a mélange as a result of interaction with outside agents.

When the Karaali massive-sulfide mineralization is examined from such a perspective, it can be associated with genetic model (2) in which several small occurrences of “Cyprus-type” massive and vein-type pyrite-chalcopyrite sulfide deposits hosted by metabasalts were incorporated into a mélange, dismembered and slightly remobilized. Although the first category also involves Cyprus-type massive pyrite-chalcopyrite deposits hosted by metabasalt, spilite or diabase, there is strong evidence that the Karaali mineralization has been slightly “remobilized” since the original time of formation. More clearly, pelagic limestones adjacent to the upper basalt unit (B2), which hosts the sulfide mineralization, are locally (especially in the vicinity of the main orebody) covered by sulfide-bearing coatings containing copper, suggestive of a possible remobilization of previously developed sulfide mineralization. If this was indeed the case, previously formed sulfide phases may have been remobilized from the basalts and moved between successions via fault-hosted veins that developed during tectonic deformation that followed the original ore formation. Nevertheless; such a scenario should be supported by geochemical evidence, especially by microthermometric and compositional analyses of fluid inclusions from the vein-type mineralizations.

7.2 Chemical Constraints

7.2.1 Hydrothermal Alteration vs. Ocean-Floor Metamorphism

Ophiolites, pieces of oceanic crust (or analogues thereof) emplaced on continents, are unsurprisingly in close association with fluids (mostly sea water) owing to their

original submarine positions. Interaction of rocks, especially basalts, gabbros and sheeted dikes comprising the uppermost part of an ophiolite sequence; with water is an unavoidable process, and this interaction in many cases brings about profound mineralogical and geochemical modifications. Circulating fluids, penetrating into the ocean crust, play the main role in the heat and chemical exchanges within rock units.

During its life span, until its recycling into the mantle by subduction since being emplaced by accretion, oceanic crust is affected by various alteration processes resulting from its interaction with seawater at sea-floor conditions and sea-water-derived fluids under hydrothermal conditions. Both processes of sea-floor metamorphism and hydrothermal alteration stem from rock/fluid interaction, so their outcomes are somewhat analogous. The term “water/rock ratio” is used to denote the volume of water that has flowed through a particular unit volume of rock during metamorphism; and where the water/rock ratio is high, the rock reacts so extensively with the fluid that it begins to take on a mineralogy and chemical composition that is dictated by the chemistry of the fluid as much as by the original nature of the rock (Honnorez, 2003). Mass and heat exchange between rocks gives rise to modifications in chemical composition of rock which can straightforwardly be investigated via mineralogical and geochemical observations. In some cases the discrimination of these different processes becomes very difficult and researchers may be mistaken because of similarities.

According to Honnorez (2003), ocean-floor metamorphism and hydrothermal alteration differ with their varying degrees of intensity, yet they are two end members of a wide range of water–rock interactions under hydrothermal conditions. They correspond, respectively to distal and non-pervasive, and proximal and pervasive cases of hydrothermal reactions between oceanic crustal rocks and discharges of seawater-derived solutions.

In their recent study of the Troodos ophiolite and its massive-sulfide deposits, Cann and Gillis (2004) recognized three sequential stages of hydrothermal circulation and hydrogeological flow. These episodes are:

1. High-temperature hydrothermal circulation close to the spreading axis that formed black smokers, sulfide deposits, and metalliferous sediments. These are underlain by stockwork zones and alteration pipes within the volcanic sequence, in which anastomosing sulfide-quartz veins cut hydrothermally altered basalt. These pipes are cored by fractured and very intensely altered basalt, chemically modified at greenschist-facies conditions.

2. Intermediate-temperature circulation within crust a few hundred thousand to a few million years old. The discharge sites of this circulation are marked by silicification and gold enrichment of basalts and the overlying umbers. At some of the discharge sites, pyrite was precipitated during the silicification, perhaps from solutions at higher temperatures. During discharge, the underlying extrusives were altered at low temperature to clays.

3. Long-term, off-axis circulation in the lavas, sheeted dikes, and gabbros. Temperatures in sheeted dikes and gabbros decreased from axial values, and fluid flow became highly localized within fault zones. In the lavas, an oxidative alteration front migrated down into the volcanic sequence, creating a zone of pervasive alteration and carbonate cementation. The thickness and distribution of this zone was controlled by the original sea-floor morphology, the rate and nature of sedimentation, and the duration of open circulation.

As can be well understood from the above explanation, volcanic rocks on the sea-floor and underlying dikes and gabbros are generally under the influence of weaker, sea-floor metamorphism due to long-term seawater circulation. This is a widespread situation observed in ancient and modern oceanic crustal materials whereas the formation of sulfide deposits, black smokers and metalliferous sediments are products of local, high-temperature hydrothermal circulation ascribed to hydrothermal alteration. Discriminating between alteration and metamorphism is a matter for detailed study that combines the petrographical, geochemical, isotopic and fluid-inclusion signatures of rock units (since one of these processes may overprint the others). Generally, hydrothermal alteration is

more intense and spatially restricted to rocks at or near active or fossil upwelling zones of hydrothermal discharges.

7.2.2 Petrographical and Geochemical Constraints

Field and petrographic analyses of basalt and gabbro samples from the Karaali area suggest that the basic rocks of the study area, as a whole, were under the influence of pervasive low-grade ocean-floor metamorphism. Apart from this, signatures of hydrothermal alteration, which was once operative, are evident around the zone of mineralization. Unlike metamorphism, hydrothermal alteration is restricted to the basaltic lavas, and in part to the fine-grained gabbros, and locally occurs around the massive orebody. However, hydrothermal alteration strongly overprints ocean-floor metamorphism proximal to the site of mineralization. Overall mineralogical modifications in the Karaali area related to secondary processes will be discussed under the “Alteration Mineralogy” heading.

In general, the Karaali basic rocks are characterized by the metamorphic mineral assemblages of quartz + calcite + albite + chlorite ± epidote ± actinolite ± prehnite ± titanite. This assemblage is representative of sub-greenschist-to-greenschist facies pressure and temperature conditions, typical of altered ophiolitic rocks. The relative proportions of these minerals may show variations from one sample to another elucidating overall alteration zones, but the mineral assemblages are more or less the same in all samples.

Spilitized pillow basalts that host the sulfide mineralization are black-dark green but, as a consequence of hydrothermal alteration, typically grayish-green in the field. These rocks are characterized by vesicles filled with secondary minerals, such as quartz, calcite and epidote. Actually, the primary mineral phases are almost completely diminished in the basalts although their primary igneous textures are partially preserved. Therefore, emphasis in research should be given to secondary mineralogies as indicated by different alteration styles, and their influences on the chemistry of basaltic rocks.

The primary mineralogy of the spilitic basalts involves mainly plagioclase feldspar and pyroxene. Relict olivine is observed in only a few of the samples. Except in areas of the most intense alteration, primary igneous textures are partially preserved.

Plagioclase, which occurs both as phenocrysts and as a groundmass constituent, is the most abundant mineral in the basalt samples. The original composition of plagioclase seems to have been labradorite but only scarce relict labradorite crystals appear to have survived in the least-altered basalt samples. Plagioclase is widely replaced by albite and less commonly by chlorite and prehnite as a result of hydrothermal alteration. The other primary mineral, clinopyroxene, is found both as phenocrysts and groundmass material. Broken pieces of pyroxene phenocrysts are scattered throughout the groundmass. Colorless to pale green pyroxenes are augitic. Phenocrysts of clinopyroxene are usually replaced by chlorite, epidote and actinolite.

7.2.2.1 Alteration Mineralogy

Together with the metamorphic assemblages that originated from low-temperature ocean-floor metamorphism, well developed alteration haloes have been observed around the massive orebody and the mineralized veins near Karaali. The intensity of alteration gradually increases towards the mineralization zone.

Looking at the alteration styles in the basalts, propylitic alteration is the most widespread. Propylitic alteration, in general, is a complex alteration type consisting of different alteration subtypes such as chloritization, albitization and carbonitization; thus obviously comprising chlorite, albite, carbonate (calcite, dolomite or ankerite) with chlorite. Minor sericite, pyrite and magnetite may also be present in propylitized rocks (Evans, 1993). Propylitized basic igneous rocks of the study area are dominated by the alteration minerals mentioned above.

In the outermost zone, a background alteration is present with an assemblage of albite+chlorite+epidote+quartz+calcite. These are representative of typical ocean-

floor metamorphism at greenschist-facies pressure and temperature conditions. However, such an assemblage may have originated by hydrothermal alteration of basic rocks, and the immediate host rocks can be hydrothermally altered in this facies. Thus, there may be an overprinting of propylitic alteration zones in metamorphosed basic lavas and hydrothermally altered basic lavas.

In the chlorite-rich zone, primary ferromagnesian mineral phenocrysts (chiefly clinopyroxene and olivine) are pseudomorphed by chlorite. Scarce olivine crystals are almost totally replaced. Chlorite also substitutes for clinopyroxene in angular interstitial areas throughout the groundmass. Furthermore, considerable amounts of chlorite occupy amygdules, found in association with epidote, calcite and quartz. Actinolite is another alteration product of clinopyroxene; it is present as fibrous aggregates or small needle-like crystals, and generally replaces pyroxene-rich groundmass material.

As mentioned previously, plagioclase was labradorite in its original composition but plagioclase crystals preserving their original features (scarce are only in the least altered samples). Calcic-plagioclase feldspars are almost entirely converted to sodic plagioclase (albite). Albitization is a widespread process in the studied basalts; almost all samples are strongly albitized. Fine, fibrous albite crystals are widely distributed throughout the groundmass. Other than albite, plagioclase feldspars are also replaced by chlorite and partially by prehnite as a result of hydrothermal alteration. Calcic-plagioclase phenocrysts are locally replaced by epidote, found in clusters in the groundmass or as an infilling material of amygdules. Calcium provided to the system by the hydrothermal fluid (sea water in this case) triggers the formation of epidote in the basaltic rocks.

Reaction with sea water implies further addition of calcium and silica and, as expected, formation of carbonate minerals and quartz. Where albite is not observed in the samples, calcite is the major alteration product. Carbonitization took place in the later stages of hydrothermal alteration. Large calcite crystals are widely distributed in the groundmass and are the chief infilling material of amygdules, along with quartz. Silicification in the basalts occurs as

microcrystalline quartz aggregates in the groundmass and in veinlets or large quartz crystals occupying the amygdules. From cross-cutting relationships among minerals, it can be stated that calcite replaced epidote and, inturn, was replaced by quartz.

The propylitized rocks are generally chlorite-rich, and the abundance of epidote minerals is relatively lower than chlorite minerals. Humphris and Thompson (1978) suggested that propylitized basic rocks can be either chlorite- or epidote-rich, and formation of chlorite-rich assemblages requires a source of magnesium, and so that these rock types must be formed while the sea-water composition is still relatively unchanged, (i.e. at an early stage in the history of circulating fluid). However, the alteration of a basaltic flow to an epidote-rich assemblage takes place with very little compositional change, thus, the reacting fluid could have been one in which much of the magnesium had been replaced by calcium due to previous uptake of magnesium into chlorite. The fluid could then provide an additional source of calcium, if required, for the formation of abundant epidote. Therefore, in light of this information, the chlorite-rich assemblages in the propylitized Karaali lavas suggest that they were formed in the earlier stages of hydrothermal-fluid circulation (Humphris and Thompson, 1978).

Massive-sulfide deposits consist of stringer zones which are discordant vein-type sulfide mineralization comprising anastomosing sulfide and quartz veins. These stockwork zones narrow downwards, and become poorer in pyrite, and contain only a few percent of pyrite. At this level the term “stockwork” becomes inappropriate, and “alteration pipe” is used as an alternative (Cann and Gillis, 2004).

At Karaali, the sulfide-bearing quartz veins are well-defined and extend for about 100 m (from northeast to southwest) on the east side of the massive orebody. It is characterized by several intertonguing veins which are 2 to 3 cm in thickness. Two different generations of veins are observed in the study area. The first group consists of ore minerals pyrite, and chalcopyrite with minor sphalerite in association with quartz. These veins later underwent weathering under oxidizing

conditions, and local malachite patches formed coevally. The second group of veins are closely associated with the first group; however, they are totally barren, devoid of ore minerals. The main mineral in these veins is quartz. The barren veins may have formed slightly before or after the formation of the mineralized veins.

The part of vein-mineralized zone is distinguished by its intensely altered basaltic rocks, which are mainly yellow or green in color. The alteration minerals in this zone are mainly quartz, chlorite, sericite, kaolinite and hematite. Sericite and kaolinite formed later than the other minerals, indicating that these rocks suffered late-stage argillic alteration. Because of the intensity of alteration, rocks of this zone the lack primary minerals and textures. Towards the margins of this zone, the effects of hydrothermal alteration cease and, instead, an assemblage of typical low-temperature ocean-floor metamorphic minerals occur.

The mineralogical aspects of ocean-floor metamorphism and hydrothermal alteration were mentioned above. Nevertheless, there is another zone of secondary minerals that is not related to any hydrothermal process but, rather, formed as a consequence of leaching of some metals in the orebody by surface waters percolating downward. This process is called supergene enrichment and causes deposition of some residual ferric hydroxide minerals, known as “gossan” (Evans, 1993). On the northeast side of the abandoned mine site, the orebody is capped by intensely leached and gossanized pillow lavas. The mineralized horizon is overlain by scattered outcrops of dark red-yellowish brown gossan surrounded by yellow gossanous scree. Primary mineralogies and textures in these gossanized lavas have been completely obliterated. Ferruginous gossans are mainly limonite- and goethite-rich, with subordinate hematite. Some outcrops display incomplete supergene enrichment, with minor pyrite surviving from the original orebody.

7.2.2.2 Metal Contents

The major base-metal constituents of the Karaali Fe-Cu sulfide mineralization are Fe, Cu, and Zn, mainly in sulfide form. In addition, Au, Ag, As, Hg, Se, Sb, Cd and Mo are present in lesser quantities. These metals within the mineralized zone are most probably derived by leaching from underlying basic host rocks during the circulation of hydrothermal fluids. Barnes and Czamanski (1967) suggested that, in order for an ore to be deposited, an aqueous solution with at least 10 ppm dissolved metals is needed and seawater, which contains less metal than this, cannot be the direct source for metal-sulfide deposition.

The bulk compositions of the Karaali ores are distinguished by their high concentrations of Cu and much lower Zn and Pb in the main ore body. The average concentration of Cu in the massive sulfides is 0.5% with a maximum concentration of 0.73%. The Cu grade significantly decreases in the disseminated and vein-type mineralized samples. On the other hand, Zn concentrations in the massive ores are very low and generally below 0.01%, whereas the vein-type ores are characterized by relatively higher concentrations of Zn (around 0.04%). However, even the most anomalous values for Zn from the Karaali ores are dissimilar from those of many ophiolite-hosted massive-sulfide deposits, such as Cyprus or Oman (Herzig et al., 1998). Similar to Zn, Pb concentrations in the Karaali ores are quite low, ranging between 47 and 59 ppm in the massive ore zone, and only about 1 ppm in the disseminated and vein-type ores.

A striking feature of the Karaali mineralization is its significant gold and silver contents. In general Cyprus-type volcanogenic massive sulfide deposits have low Au contents (Table 7.1). Most deposits within the Troodos Massif of Cyprus have insignificant Au concentrations (less than 1 ppm) with the exception of few deposits, such as Limni and Kalavasos-Mousoulos deposits (3.4 and 1.7 ppm Au, respectively) (Hannington et al., 1998). At Karaali, the massive ores have Au concentrations around 1 ppm (with a maximum of 1.2 ppm). These values are similar to a few well-known deposits from North America that are distinguished by their considerably high Zn concentrations. These Zn-rich ophiolite-hosted

massive-sulfide deposits are the Turner-Albright (Oregon, USA), and Betts Cove and Tilt Cove (Newfoundland, Canada) deposits (Seal et al., 2002).

Table 7-1. Comparison of selected metal concentrations from the Karaali and Cyprus ores (data for Cyprus from Kortan, 1970; Constantinou and Govett, 1973 and Hannington et al., 1998).

	KARAALİ			CYPRUS		
	Average basalts	**Massive ore**	**Vein-type**	**Skouriotissa**	**Mathiati**	**Agrokipia**
Cu (%)	0.01	0.50	0.07	2.78	0.17	0.07
Zn (%)	<0.01	<0.01	0.05	<100	0.26	0.03
Pb (%)	<0.01	<0.01	<0.01	0.02	97	30
Au (ppb)	2.98	1036.25	14.45	500	800	135
Mo (ppm)	2.3	35.5	4.85	62	35	13
Ni	72.32	39.95	78.15	20	33	<10
Sb	0.175	41.55	0.35	3	11	3
Bi	<0.1	9.05	0.35	-	-	-
Hg	<0.01	1.345	0.025	-	-	-
Tl	<0.1	4.45	<0.1	-	-	-
Ag	<0.1	6.65	0.1	5	4	1
As	2.89	2260.5	11	74	160	201
Cd	<0.1	0.15	0.5	-	29	1
Se	<0.5	80.9	1.45	296	20	144

The Turner-Albright Zn-Cu-Ag-Au-Co deposit, regarded as an important ophiolite-hosted massive-sulfide occurrence, is located in Josephine County, Oregon, USA (Kuhns and Baitis, 1987). The Turner-Albright sulfide bodies have anomalously high gold values, with an average gold content of 1.56 g/ton (Strickler, 1986). Likewise, samples of massive sulfide ores from Karaali yield an average gold content of around 1.03 g/ton. However, the Karaali mineralization differs from Zn-rich Turner-Albright massive-sulfide deposit due to its very low Zn content.

Besides these metals, whole-rock geochemical analyses indicate that the Karaali Fe-Cu massive-sulfide mineralization contains important concentrations of metals, such as Mo, Sb, Bi, Hg, Tl, Cd, Se, Ag, and As. Frost et al. (2002) some indicated that such minor elements may be remobilized and concentrated in the form of discrete pockets in massive-sulfide deposits that have undergone metamorphism. The high Au contents of the sulfide-mineralized Karaali basalts, which have been subjected to metamorphic conditions, may be explained thus. In a similar way, the regionally metamorphosed Turner-Albright host rocks may have relatively high Au contents as compared to the majority of ophiolite-hosted massive sulfide deposits.

At Karaali, anomalous Mo contents can be attributed to high Cu contents and, similarly, anomalous As and Au values may be related to high pyrite content of the sulfide mineralization in the absence of arsenopyrite. Additionally, in massive-sulfide deposits, Hg is derived primarily from pyrite, sphalerite and sulfosalts. In the Karaali ores, which are significantly Zn-poor, high concentrations of Hg may be related to pyrite mineralization. Cd, on the other hand, usually occurs as a solid solution within sphalerite and is found in higher concentrations in sulfide-bearing veins that contain sphalerite (Ryall, 1981; Seal et al., 2002).

A comparison of metal contents in the Karaali and Küre massive-sulfide deposits, shows that the Küre ores are distinguished by their higher Cu and Au contents. Çağatay et al. (1980) reported that the average Cu contents of the Küre massive-sulfide deposit are 1.69% in the Aşıköy district and 3.42% in the Bakibaba district. Also, an average Au concentration of 2.48 g/ton and an Ag concentration of 11.4 g/ton were reported for Küre area in that study.

7.2.3 Comparison with the Cyprus and Küre Massive Sulfides

In order to classify, the Karaali sulfide mineralization, corresponding field and geochemical signatures should be further correlated with selected ore deposits mineralization that can be regarded as representative of that particular mineralization style. For this reason, two well-known ophiolite-related massive sulfide deposits from Cyprus and Turkey have been selected. Extensive copper deposits in Cyprus are the type example of sulfide deposits that have formed within an ophiolite succession, and the Küre massive-sulfide deposit in northern Turkey is quite similar (but not identical) to the Cyprus-type deposits. As a result a thorough comparison with these two deposits may be useful for categorizing the Karaali massive-sulfide mineralization.

Alteration styles around the massive sulfide orebody near Karaali shows similarities to alteration styles of the Cyprus and Küre deposits and their host rocks. Mineralogical characteristics of the altered pillow lava sequence in Troodos, Cyprus are described well by Constantinou (1980). Numerous isotopic and fluid inclusion studies of these zones (e.g. Heaton and Sheppard, 1977; Spooner, 1977; Spooner and Bray, 1977; Gillis and Robinson, 1985; Schiffman et al., 1987; Richardson et al., 1987) have established the temperature and compositions of the ore-forming fluids.

The Cyprus lavas hosting the sulfide mineralization are altered to a typical greenschist facies metabasaltic assemblage (albite + chlorite + quartz + actinolite + titanite ± epidote ± pyrite ± relict primary phases). Massive sulfides are underlain by stockworks of hydrothermally altered lavas that are cut by networking quartz and sulfide veins. These lavas lack plagioclase, clinopyroxene, magnetite, and most of the zeolite minerals. Plagioclase and pyroxene have been replaced by quartz, and chalcedony replaces the glassy matrix of the basalt. Chlorite and minor illite are other secondary minerals observed in the altered lavas (Franklin et al., 1981).

According to Richards et al. (1989), alteration pipes are concentrically zoned into two distinct types of alteration. In the most common type, pipe centers are dominated by illite, pyrite, and quartz. More rarely the mineral assemblage at the center of the pipe is dominantly chlorite + quartz. Outward from these central zones, other phases may enter the assemblage. Some pipes display late silicification, though most pipes are relatively unsilicified. Richards et al. (1989) interpreted the concentric zonation as having been caused by variation in water/rock ratio across the diameter of the pipe, with the highest ratios at the center, and low ratios in the marginal zone (Cann and Gillis, 2004).

At Küre, the hydrothermally unaltered fresh spilites have been affected by low-temperature, ocean-floor metamorphism and consist of mostly albitized labradorite and chloritized augite phenocrysts in a groundmass of albite, chlorite, epidote, calcite, quartz, prehnite, magnetite, and pyrite.

Similar to Cyprus, the Küre massive sulfides are underlain by alteration pipes consisting of networks of veins and veinlets of secondary minerals in basaltic pillow lavas (Çağatay, 1993). Primary mafic minerals and feldspars have been completely altered and original textures completely obliterated. The footwall alteration assemblage in the pipe is characterized by chlorite, quartz, and sulfides, with lesser amounts of epidote, calcite, siderite, and hematite. At the top of the pipe illite-mica occurs. Silicification occurs as microcrystalline quartz aggregates and veinlets. Some hematite also occurs in the stringer ore as veins and cavity linings. Siderite is found as veinlets and impregnations in the upper levels of the alteration pipe beneath the massive ore and decreases laterally toward the margins of the pipe. Carbonate and epidote veining is later than the formation of chlorite. Laterally, the alteration pipe assemblage grades into a background assemblage of chlorite+albite+calcite (Çağatay, 1993). Additionally, argillic alteration has been also identified at Küre. In the Bakibaba mine, 0.5- to 0.8-m-thick kaolinite zones envelop the massive orebodies (Güner, 1980). This zone typically associated with siderite and devoid of sulfides, containing only local

euhedral pyrite at the contact between the massive and stringer ores (Çağatay, 1993).

The Karaali deposits resemble those of the Cyprus and Küre deposits in terms of both mineralogical and geochemical properties. All three deposits are hosted by basalts which have been altered into assemblages of quartz, chlorite, and sulfides with minor hematite. Primary mafic minerals and feldspars no longer exist. One major difference is that the Karaali and Küre deposits are devoid of the mixed layer chlorite-smectite facies which is typical of the Cyprus deposits; according to Çağatay (1993), this may be a result of the overprint of low-grade ocean-floor metamorphism in those areas. Also, in the Cyprus deposits evidence for argillic alteration is not given; however, in the Küre and Karaali deposits, argillic alteration is more apparent. Differing from Küre, the Karaali argillic alteration is demonstrated by increasing abundance of sericite towards the orebody. Contrary to Cyprus and Küre, which have local K_2O enrichments in their alteration pipes, the hydrothermally altered Karaali basalts do not display such a trend. The reason for this difference is the absence of K-feldspar in the Karaali basalts, whereas in Cyprus and Küre the host rocks immediately underlying the orebodies consist of K-feldspar.

The geochemical characteristics of Karaali lavas and gabbros were described in Chapter 6. Major- and trace-element compositions of spilitic basalts and gabbros seem to be strongly modified as a result of both long-term, low-grade ocean-floor metamorphism and short-term hydrothermal alteration. CaO, Na_2O and K_2O are the most mobile phases in these rocks and are significantly depleted. Initial replacement of calcic-plagioclase (labradorite) by sodic varieties (albite) is the main reason for Ca depletion in these rocks. Following this, sodic-plagioclase was replaced by secondary mineral assemblages (such as calcite and quartz), and Na was removed from the system.

Likewise, trace-element patterns seem variable with significant modifications. Large-ion lithophile elements (LILE), such as Rb, K, Ba and Sr, are those most affected by secondary processes. The abundances of these elements in the

Karaali basic rocks apparently were reduced by the effects of ocean-floor metamorphism and hydrothermal alteration. High-field-strength elements (HFSE), which are relatively immobile, are also found in low concentrations. Multi-element variation diagrams using trace and rare-earth elements display typical island-arc tholeiite signatures for the Karaali basic rocks, with large-ion lithophile element (LILE) enrichment and high-field strength element (HFSE) depletion compared to N-MORB. However, the enrichment levels of large-ion lithophile elements (LILE) are lower than typical island-arc tholeiites, whereas high-field-strength element (HFSE) depletion is consistent with island-arc tholeiite levels. This is mainly due to the inconsistent behavior of large-ion lithophile elements under hydrothermal conditions.

The tholeiitic Troodos lavas are more andesitic than the Karaali lavas (Figures 7.1 and 7.2). They exhibit geochemical characteristics of both mid-ocean ridge basalts (MORB) and island-arc tholeiites (IAT). However, the tectonic setting of the erupted lavas of the Troodos ophiolite is a matter of a long debate. Most widely accepted tectonic setting for the origin of Troodos lavas is a supra-subduction zone environment. As suggested by Pearce et al. (1984), supra-subduction zone ophiolites have the geochemical characteristics of island-arc tholeiites (IAT) and mid-ocean ridge basalts (MORB). To assign a definite tectonomagmatic setting by evaluating the limited geochemical data from Karaali is beyond the scope of this work. However; almost similar results have been obtained in comparison with the current literature. The majority of tectonic discrimination diagrams suggest an island-arc geochemistry for Troodos lavas which host the main massive-sulfide mineralization. Numerous studies on the origin of the Troodos lavas suggest a supra-subduction zone setting and this suggestion is not solely based on geochemical data; it also considers the general geological and petrographical features as compared to many mid-ocean ridge and arc systems.

On the other hand, the Küre lavas that host massive-sulfide mineralization are geochemically analogous to the Karaali lavas. When lava samples from Küre are plotted on geochemical discrimination diagrams, they plot very near the Karaali

samples. The Küre lavas are tholeiitic basalts, and selective enrichment of large-ion lithophile elements (LILE) and depletion of high-field-strength elements (HFSE) indicate that they are of arc origin. Detailed geochemical work on the Küre lavas was conducted by Ustaömer and Robertson (1994) who proposed a possible back-arc tectonic setting for the magmatic rocks of the Küre area. (Figures 7.1 and 7.2).

In the light of these data; it is proposed that the Karaali, Troodos and Küre lavas, all of which host massive-sulfide mineralization, originated from subduction-related systems (either in an island-arc or supra-subduction zone setting), not from a mid-ocean ridge. However, in Karaali there is no field geological evidence which indicates a possible tectonic setting for the magmatic rocks. Thus, the present suggestion of a possible tectonic setting for the Karaali magmatic rocks is based solely on the geochemical signatures of the rocks.

The tectonic setting of the host rocks of massive-sulfide deposits actually is not definitive for the classification of ophiolite-hosted massive-sulfide deposits since there is broad agreement that, whatever the tectonic setting, many ocean-crust generating systems may produce massive-sulfide deposits. Numerous studies around the world have shown that most ophiolite-hosted volcanogenic massive-sulfide deposits have formed in mature back-arc basins or supra-subduction zone spreading axes occurring in fore-arc and immature back-arc environments *rather* than in “typical” mid-ocean ridge tectonic settings (Koski, 2003).

7.3 Sulfur Isotopes

In Chapter 6, results of sulfur-isotopic analyses were presented. According to these data, sulfide minerals in the ore-bearing Karaali samples have δS^{34} values between 1.9 and 6.8‰, with an average of 3.7‰. Consistently, the Troodos and Küre ores have similar sulfur-isotope abundances.

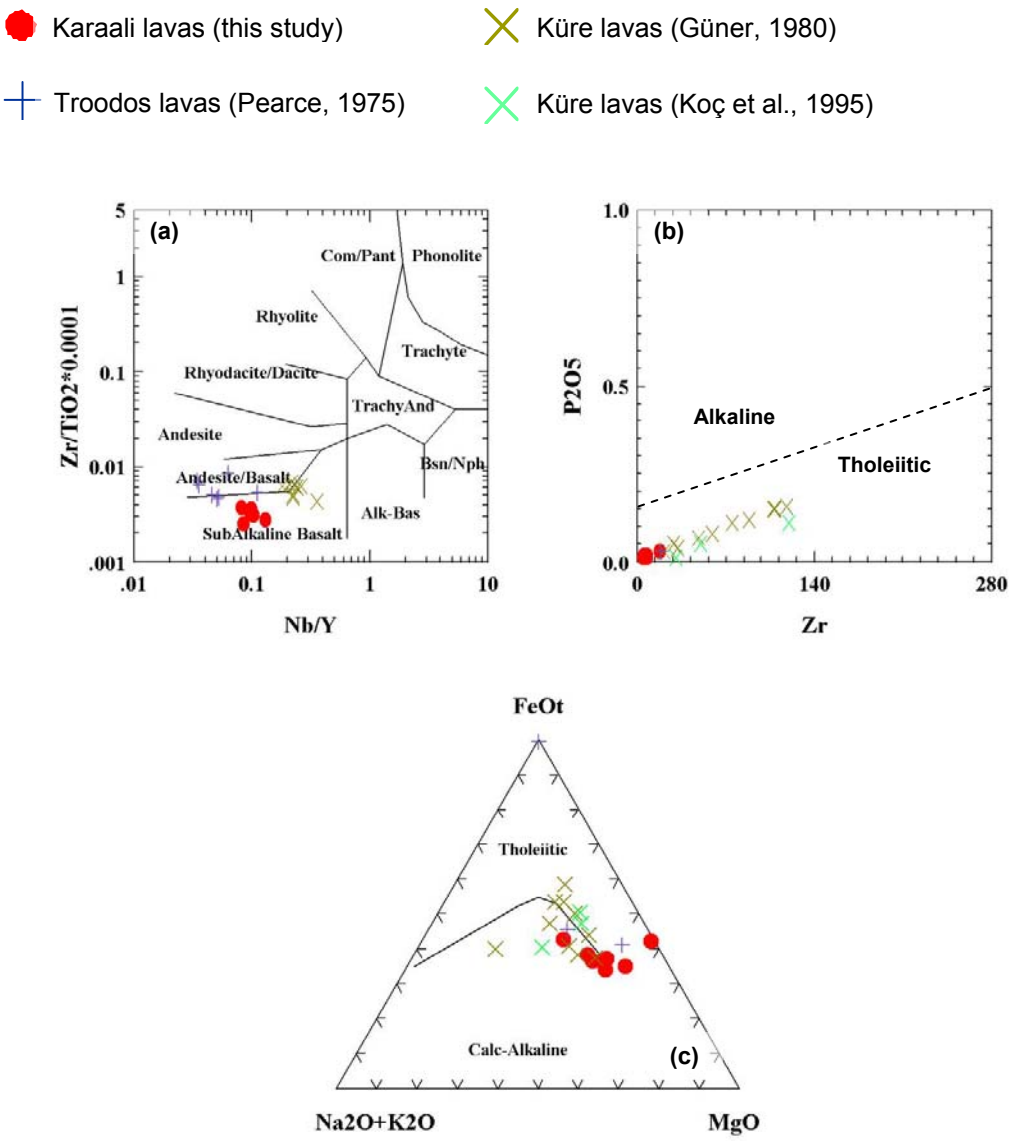

Figure 7-1. Plots of the Karaali, Troodos and Küre lavas on the rock classification diagrams of (a) Winchester and Floyd (1977), (b) Floyd and Winchester (1975), and (c) Irvine and Baragar (1971).

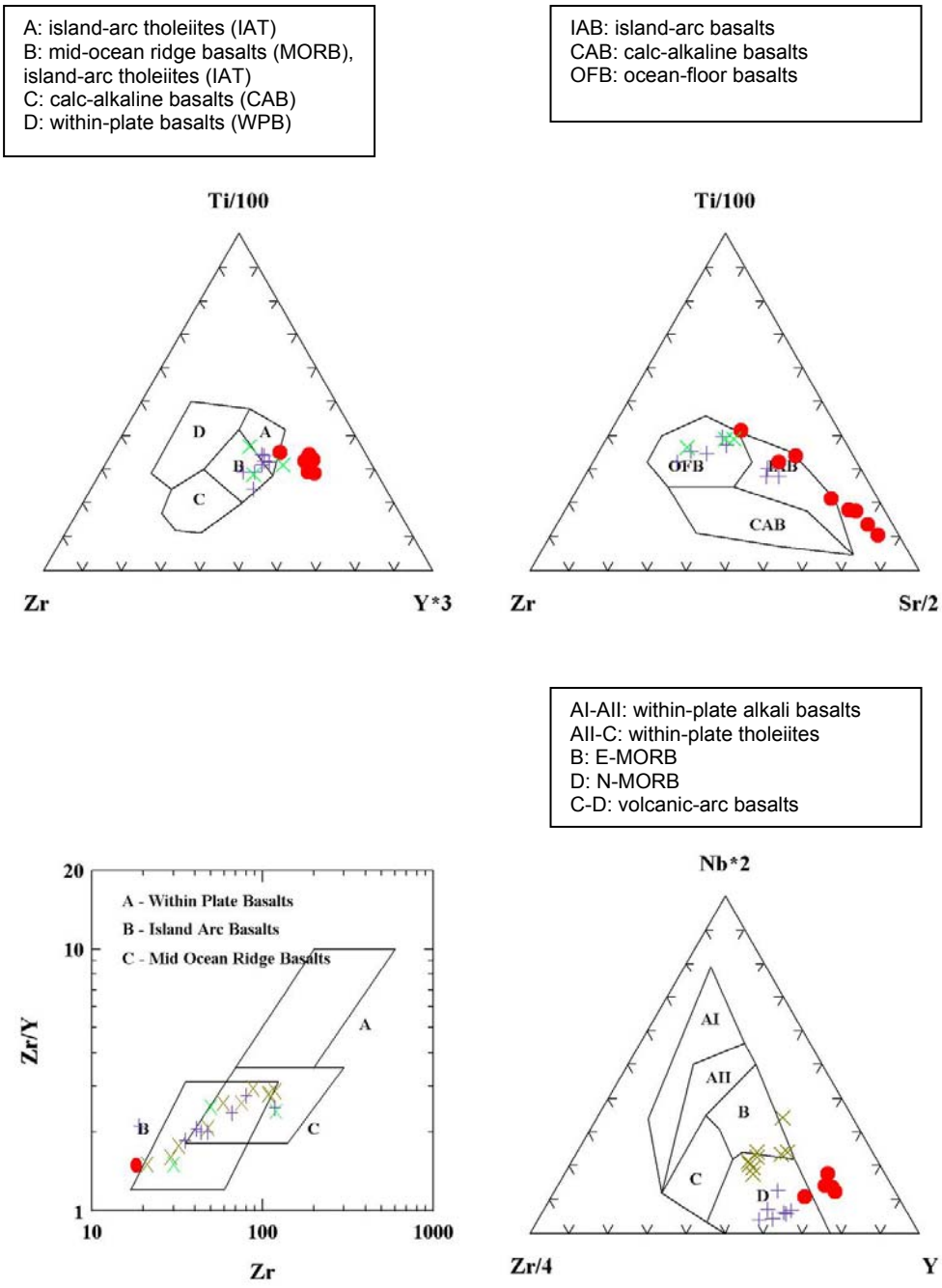

Figure 7-2. Selected tectonic discrimination diagrams for the Karaali, Troodos and Küre lavas; (a) Ti/100-Zr-Y*3 (after Pearce and Cann, 1973), (b) Ti/100-Zr-Sr/2 (Pearce and Cann, 1973), (c) Zr versus Zr/Y (after Pearce and Norry, 1979) and (d) Nb*2-Zr/4-Y (after Meschede, 1986) (Symbols as in Figure 7.1)

Pyrite from massive-sulfide deposits in the Troodos ophiolite has $\delta^{34}S$ values ranging from -1.1 to 7.5‰, but most fall between +4 and +7‰ (Clark, 1971; Hutchinson and Searle, 1971; Johnson, 1972; Jamieson and Lydon, 1987). These values are slightly higher than those for the Karaali massive-sulfides. The Küre deposits have a narrower range of $\delta^{34}S$ values, between 6.5 and 9.5‰.

These values are quite similar to those of Troodos and Karaali but the contribution from seawater sulfate is more apparent. However, in general terms, the Karaali, Troodos and Küre massive-sulfide deposits all have similar $\delta^{34}S$ values, restricted to a range from 2 to 9‰. Even in the same deposit such variations may appear, but it is obvious that the sulfur in all of these sulfide deposits mainly originated from magmatic rocks.

7.4 Fluid Inclusions

It was previously reported presented in Chapter 5 that studies of fluid inclusions in syngenetic quartz and sphalerite from the vein-mineralized zone of the Karaali area were not possible due to the lack of well-developed primary fluid inclusions.

Many fluid-inclusion studies from different massive-sulfide deposits around the world suggest that the majority of these massive-sulfide deposits formed under hydrothermal conditions in which homogenization temperatures of inclusions in the syngenetic vein-filling minerals were higher than 200°C (e.g., Spooner and Bray, 1977; Spooner, 1981; Wilson and Petersen, 1989) .

Fluid-inclusion data from Cyprus (Spooner and Bray, 1977; Spooner, 1981) yielded temperatures of 301 to 380°C, while Wilson and Petersen (1989) reported that late-stage quartz in the Oxec massive-sulfide deposit of Guatemala was deposited at an average, pressure-corrected temperature of 314°C. When modern mid-ocean-ridge hydrothermal environments are considered, the situation is not significantly different from ancient massive-sulfide deposits. From their studies on the Mid-Atlantic ridge, Styrt et al. (1981) obtained pressure-corrected temperatures of 280 to 285°C while Delany et al. (1982) reported fluid inclusions

in quartz from the Kane fracture zone with maximum entrapment temperatures of 310°C. In addition to these, other fluid-inclusion studies on different massive-sulfide deposits suggest that (syngenetic with the ore formation), many instances of stockwork mineralization formed between200 and 350°C (Petersen et al. 2000; Zengqian et al., 2001; Solomon et al., 2002; Alm et al. 2003).

However, in the present study, minerals thought to be syngenetic with the sulfide mineralization did not yield temperature data and, instead, temperature measurements were only available from dolomite. The primary, two-phase (L+V) fluid inclusions from dolomites yielded a homogenization-temperature interval of 82 to 104°C. These data do not seem to reflect the original temperature conditions for the formation of Karaali massive-sulfide deposit. Rather, the microthermometric data obtained from dolomites within the quartz-sulfide veins indicate a late-stage, low temperature hydrothermal event that followed the massive-sulfide mineralization.

7.5 Concluding Remarks

In light of field-geological, petrographical and geochemical examination of the Karaali massive sulfide mineralization and the adjacent rock units, it can be concluded that the Karaali Fe-Cu sulfides show similarities to other ophiolite-related massive-sulfide deposits. Although tectonic deformation extensively modified the development and significance of the sulfide mineralization, the Karaali ores still preserve some genetic features. A comparison with Cyprus-type massive-sulfide deposits shows that there are many similarities between these two different occurrences. In particular, a comparison of host-rock lithology and geochemistry, metal content, mineral paragenesis and alteration zoning show that the Karaali massive sulfides may be a counterpart of Cyprus-type massive-sulfide mineralization which is developed within a mélange with a simpler mineralogy, lower grade/tonnage and uncertain deposit morphology (Table 7.2). Likewise, the Küre massive-sulfide mineralization displays strong correlations with the Karaali sulfides. With these characteristic features, the Karaali Fe-Cu sulfide

mineralization can be easily distinguished from other major massive-sulfide deposit types (e.g., Kuroko and Besshi).

Table 7-2. Comparison of the Karaali massive-sulfide mineralization with selected massive-sulfide deposits.

		KARAALİ	CYPRUS	KÜRE
WALL-ROCK ALTERATION	**Alteration Mineralogy**	chlorite+albite+quartz+calcite ±epidote±actinolite±prehnite	albite+chlorite+quartz +actinolite+titanite±epidote	albite+chlorite+epidote +calcite+quartz+prehnite
	Alteration Styles	propylitization, argillic alteration, silicification, carbonatization supergene enrichment	propylitization, silicification, supergene enrichment	propylitization, argillic alteration, silicification, carbonatization supergene enrichment
Ore Minerals		pyrite, chalcopyrite, bornite, covellite, sphalerite	pyrite, chalcopyrite, magnetite, sphalerite, galena, marcasite, pyrrhotite, hematite, sphalerite	pyrite, chalcopyrite, bornite, covellite, sphalerite, marcasite, tennantite
Host-Rock Geochemical Signatures		tholeiitic basalts	tholeiitic basaltic andesites	tholeiitic basalts
Sulfur-isotopic signatures		1.9 and 6.8‰ (magmatic source)	1.1 to 7.5‰ (magmatic source)	6.5 – 9.5 ‰ (magmatic source)
Tectonic Settings		arc-related	supra-subduction setting (two-stage evolution)	arc-related (back-arc) (Ustaömer and Robertson, 1994)

REFERENCES

Adamides, N., 1980. Kalavasos Mining District. In: (ed.) Panayioutou, A., Ophiolites, Proceedings, International Ophiolite Symposium, Cyprus, 1979, Nicosia, Cyprus Geological Survey Department, 80-93.

Akyürek, B., 1981. Ankara Melanjının kuzey bölümünün temel jeoloji özellikleri. Proceedings of the Symposium on the Geology of Central Anatolia, 41-45, (in Turkish, with English abstract).

Akyürek, B., Bilginer, E., Çatal, E., Dağer, Z., Soysal, Y. and Sunu, O., 1979. Eldivan Şabanözü (Çankırı) dolayında ofiyolit yerleşmesine ilişkin bulgular. Jeoloji Mühendisliği 9, 5-11.

Akyürek, B., Bilginer, E., Dağer, Z., Soysal, Y. and Sunu, O., 1980. Eldivan Şabanözü (Çankırı), Hasayaz-Çankırı (Kalecik, Ankara) dolayının jeolojisi. MTA rapor no: 6741.

Akyürek, B., Bilginer, E., Akbas, B., Hepşen, N., Pehlivan, S.¸ Sunu, O., Soysal, Y., Dağer, Z., Çatal, E., Sözeri, B., Yıldırım, H. and Hakyemez, Y., 1984. Fundamental geological characteristics of Ankara–Elmadağ Kalecik area. Chamber Geol. Eng. 20, 31–47, (in Turkish).

Akyürek, B., Duru, M., Sütçü, Y.F., Papak, İ. Şaroğlu, F., Pehlivan, N., Gönenç, O., Granit, S., and Yaşar, T., 1996. Ankara ilinin çevre jeolojisi ve doğal kaynaklar projesi (1994 yılı Jeoloji Grubu çalışmaları). Maden Tetkik ve Arama Enstitüsü, Rapor No: 9961 (unpublished).

Alm, E., Broman, C., Billström, K., Sundblad, K. and Torssander, P., 2003. Fluid characteristics and genesis of early Neoproterozoic orogenic gold-quartz veins in the Harnäs area, southwestern Sweden. Economic Geology 98, 1311-1328.

Anonymous, 1972. Penrose Field Conference on ophiolites. Geotimes 17, 24-25.

Arnold, M. and Sheppard, S.M.F., 1981. East Pacific Rise at latitude 2l^{o}N: isotopic composition and origin of the hydrothermal sulphur. Earth and Planetary Science Letters 56, 148-56.

Bailey, E.B. and McCallien, W.J., 1950. The Ankara mélange and the Anatolian thrust. Mineral Research and Exploration Institute of Turkey (MTA) Bulletin 40, 17-21.

Bailey, E.B. and McCallien, W.J., 1953. Serpentine lavas, the Ankara mélange and the Anatolian thrust. Trans. R. Soc. Edinburgh 62, 403–442.

Bamba, T., 1976. Ophiolite and related copper deposits in Ergani–Maden area, Southeast Anatolian. Mineral Research and Exploration Institute of Turkey (MTA) Bulletin 86, 35–49, (in Turkish, with English abstract).

Barnes, H.L. and Czamanski, G.L., 1967. Solubilities and transport of ore minerals. In: Barnes, H.L., (ed.), Geochemistry of Hydrothermal Ore Deposits. New York: Holt, Rinehart and Winston, 336-381.

Batman, B., 1978. Haymana kuzeyinin jeolojik evrimi ve yöredeki melanjin incelenmesi - stratigrafi birimleri. Hacettepe University, Earth Sciences 4, 95-124, (in Turkish, with English abstract).

Best, M.G., 1982. Igneous and Metamorphic Petrology. New York, W.H. Freeman & Co., San Francisco, 630 p.

Birgi, Ş., 1944. Karaali bakır madenine yapılan bir gezi hakkında rapor. MTA Derleme Rapor No. 1512 (unpublished).

Boccaletti, M., Bortolotti, V. and Sagri, M. 1966. Ricerche sulle ofioliti della Catene Alpine; Osservazioni sull'Ankara mélange nella zona di Ankara. Bollettino della Societa Geologica Italiana 85, 485-508.

Bowers, T.S., 1989. Stable isotope signatures of water-rock interaction in mid-ocean ridge hydrothermal systems: sulfur, oxygen, and hydrogen. Journal of Geophysical Research 94, 5775-5786.

Bozkurt E. and Mittwede S.K., 2001. Introduction to the geology of Turkey - a synthesis. International Geological Review 43 (7), 578-594.

Brabers, A.J.M., 1964. Ankara vilayeti, Bala yakınlarındaki altın ve bakır ruhsat sahaları. MTA Derleme Rapor No. 3364 (unpublished).

Brongniart, A., 1813. Essai de classification minéralogique des roches mélanges. Journal des Mines, v. XXXIV, 190-199.

Cann, J.R., 1970. Rb, Sr, Y, Zr and Nb in some ocean floor basaltic rocks. Earth and Planetary Science Letters 10, 7– 11.

Cann, J.R. and Gillis, K.M., 2004. Hydrothermal insights from the Troodos ophiolite, Cyprus. In: Elderfield, H. and Davis, E. (eds.), The Hydrology of the Oceanic Lithosphere, Cambridge University Press, 274-310.

Clague, D.A. and Frey, F.A., 1982. Petrology and trace element geochemistry of the Honolulu volcanics, Oahu: implications for the oceanic mantle below Hawaii. Journal of Petrology 23, 447-504.

Clark, L.A., 1971. Volcanogenic ores: comparison of cupriferous pyrite deposits of Cyprus and Japanese Kuroko deposits. Soc. Mining Geologists Japan, Special Issue 3, 206-215.

Coleman, R.G., 1971. Plate tectonic emplacement of upper mantle peridotites along continental edges. Journal of Geophysical Research 76, 1212-1222.

Coleman, R.G., 1977. Ophiolites, Ancient Oceanic Lithosphere. New York: Springer-Verlag, 229 p.

Constantinou, G., 1980. Metallogenesis associated with the Troodos ophiolite. In: Panayioutou, A., (ed.), Ophiolites, Proceedings, International Ophiolite Symposium, Cyprus 1979: Nicosia, Cyprus, Cyprus Geological Survey Department, 663-674.

Constantinou, G. and Govett, G.J.S., 1972. Genesis of sulphide deposits, ochre and umber of Cyprus. Institution of Mining and Metallurgy, Transactions 8, B36-B46.

Constantinou, G. and Govett, G.J.S., 1973. Geology, geochemistry, and genesis of Cyprus sulfide deposits. Economic Geology 68, 843-858.

Cox, D.P. and Singer, D.A., 1986. Mineral Deposit Models. U.S. Geological Survey Bulletin 1693, 379 p.

Craig, J.R. and Vaughan, D.J., 1981. Ore Microscopy and Ore Petrology. John Wiley and Sons, 406 p.

Çağatay, M.N., 1993. Hydrothermal alteration associated with volcanogenic massive sulfide deposits, Examples from Turkey. Economic Geology 88, 606–621.

Çağatay, N., Pehlivanoğlu, H. and Altun. Y., 1980. Küre piritli bakır yataklarının kobatt-altın mineralleri ve yataklarının bu metaller acısından ekonomik değeri. Mineral Research and Exploration Institute of Turkey (MTA) Bulletin 93/94,110-117.

Çapan, U.Z. and Buket, E., 1975. Aktepe-Gökdere bölgesinin jeolojisi ve ofiyolitli melanj. Geological Society of Turkey Bulletin 18, 11-16.

Delany, J.R., Mogk, D.M. and Cosens, B., 1982. Indirect evidence of boiling hydrothermal systems on the Mid-Atlantic Ridge [abs.]. Am. Geophys. Union Trans. 63, 472.

Dewey, J.F., 1976. Ophiolite obduction. Tectonophysics 31, 93-120.

Dewey, J.F., 2003. Ophiolites and lost oceans: Rifts, ridges, arcs, and/or scrapings? In: Dilek, Y., Newcomb, S., (eds.), Ophiolite Concept and the Evolution of Geological Thought. Geological Society of America Special Paper 373, 1–16.

Dewey, J.F. and Bird, J.M., 1971. Origin and emplacement of the ophiolite suite: Appalachian ophiolites in Newfoundland. Journal of Geophysical Research 76, 3179-3206.

Dilek, Y., 2003. Ophiolite concept and its evolution. In: Dilek, Y., Newcomb, S., (eds.), Ophiolite Concept and the Evolution of Geological Thought. Geological Society of America Special Paper 373, 1–16.

Edwards, R. and Atkinson, K., 1986. Ore Deposit Geology. Chapman and Hall, 466 p.

Erdoğan, B., 1977. Geology, geochemistry, and genesis of the sulfide deposits of the Ergani–Maden region, SE Turkey. Unpublished PhD Thesis, New Brunswick University, 289 p.

Erler, A., 1984. Tectonic setting of the massive sulfide deposits of the Southeast Anatolian thrust belt. In: Tekeli, O., Göncüoğlu, M.C., (eds.), The Geology of the Taurus Belt, Proceedings of the International Symposium, 309–316.

Erler, A., Güleç, N., Eseller, G., Kuşçu, İ. And Yavuz, N., 1994. Güneydoğu Anadolu Bindirme Kuşağı ve Küre-Kastamonu yöresi masif sülfid yataklarının kükürt izotop bileşimlerinin karşılaştırılması. ODTÜ AFP Project No. 92-03-09-02.

Evans, A. M., 1993. Ore Geology and Industrial Minerals: An Introduction, (3rd edition). Blackwell, 390 p.

Floyd, P.A. and Winchester, J.A., 1975. Magma type and tectonic setting discrimination using immobile elements. Earth and Planetary Science Letters 27, 211-218.

Franklin, J.M., Lydon, J.W. and Sangster, D.F., 1981. Volcanic-associated massive sulfide deposits: Economic Geology, 75th Anniversary Volume, 485–627.

Frost, B.R., Mavrogenes, J.A. and Tomkins, A.G., 2002. Partial melting of sulfide ore deposits during medium- and high-grade metamorphism. Canadian Mineralogist 40, 1-18.

Gansser, A., 1959. Ausseralpine ophiolitith probleme. Eclogae Geol. Helv. 52, 2, 327-354.

Garson, M. and Mitchell, A.H.G, 1977. Mineralization at destructive plate boundaries: a brief review. Volcanic Processes in Ore Genesis. In: Proceedings of a joint meeting of the Volcanic Studies Group of the Geological Society of London and the Special Publication of the Geological Society of London 7, 81-97.

Gillis, K.M. and Robinson, P.T., 1985. Low-temperature alteration of the extrusive sequence, Troodos ophiolite, Cyprus. Canadian Mineralogist 23, 431-441.

Gorton, M.P. and Schandl, E.S., 2000. From continents to island arcs: a geochemical index of tectonic setting for arc-related and within-plate felsic to intermediate volcanic rocks. Canadian Mineralogist 38, 1065-1073.

Göncüoğlu, M.C., Dirik, K. and Kozlu, H., 1997. Pre-Alpine and Alpine Terranes in Turkey: explanatory notes to the terrane map of Turkey: IGCP Project No 276. Terrane Maps and Terrane Descriptions, Annales Géologiques Des Pays Helléniques 37, 515-536.

Görür, N., Oktay, F. Y., Seymen, İ., and Şengör, A.M.C., 1984. Paleotectonic evolution of Tuzgölü basin complex, Central Turkey. In: Dixon, J. E., and Robertson, A.H.F., (eds.), The Geological Evolution of the Eastern Mediterranean. Geological Society of London Special Publication 17, 81–96.

Güner, M., 1980. Küre civarının masif sülfid yatakları ve jeolojisi, Pontidler (Kuzey Türkiye). Mineral Research and Exploration Institute of Turkey (MTA) Bulletin 93/94, 65-109.

Hannington, M.D., Galley, A.G., Herzig, P.M. and Petersen, S., 1998. Comparison of the TAG mound and stockwork complex with Cyprus-type massive sulfide deposits, In: Herzig, P.M., Humphris, S.E., Miller, D.J., and Zierenberg, R.A., (eds.), 1998. Proceedings of the Ocean Drilling Program, Scientific Results 158, 389-415.

Hart, S. R., A. J. Erlank and Kable, E.J.D., 1974. Sea floor basalt alteration: Some chemical and Sr isotopic effects. Contributions to Mineralogy and Petrology 44, 219-230.

Heaton, T.H.E and Sheppard, S.M.F., 1977. Hydrogen and oxygen isotope evidence for sea-water hydrothermal alteration and ore deposition, Troodos Complex, Cyprus. Geological Society of London Special Publication 7, 42-57.

Hoefs, J., 1987. Stable isotope geochemistry (3rd edition), New York: Springer Verlag, 241 p.

Honnorez, J., 2003. Hydrothermal alteration vs. ocean-floor metamorphism. A comparison between two case histories: the TAG hydrothermal mound (Mid-Atlantic Ridge) vs. DSDP/ODP Hole 504B (Equatorial East Pacific). C. R. Geoscience 335, 781-824.

Horihoshi, E., 1969. Volcanic activity related to the formation of the Kuroko-type deposits in the Kosaka District, Japan. Mineralium Deposita 4, 321-345.

Höy, T., 1991. Volcanogenic massive sulphide deposits in British Columbia. In: Ore Deposits, Tectonics and Metallogeny in the Canadian Cordillera, McMillan, W.J., Coordinator, B. C. Ministry of Energy, Mines and Petroleum Resources, Paper 1991-4, 89-123.

Hsü, K. J., 1971. Franciscan mélanges as a model for eugeosynclinal sedimentation and underthrusting tectonics. Journal of Geophysical Research 76, 1162-1170.

Hughes, C.J., 1982. Igneous Petrology. New York: Elsevier, 551 p.

Humphris, S.E. and Thompson, G., 1978. Hydrothermal alteration of oceanic basalts by seawater. Geochimica et Cosmochimica Acta 42, 107–125.

Hutchinson, R.W., 1973. Volcanogenic sulfide deposits and their metallogenic significance. Economic Geology 68, 1223-1246.

Hutchinson, R.W., 1980. Massive base metal sulphide deposits as guides to tectonic evolution. In: Strangway, D.W., (ed.), The Continental Crust and its Mineral Deposits, Geological Association of Canada Special Paper 20, 659-684.

Hutchinson, R.W. and Searle, D.L., 1970. Stratabound pyrite deposits in Cyprus and relations to other sulfide ores. Soc. Min. Geol. Jpn. Spec. Iss. 3, 198-205.

Irvine, T.N. and Baragar, W.R.A., 1971. A guide to the chemical classification of the common volcanic rocks. Canadian Journal of Earth Sciences 8, 523-548.

Jamieson, H. E. and Lydon, J. W., 1987. Geochemistry of a fossil ore-solution aquifer: chemical exchange between rock and hydrothermal fluid recorded in the lower portion of research drill hole CY-2a, Agrokipia, Cyprus. In: Robinson, P. T., Gibson, I. L. and Panayiotou, A., (eds.), Cyprus Crustal Study Project: Initial Report, Holes CY-2 and 2a. Ottawa, Ontario, Canada, Geological Survey of Canada, 139-152.

Johnson, A.E., 1972. Origin of Cyprus pyrite deposits: International Geological Congress, 24th, Montreal 1972, sec. 4, 291-298.

Klau, W. and Large, D.E., 1980. Submarine exhalative Cu-Pb-Zn deposits, a discussion of their classification and metallogenesis. Geol. Jahrb. Sect. D. 40, 13-58.

Koç, Ş¸ Ünsal, A. and Kadıoğlu, Y., 1995. The geology, geochemistry and geotectonic position of volcanics including Küre (Kastamonu) mineralizations. Bulletin of Mineral Research and Exploration (MTA) 117, 41–54, (in Turkish, with English abstract).

Koçyiğit, A. 1987. Hasanoğlan (Ankara) yöresinin tektonostratigrafisi: Karakaya orojenik kuşağının evrimi. Hacettepe University, Earth Sciences 14, 269-293, in Turkish with English abstract.

Koçyiğit, A., 1991. An example of an accretionary fore arc basin from Northern Central Anatolia and its implications for the history subduction of Neo-Tethys in Turkey. Geological Society of America Bulletin 103, 22-36.

Kortan, K., 1970. Zur Bildung der Scwefelkies-Kupferkies-Vorkommem Cyperns unter besonderer Berucksichtigung der Lagerstatte Skouriotissa [Ph.D. thesis]. Tech. Univ. Clausthal, Germany.

Koski, R.A., 2003. Ophiolite-hosted volcanogenic massive sulfide deposits: a view in 2003. Modern and Ancient Mineralizing Seafloor Hydrothermal Systems I, Geological Society of America Annual Meeting, Paper No. 1-4.

Kuhns, R.J. and Baitis, H.W., 1987. Preliminary study of the Turner Albright Zn-Cu-Ag-Au-Co massive sulfide deposit, Josephine County, Oregon. Economic Geology 82 (5), 1362-1376.

Kuşçu, Ü. and Erler, A., 1994. Pyrite deformation textures in the Küre volcanogenic massive sulfide deposits (Kastamonu-Turkey): an approach for P-T conditions of deformation. International Volcanological Congress 94 Special Publication No. 2.

Kuşçu, İ. and Erler, A., 1999. Deformation of stibnites and pyrites in the Madsan antimony deposit (Niğde, Turkey): implications for pressure-temperature conditions of local deformation. Turkish Journal of Earth Sciences 8, 57-66.

Kuşçu, İ. and Erler, A., 2002. Pyrite deformation textures in the deposits of the Küre mining district (Kastamonu, Turkey). Turkish Journal of Earth Sciences 11, 205-215.

Laznicka, P., 1985. Subaqueous-hydrothermal deposits. Empirical Metallogeny, Elsevier, Amsterdam, 1758 p.

Lydon, J.W., 1984. Volcanogenic massive sulphide deposits, Part 1: A descriptive model. Geoscience Canada 11, 195-202.

McClay, K.R. and Ellis, P.G., 1984. Deformation of pyrite. Economic Geology 79, 400-403.

Meschede, M., 1986. A method of discriminating between different types of mid-ocean ridge basalts and continental tholeiites with the Nb-Zr-Y diagram. Chemical Geology 56, 207-218.

Miyashiro, A., 1974. Volcanic rock series in island arcs and active continental margins. American Journal of Science 274, 321–355.

Miyashiro, A., 1975. Classification characteristics and origin of ophiolites. Journal of Geology 83, 249-281.

Miyashiro, A., Shido, F., and Ewing, M., 1971. Metamorphism in the Mid-Atlantic Ridge near 24° and 30°N, Phil. Trans. R. Soc. A 268, 589–603.

Moores, E.M., 2003. A personal history of the ophiolite concept. In: Dilek, Y., Newcomb, S., (eds.), Ophiolite Concept and the Evolution of Geological Thought. Geological Society of America Special Paper 373, 17–29.

Norman, T., 1972. Ankara Yahşihan bölgesinde Üst Kretase-Alt Tersiyer istifinin stratigrafisi. TJK Bülteni XV (2), 180-277.

Norman, T., 1973. Ankara melanjının yapısı hakkında. Proceedings of the Symposium on the Occasion of the 50th Anniversary of Turkish Republic. Mineral Research and Exploration Institute of Turkey (MTA) Special Publication, 77-94, (in Turkish, with English abstract).

Norman, T., 1984. The role of the Ankara mélange in the development of Anatolia Turkey. In: Dixon, J.E., Robertson, A.H.F., (eds.), The Geological Evolution of the Eastern Mediterranean. Geological Society of London Special Publication 17, 441–447.

Norman, T., Gökçen, S.L. and Şenalp, M., 1980. Sedimentation pattern in Central Anatolia at the Cretaceous-Tertiary boundary. Cretaceous Research l, 61-84.

O'Hanley, D.S., 1996. Serpentinites: Records of Tectonic and Petrological History. Oxford University Press, New York - Oxford, 277 p.

Obolenskiy, A.A., Rodionov, S.M., Ariunbileg, S., Dejidmaa, G., Distanov, E.G., Dorjgotov, D., Gerel, O., Hwang, D.H., Sun, F., Gotovsuren, A., Letunov, S.N., Li, X., Nokleberg, W.J., Ogasawara, M., Seminsky, Z.V., Smelov, A.P., Sotnikov, V.I., Spiridonov, A.A., Zorina, L.V. and Yan, Hongquan, 2003. Mineral deposit models for northeast Asia. In: Nokleberg, W.J., and 10 others, (eds.), Preliminary Publications Book 2 from Project on Mineral Resources, Metallogenesis, and Tectonics of Northeast Asia: U.S. Geological Survey Open-File Report 03-203 (CD-ROM), 47 p.

Ohmoto, H. and Rye, R.O., 1979. Isotopes of sulphur and carbon. In: Barnes, H.L., (ed.), Geochemistry of Hydrothermal Ore Deposits. New York: Wiley, 506-567.

Okay, A.İ. and Tüysüz, O., 1999. Tethyan sutures of northern Turkey. In: Duran, B., Jolivet, L., Horvath, F. and Séranne, M. (eds.), The Mediterranean Basins: Tertiary Extension within the Alpine Orogen. Geological Society of London Special Publication 156, 475-515.

Pearce, J.A., 1975. Basalt geochemistry used to investigate past tectonic environments on Cyprus. Tectonophysics 25, 41-67.

Pearce, J.A., 1976. Statistical analyses of major element patterns in basalts. Journal of Petrology 17, n. 1, 15-43.

Pearce, J.A., 1982. Trace element characteristics of lavas from destructive plate boundaries. In: Thorpe, R.S., (ed.), Orogenic Andesite Related Rocks. Wiley, Chichester: Wiley, 525–548.

Pearce, J.A., 2003. Supra-subduction zone ophiolites: The search for modern analogues. In: Dilek, Y., Newcomb, S., (eds.), Ophiolite Concept and the Evolution of Geological Thought. Geological Society of America Special Paper 373, 269–293.

Pearce, J.A. and Cann, J.R., 1971: Ophiolite origin investigated by discriminant analysis using Ti, Zr and Y. Earth and Planetary Science Letters 12, 339-349.

Pearce, J.A. and Cann, J.R., 1973. Tectonic setting of basic volcanic rocks determined using trace element analyses. Earth and Planetary Science Letters 19, 290-300.

Pearce, J.A. and Norry, M.J., 1979. Petrogenetic implications of Ti, Zr, Y, and Nb: variations in volcanic rocks. Contributions to Mineralogy and Petrology 69, 33-47.

Pearce, T.H., Gorman, B.E. and Birkett, T.C., 1977. The relationships between major element chemistry and tectonic environment of basic and intermediate volcanic rocks. Earth and Planetary Science Letters 36, 121-132.

Perfit, M.R., Gust, D.A., Bence, A.E., Arculus, R.J. and Taylor, S.R., 1980. Chemical characteristics of island-arc basalts; implications for mantle source. Chemical Geology 30, 227-256.

Pearce J.A., Lippard S.J. and Roberts, S., 1984. Characteristics and tectonic significance. of supra-subduction zone ophiolites. In: Kokelaar, B.P., Howells, M.F., (eds) Marginal basin geology. Geological Society of London Special Publication 14, 77-93.

Petersen, S., Herzig, P.M. and Hannington, M.D., 2000. Third dimension of a presently forming VMS deposit: TAG hydrothermal mound, Mid-Atlantic Ridge, 26°N. Mineralium Deposita 35, 233-259.

Piercey, S.J., Ryan, J.J., Gordey, S.P., and Villeneuve, M.E., 2003. Geochemistry of tectonic significance of amphibolites from the Yukon-Tanana terrane (YTT),

Stewart River, Yukon: Preliminary results. Geological Association of Canada-Mineralogical Association of Canada Annual Meeting, Program with Abstracts, 134.

Pouit, G., 1984. Les gisements à sulfures massifs exhalatifs sédimentaires: une mise au point sur leur classification et la méthodologie de leur recherche. Chron. Rech. Min. 476, 31-34.

Richards, H.G., Cann, J.R. and Jensensius, J., 1989. Mineralogical zonation and metasomatism of the alteration pipes of Cyprus sulfide deposits. Economic Geology 84, 91–115.

Richardson, C.J., Cann, J.R., Richards, H.G. and Cowan, J.G., 1987. Metal-depleted root zones of the Troodos ore-forming hydrothermal systems, Cyprus. Earth and Planetary Science Letters 84, 243-253.

Robinson, P.T., Malpas, J. and Xenophontos, C., 2003. The Troodos Massif of Cyprus: its role in the evolution of the ophiolite concept. In: Dilek, Y., Newcomb, S., (eds.), Ophiolite Concept and the Evolution of Geological Thought. Geological Society of America Special Paper 373, 295–308.

Roedder E. 1984. Fluid inclusions. Reviews in Mineralogy 12, 646 p.

Rojay, B., Yalınız, K. and Altıner, D., 2001. Tectonic implications of some Cretaceous pillow basalts from the North Anatolian Ophiolitic Mélange (Central Anatolia-Turkey) to the Evolution of Neo-Tethys. Turkish Journal of Earth Sciences 10, 93-102.

Rojay, B., Altıner, D., Altıner, S.Ö., Önen, A.P., James, S. and Thirlwall, M.F., 2004. Geodynamic significance of the Cretaceous pillow basalts from North Anatolian Ophiolitic Mélange Belt (Central Anatolia, Turkey): geochemical and paleontological constraints. Geodinamica Acta 17/5, 349-361.

Rollinson, H., 1993. Using Geochemical Data: Evaluation, Presentation, Interpretation. Longman Scientific & Technical, John Wiley and Sons, 352 p.

Ryall, W.R., 1981. The forms of mercury in some Australian stratiform Pb-Zn-Ag deposits of different regional metamorphic grades. Mineralium Deposita 16, 425-435.

Sangster, D.F., 1968. Relative sulphur isotope abundances of ancient seas and strata-bound sulphide deposits. Geological Association of Canada Proceedings 19, 79–91.

Sangster, D.F. and Scott, S.D., 1976. Precambrian, strata-bound, massive Cu-Zn-Pb sulphide ores of North America. In: Wolf, K.H. (ed.), Handbook of Strata-bound and Stratiform Ore Deposits, Elsevier Scientific Publishing, Amsterdam 6, 130-221.

Sangster, D.F. and Brook, W.A., 1977. Primitive lead in an Australian Zn-Pb-Ba deposit. Nature 270, 423.

Sawkins, F.J., 1976. Massive sulphide deposits in relation to geotectonics. Geological Association of Canada Special Publication 14, 221-240.

Schiffman, P., Smith, B.M., Varga, R.J. and Moores, E.M., 1987. Geometry, conditions, and timing of off-axis hydrothermal metamorphism and ore deposition in the Solea Graben. Nature 325, 423-425.

Seal, R.R., II, Hammarstrom, J.M., Foley, N.K., and Alpers, C.N., 2002. Geoenvironmental models for seafloor massive sulfide deposits. In: Seal, R.R., II, and Foley, N.K., (eds.), Progress on geoenvironmental models for selected mineral deposit types: U.S Geological Survey Open-File Report 02-0195, 196-212.

Sestini, G., 1971. The relations between flysch and serpentinites in north-central Turkey. In: Campbell, A. S., (ed.), Geology and History of Turkey, The Petroleum Exploration Society of Libya, Tripoli, 369-383.

Shanks, W. C., III, and Seyfried, W. E., Jr., 1987. Stable isotope studies of vent fluids and chimney minerals, southern Juan de Fuca Ridge: sodium metasomatism and seawater sulfate reduction. Journal of Geophysical Research 92, 11387–11399.

Shepherd, T.J., Rankin, A.H. and Alderton, D.H.M., 1985. A practical guide to fluid inclusion studies. Glasgow: Blackie, 239 p.

Shervais, J. W., 1982. Ti-V plots and the petrogenesis of modern and ophiolitic lavas. Earth and Planetary Science Letters 59, 101-118.

Solomon, M., 1976. “Volcanic” massive sulphide deposits and their host rocks- a review and an explanation. In: Wolf, K. A., (ed.), Handbook of strata-bound and stratiform ore deposits, II, Regional studies and specific deposits. Amsterdam: Elsevier, 21-50.

Solomon, M., Tornos, F. and Gaspar, O.C., 2002. Explanation for many of the unusual features of the massive sulfide deposits of the Iberian pyrite belt. Geology 30, 87-90.

Spooner, E.T.C., 1977. Hydrodynamic model for the origin of the ophiolitic cupriferous pyrite ore deposits of Cyprus. Geological Society of London Special Publication 7, 58-71.

Spooner, E.T.C., 1981. Fluid inclusion studies of hydrothermal ore deposits. Mineralogical Association of Canada Short Course Handbook 6, 232-240.

Sillitoe, R. H., 1972. Formation of certain massive sulfide deposits at sites of sea-floor spreading. Trans. Inst. Mining and Metallurgy (section B) 81, B 141-148.

Spooner, E.T.C. and Bray, C.J., 1977. Hydrothermal fluids of sea water salinity in ophiolitic sulphide ore deposits in Cyprus. Nature 266, 808-812.

Stanton, R.L., 1972. Ore Petrology. New York: McGraw-Hill, 713 p.

Stanton, R. L., 1978. Mineralization in island arcs with particular reference to the southwest Pacific region. Proceedings Australian Institution of Mining and Metallurgy 268, 9-19.

Staudigel, H., Hart, S.R., and Richardson, S.H., 1981. Alteration of the oceanic crust - processes and timing. Earth and Planetary Science Letters 52, 2, 311-327.

Strickler, M.D., 1986. Geologic setting of the Turner-Albright massive sulfide deposit, Josephine County, Oregon. Oregon Geology 48 (10), 115-122.

Styrt, M.M., Brackmann, A.J., Holland, H.D., Clark, B.E., Pisutha-Arnond, V., Eldridge, C.S. and Ohmoto, H., 1981. The mineralogy and the isotopic

composition of sulphur in hydrothermal sulphide/sulphate deposits on the East Pacific Rise, 2l°N latitude. Earth Planetary Science Letters 53, 382-390.

Sun, S.-S., 1980. Lead isotopic study of young volcanic rocks from mid-ocean ridges, ocean islands and island arcs. Phil. Trans R. Soc. Lond. A297, 409-445.

Sun, S.-S. and McDonough, W.F., 1989. Chemical and isotope systematics basalts: implications for mantle composition and processes. In: Saunders, A.D., Norry, M.J., (eds.), Magmatism in the Ocean Basins. Geol. Soc. London Special Publication 42, 441-447.

Şengör, A.M.C. and Yılmaz, Y., 1981. Tethyan evolution of Turkey: a plate tectonic approach. Tectonophysics 75, 181–241.

Tankut, A. 1990. Geochemical implications for tectonic setting of the ophiolitic rocks from the ophiolite mélange belt of the Ankara Mélange. Mineral Research and Exploration Institute of Turkey (MTA) Bulletin 110, 17-28.

Tankut, A. and Gorton, M.P., 1990. Geochemistry of a mafic-ultramafic body in the Ankara Mélange, Anatolia, Turkey: evidence for a fragment of oceanic lithosphere. Ophiolites- Oceanic Crustal Analogues. Troodos 1987 Symposium Proceedings, 339-349.

Tankut, A. and Sayın, M.N., 1990. Mineral phases in the Edige ultramafic body. Mineral Research and Exploration Institute of Turkey (MTA) Bulletin 110, 11–97.

Tankut, A., Dilek, Y. and Önen, P., 1998. Petrology and geochemistry of the Neo-Tethyan volcanism as revealed in the Ankara mélange, Turkey. Journal of Volcanology and Geothermal Research 85, 1-4, 265-284.

Taylor, C.D., Zierenberg, R.A., Goldfarb, R.J., Kilburn, J.E., Seal II, R.R. and Kleinkopf, M.D., 1995. Volcanic-associated massive sulfide deposits. In: E.A., du Bray, (ed.), Preliminary compilation of geoenvironmental mineral deposit models: U.S. Geological Survey Open-File Report 95-831, 137-144.

Tüysüz, O., 1993. Karadeniz'den Orta Anadolu'ya bir jeotravers: Kuzey Neo-Tetis'in tektonik evrimi. Türkiye Petrol Jeologları Derneği Bülteni 5, 1-33.

Tüysüz, O., Dellaloğlu, A.A. and Terzioğlu, N., 1995. A magmatic belt within the Neo-Tethyan zone and its role in the tectonic evolution of northern Turkey. Tectonophysics 243, 173-191.

Ueda, A.A.H.R.K., 1986. Direct conversion of sulphide and sulphate minerals to SO_2 for isotope analysis. Geochemical Journal 20, 209-212.

Ustaömer, T. and Robertson, A.H.F., 1994. Late Palaeozoic marginal basin and subduction – accretion: evidence from the Palaeotethyan Küre Complex, Central Pontides, N. Turkey. J. Geol. Soc. London 151, 291–305.

Ünalan, G., 1981. Ankara Güneyindeki Ankara Melanjının stratigrafisi. Proceedings of the Symposium on the Geology of Central Anatolia. Geological Society of Turkey 35th Annual Meeting, 46-52, in Turkish with English abstract.

Vokes, F.M., Constantinou, G., Panayiotou, A. and Prestvik, T., 1990. In: Malpas, J.G., Moores, E.M., Panayiotou, A. and Xenophontos, C., (eds.), Ophiolites. Oceanic Crustal Analogues. Proceedings of the Symposium Troodos 1987. Geological Survey Department, Cyprus, 627-638.

White, W.M., 2005. Geochemistry. New York: Cornell University Press, 700 p.

Wilcox, R.E., 1979. The liquid line of descent and variation diagrams. The Evolution of the Igneous Rocks: 50th Anniversary Perspectives, Chapter 7, 206-232.

Wilson, M., 1989. Igneous Petrogenesis. Kluwer: Dordrecht, 450 p.

Wilson, P.N. and Petersen, E.U., 1989. Fluid inclusion evidence for fluid mixing in the Oxec Cyprus-type copper deposit, Guatemala. Economic Geology 84, 444-449.

Winchester, J. A. and Floyd, P. A., 1975. Geochemical magma type discrimination: application to altered and metamorphosed basic igneous rocks. Earth and Planetary Science Letters 28, 459-469.

Winchester, J.A. and Floyd, P.A., 1977. Geochemical discrimination of different magma series and their differentiation products using immobile elements. Chemical Geology 20, 325-343.

Wood, D.A., 1980. The application of a Th-Hf-Ta diagram to problems of tectonomagmatic classification and to establishing the nature of crustal contamination of basaltic lavas of the British Tertiary Volcanic Province. Earth and Planetary Science Letters 56, 11-30.

Zengqian, H., Zaw, K., Xiaoming, Q., Qingtong,Y., Jinjie, Y., Mingji, X., Deming, F. and Xianke, Y., 2001. Origin of the Gacun volcanic-hosted massive sulfide deposit in Sichuan, China; fluid inclusion and oxygen isotope evidence. Economic Geology 96/7, 1491-1512.

APPENDIX A

XRD DIFFRACTOGRAM OF SAMPLE KA-18

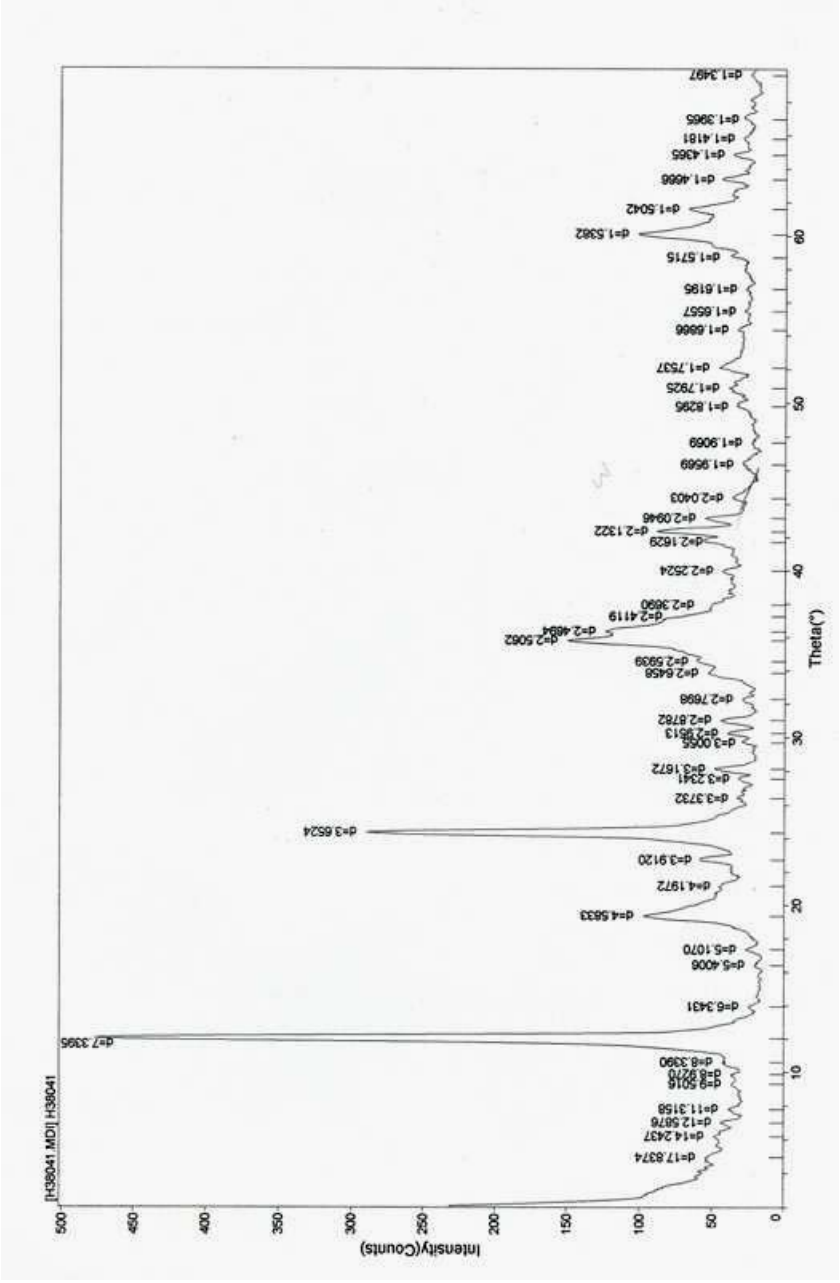

APPENDIX B

WHOLE ROCK GEOCHEMICAL DATA

		KD 3	KA 36	KA 40	KA 44	KA 46	KA 63	KA 74	KA 75	KD 2
		G	B	B	B	B	B	B	B	B
SiO_2	%	52.16	53.73	52.82	54.07	54.42	52.51	57.13	51.37	50.99
Al_2O_3	%	15.71	13.81	11.83	11.81	14.91	13.83	14.37	13.08	13.69
$Fe_2O_{3(T)}$	%	12.04	7.8	9.42	7.43	7.39	7.47	8.4	7.82	7.52
MgO	%	6.64	9.35	10.97	10.42	7.56	9.86	6.24	9.54	8.41
CaO	%	4.87	5.85	7.85	9.18	7.6	7	4.95	12.51	8.05
Na_2O	%	3	3.04	3.23	1.99	2.93	3.18	3.9	0.09	3.28
K_2O	%	0.19	0.07	0.05	0.07	0.28	0.04	0.1	0.04	0.06
TiO_2	%	0.44	0.24	0.19	0.17	0.25	0.19	0.49	0.19	0.24
P_2O_5	%	0.03	0.02	0.02	0.01	0.01	0.01	0.03	0.01	0.02
MnO	%	0.15	0.08	0.11	0.12	0.1	0.14	0.1	0.14	0.12
Cr_2O_3	%	0.024	0.075	0.115	0.127	0.029	0.06	0.019	0.12	0.041
LOI	%	4.5	5.8	3.2	4.5	4.4	5.6	4.1	5.1	7.4
SUM	%	99.76	99.89	99.83	99.92	99.89	99.88	99.84	100	99.84
Ni	ppm	29.6	69.2	53.5	105.9	28.9	98.7	36.8	122.6	63
Sc	ppm	42	47	48	45	44	46	34	42	43
Mo	ppm	3.3	1.8	1.7	2.4	1.2	1.7	3	4.1	2.5
Cu	ppm	1196	156.4	504.4	46.3	5.4	52.9	195	97	80.8
Pb	ppm	0.2	0.8	0.4	1.7	0.2	2.6	0.3	1.2	0.5
Zn	ppm	48	55	14	41	10	95	54	61	61
As	ppm	1	1.7	1.1	1.7	0.6	12.8	2.9	1.5	0.8
Cd	ppm	<.1	<.1	<.1	<.1	<.1	0.1	<.1	<.1	<.1
Sb	ppm	0.1	0.1	0.1	0.3	0.1	0.1	0.2	0.3	0.2
Ag	ppm	0.1	<.1	<.1	<.1	<.1	<.1	0.1	<.1	<.1
Au	ppb	3.8	1.7	<.5	1	<.5	8.6	1.2	2.4	<.5
Hg	ppm	<.01	<.01	<.01	<.01	<.01	0.02	<.01	<.01	0.01
Se	ppm	0.6	<.5	<.5	<.5	<.5	<.5	<.5	<.5	<.5

G: gabbro, B: basalt

		KD 3	KA 36	KA 40	KA 44	KA 46	KA 63	KA 74	KA 75	KD 2
		G	B	B	B	B	B	B	B	B
Ba	ppm	19.1	34.7	7.1	15.9	73.4	23.5	22.2	5.8	20.9
Be	ppm	<1	<1	<1	<1	<1	<1	<1	1	1
Co	ppm	40	34.1	35.7	34.7	34	24.1	28.9	33.9	29.3
Cs	ppm	0.1	<.1	<.1	0.1	0.4	<.1	0.2	<.1	<.1
Ga	ppm	14.3	11.1	9.2	9.7	10.1	11.4	11.5	10.6	11.3
Hf	ppm	<.5	<.5	<.5	<.5	<.5	<.5	0.7	<.5	<.5
Nb	ppm	0.6	0.8	<.5	0.7	0.8	0.7	1	0.7	0.6
Rb	ppm	3.3	1.3	0.9	1.4	4	0.7	2.1	<.5	1
Sr	ppm	111.4	117.9	34.6	117.7	243.1	71.5	87.6	18.3	123.1
Ta	ppm	<.1	<.1	<.1	<.1	<.1	<.1	<.1	<.1	<.1
Th	ppm	0.4	0.2	0.3	0.1	0.4	0.2	0.2	0.1	0.2
U	ppm	<.1	<.1	<.1	0.2	0.2	0.1	0.1	<.1	<.1
V	ppm	256	268	230	225	292	242	260	233	241
W	ppm	0.4	0.3	0.2	0.3	0.6	0.9	0.6	0.5	0.2
Zr	ppm	15.1	7.4	5	4.7	7.7	6.4	18.2	6.8	6.1
Y	ppm	11.8	7.7	6.1	5.4	7.8	7.3	12.2	7	7.1
La	ppm	1.2	0.9	0.7	0.6	1.1	0.8	1.3	0.6	0.8
Ce	ppm	2.8	1.6	1.3	1	2.1	1.6	3.1	1.4	1.4
Pr	ppm	0.41	0.19	0.15	0.11	0.24	0.15	0.44	0.15	0.16
Nd	ppm	2.5	0.7	0.7	<.4	1.2	0.7	2.4	0.6	1.1
Sm	ppm	0.9	0.3	0.3	0.3	0.3	0.3	0.8	0.3	0.4
Eu	ppm	0.34	0.12	0.13	0.12	0.17	0.15	0.34	0.12	0.19
Gd	ppm	1.35	0.65	0.58	0.47	0.74	0.58	1.54	0.57	0.7
Tb	ppm	0.31	0.17	0.13	0.12	0.15	0.14	0.31	0.14	0.14
Dy	ppm	1.92	1.12	1.03	0.76	1.06	1.1	1.9	0.92	1.04
Ho	ppm	0.43	0.3	0.22	0.2	0.27	0.25	0.45	0.25	0.26
Er	ppm	1.25	0.81	0.7	0.65	0.89	0.86	1.39	0.74	0.78
Tm	ppm	0.19	0.13	0.11	0.11	0.13	0.15	0.21	0.12	0.14
Yb	ppm	1.23	0.87	0.74	0.67	0.93	0.97	1.33	0.79	0.85
Lu	ppm	0.22	0.14	0.14	0.1	0.16	0.16	0.23	0.16	0.17

G: gabbro, B: basalt

		KA 22-1	KA 29-1	KA 11	KA 12	KA 18	KA 19	KA 29-2	KA 22-2	KA 59
		G	G	S	S	V	V	D	M	M
SiO2	%	48.32	51.19	42.3	41.26	60.81	58.81	60.7	16.41	15.91
Al2O3	%	14.83	18.41	1.63	1.95	14.37	11.02	12.67	0.07	0.04
Fe2O3	%	7.01	6.22	8.63	8.66	7.91	8.79	9.82	54.32	54.41
MgO	%	5.84	6.42	33.29	32.48	7.69	10.78	7.73	0.01	0.17
CaO	%	12.33	11.1	0.73	0.26	0.4	3.38	0.07	0.1	0.01
Na2O	%	4.73	2.49	0.07	0.01	3.95	0.04	0.07	0.01	0.01
K2O	%	0.26	0.22	0.04	0.04	0.05	0.04	0.89	0.04	0.04
TiO2	%	1.08	0.25	0.02	0.03	0.21	0.2	0.22	0.01	0.01
P2O5	%	0.11	0.01	0.01	0.01	0.01	0.01	0.02	0.01	0.01
MnO	%	0.14	0.07	0.11	0.13	0.13	0.21	0.07	0.01	0.01
Cr2O3	%	0.037	0.019	0.024	0.481	0.05	0.101	0.058	0.079	0.044
LOI	%	5.1	3.5	12.3	14.3	4.2	6.6	7	28.8	29.3
SUM	%	99.82	99.9	99.15	99.88	99.79	100	99.33	99.82	99.91
Ni	ppm	128.5	8.6	2011	2266	57.7	98.6	62.1	38.5	41.4
Sc	ppm	37	37	11	15	40	41	39	1	1
Mo	ppm	2	1.9	0.9	0.8	6.3	3.4	3.3	42.5	28.4
Cu	ppm	51.4	7.9	35.4	33	127.8	18	7971	2759	7271
Pb	ppm	1	<.1	0.1	<.1	1.7	1.3	0.5	46.9	59.1
Zn	ppm	60	4	17	30	731	214	169	82	84
As	ppm	1.5	<.5	1.4	0.6	9.1	12.9	9.8	1632	2889
Cd	ppm	0.4	<.1	<.1	<.1	0.9	0.1	<.1	0.1	0.2
Sb	ppm	0.1	<.1	<.1	<.1	0.5	0.2	0.4	33.7	49.4
Ag	ppm	0.1	<.1	<.1	<.1	0.1	0.1	0.5	4.8	8.5
Au	ppb	2	0.5	1.5	2.1	19.2	9.7	68	848.2	1224
Hg	ppm	0.01	0.07	0.01	0.01	0.04	0.01	0.02	0.91	1.78
Se	ppm	<.5	<.5	0.7	<.5	0.7	2.2	6.1	>100	80.9

G: gabbro, B: basalt, S: serpentinite, V: vein-type ore,
D: disseminated ore, M: massive ore

		KA 22-1	KA 29-1	KA 11	KA 12	KA 18	KA 19	KA 29-2	KA 22-2	KA 59
		G	G	S	S	V	V	D	M	M
Ba	ppm	45.6	40.8	1.8	1.9	16.2	23.2	125.2	589.8	117
Be	ppm	<1	<1	<1	<1	<1	<1	<1	<1	<1
Co	ppm	74.1	30.6	107.3	107.8	27.9	33.8	30.6	68.7	16.5
Cs	ppm	0.2	1.1	<.1	0.1	<.1	0.1	0.2	0.2	0.3
Ga	ppm	11.9	14	2.2	2.4	11.4	11.8	23.9	0.7	<.5
Hf	ppm	2.1	<.5	<.5	<.5	<.5	<.5	<.5	<.5	<.5
Nb	ppm	2.4	0.9	<.5	<.5	1	0.7	0.9	<.5	<.5
Rb	ppm	3.9	4.8	<.5	0.7	1.5	0.9	18.7	0.8	0.6
Sn	ppm	149.9	246.4	<1	<1	<1	<1	<1	<1	<1
Sr	ppm	0.2	<.1	2.2	1.3	37.2	7.1	2.6	5.3	2.3
Ta	ppm	0.2	0.3	<.1	<.1	<.1	<.1	<.1	<.1	<.1
Th	ppm	2.9	<.1	<.1	<.1	0.3	0.2	0.3	0.1	<.1
U	ppm	247	283	<.1	<.1	0.2	0.2	0.5	<.1	<.1
V	ppm	0.5	0.3	68	71	242	221	236	8	<5
W	ppm	58.6	7.3	0.3	0.3	1.3	0.6	0.8	0.3	0.8
Zr	ppm	27.1	7	<.5	<.5	7.2	6.6	8	0.8	<.5
Y	ppm	3.9	1.1	0.8	1	15.9	7.7	4.5	0.2	<.1
La	ppm	10.8	1.9	<.5	<.5	<.5	0.6	0.9	<.5	<.5
Ce	ppm	1.62	0.19	<.5	<.5	0.6	0.9	1.9	<.5	<.5
Pr	ppm	8.2	0.7	<.02	<.02	0.11	0.12	0.22	0.03	<.02
Nd	ppm	3	0.3	<.4	<.4	0.7	0.7	1	<.4	<.4
Sm	ppm	1.06	0.18	<.1	<.1	0.5	0.3	0.3	<.1	<.1
Eu	ppm	3.95	0.68	<.05	<.05	0.21	0.14	0.11	<.05	<.05
Gd	ppm	0.78	0.16	0.08	0.07	1.28	0.61	0.53	<.05	<.05
Tb	ppm	4.42	1.03	0.02	0.01	0.35	0.17	0.1	0.01	<.01
Dy	ppm	0.96	0.27	0.12	0.1	2.69	1.23	0.79	0.05	<.05
Ho	ppm	2.87	0.78	<.05	<.05	0.59	0.28	0.21	<.05	<.05
Er	ppm	0.4	0.14	0.1	0.1	1.74	0.88	0.59	<.05	<.05
Tm	ppm	2.46	0.8	<.05	<.05	0.25	0.13	0.09	<.05	<.05
Yb	ppm	0.41	0.15	0.13	0.17	1.43	0.98	0.64	<.05	<.05
Lu	ppm	45.6	40.8	0.02	0.02	0.21	0.16	0.12	<.01	<.01

G: gabbro, B: basalt, S: serpentinite, V: vein-type ore,
D: disseminated ore, M: massive ore